THESIS REPORT
Ph.D.

SYSTEMS
RESEARCH
CENTER

Supported by the National Science Foundation Engineering Research Center Program (NSFD CD 8803012), the University of Maryland, Harvard University, and Industry

Wavelets and Time-Frequency Methods in Linear Systems and Neural Networks

by Y.C. Pati
Advisor: P.S. Krishnaprasad

Ph.D. 92-13

Report Documentation Page

Form Approved
OMB No. 0704-0188

1. REPORT DATE	2. REPORT TYPE	3. DATES COVERED
1992		**00-00-1992 to 00-00-1992**

4. TITLE AND SUBTITLE	5a. CONTRACT NUMBER
Wavelets and Time-Frequency Methods in Linear Systems and Neural Networks	5b. GRANT NUMBER
	5c. PROGRAM ELEMENT NUMBER
6. AUTHOR(S)	5d. PROJECT NUMBER
	5e. TASK NUMBER
	5f. WORK UNIT NUMBER
7. PERFORMING ORGANIZATION NAME(S) AND ADDRESS(ES) **University of Maryland,The Graduate School,2123 Lee Building,College Park,MD,20742**	8. PERFORMING ORGANIZATION REPORT NUMBER
9. SPONSORING/MONITORING AGENCY NAME(S) AND ADDRESS(ES)	10. SPONSOR/MONITOR'S ACRONYM(S)
	11. SPONSOR/MONITOR'S REPORT NUMBER(S)

12. DISTRIBUTION/AVAILABILITY STATEMENT
Approved for public release; distribution unlimited

13. SUPPLEMENTARY NOTES

14. ABSTRACT
see report

15. SUBJECT TERMS

16. SECURITY CLASSIFICATION OF:			17. LIMITATION OF ABSTRACT	18. NUMBER OF PAGES	19a. NAME OF RESPONSIBLE PERSON
a. REPORT **unclassified**	b. ABSTRACT **unclassified**	c. THIS PAGE **unclassified**		**196**	

Wavelets and Time-Frequency Methods in Linear Systems and Neural Networks

by

Yagyensh C. Pati

Dissertation submitted to the Faculty of The Graduate School
of The University Of Maryland in partial fulfillment
of the requirements for the degree of
Doctor of Philosophy
1992

Advisory Committee:

Professor P. S. Krishnaprasad, Chairman/Advisor
Associate Professor W. Dayawansa
Professor S. Marcus
Professor M. C. Peckerar
Professor C. A. Berenstein

ABSTRACT

Title of Dissertation: Wavelets and Time-Frequency Methods in Linear Systems and Neural Networks

Yagyensh C. Pati, Doctor of Philosophy, 1992

Dissertation directed by: Professor P. S. Krishnaprasad

Department of Electrical Engineering

In the first part of this dissertation we consider the problem of rational approximation and identification of stable linear systems. Affine wavelet decompositions of the Hardy space $H^2(\Pi^+)$, are developed as a means of constructing rational approximations to nonrational transfer functions. The decompositions considered here are based on frames constructed from dilations and complex translations of a single rational function. It is shown that suitable truncations of such decompositions can lead to low order rational approximants for certain classes of time-frequency localized systems. It is also shown that suitably truncated rational wavelet series may be used as 'linear-in-parameters' black box models for system identification. In the context of parametric models for system identification, time-frequency localization afforded by affine wavelets is used to incorporate *a priori* knowledge into the formal properties of the model. Comparisons are made with methods based on the classical Laguerre filters.

The second part of this dissertation is concerned with developing a theoretical framework for feedforward neural networks which is suitable for both analysis and synthesis of such networks. Our approach to this problem is via affine wavelets and the theory of frames. Affine frames for L^2, are constructed using combinations of sigmoidal functions and the inherent translations and dilations of feedforward network architectures. Time-frequency localization is used in developing methods for the synthesis of feedforward networks to solve a given problem.

These two seemingly disparate problems both lie within the realm of approximation theory, and our approach to both is via the theory of frames and affine wavelets.

Acknowledgements

I would like to express my gratitude to my thesis advisor Professor P. S. Krishnaprasad for providing an abundance of opportunity to explore new and diverse areas of research, and for providing encouragement, guidance, and inspiration throughout the course of my graduate studies and this research. I am indebted and grateful to Professor Martin C. Peckerar, who gave me the opportunity and inspiration to broaden my interests and research in many ways, and served as a constant source of encouragement. I thank the other members of my advisory committee, Professor C. Berenstein, Associate Professor W. Dayawansa, and Professor S. I. Marcus for their efforts in providing many useful comments and suggestions regarding this dissertation. I am also grateful to Professor J. Benedetto for providing considerable insight and assistance on the topic of wavelet transforms. I thank Associate Professor Shihab Shamma for his support over the past few years.

A number of colleagues and fellow students also merit special acknowledgement for serving as sounding boards for ideas, offering suggestions, comments, and support over the years. I thank Bill Byrne, Svetlana Vranic, Tony and Carole Teolis, Zeev Berman, and Nick Sidiropoulis, among others for making the past few years more enjoyable. I also thank Helen Pickett for her assistance in numerous projects.

This research was supported in part by the National Science Foundation's Engineering Research Centers Program: NSFD CDR 8803012, the Air Force Office of Scientific Research under contract AFOSR-88-0204, the AFOSR University Research Initiative Program under grant AFOSR-90-0105, and by the Naval Research Laboratories through summer employment.

Contents

List of Tables

List of Figures

Chapter 1

Introduction

As is perhaps suggested by the title, this dissertation is composed of two somewhat distinct parts. The first part (Chapters 3 and 4) is concerned with the approximation and identification of causal linear time-invariant systems using time-frequency localized rational (wavelet) representations. In Section 1.2 below we give a brief description of the problem and an outline of the work done.

In the second part of this dissertation (Chapter 5) we address the problem of developing a formal mathematical framework suitable for both analysis and synthesis of feedforward neural networks using wavelet theory. An outline of the problem and a summary of our results are given in Section 1.3.

A common thread in the approach taken here to the above two problems is the theory of frames and affine wavelets. A second area of commonality in these two seemingly disparate problems is that both fall within the realm of approximation theory.

1.1 Affine Wavelet Transforms

In its continuous form, the (affine) wavelet transform is an integral transform against dilations and translations of a single function called the *analyzing wavelet*, where for an analyzing wavelet g, the translations and dilations are of the form $g^{(a,b)}(x) =$

$a^{1/2}g(ax-b)$. In Chapter 2 we define, and briefly review some properties of, wavelet transforms on $L^2(\mathbb{R})$. Although the use of dilations and translations of a single function is not new (c.f. [AK69]), the more recent application of these techniques to signal analysis may be traced to J. Morlet [MAFG82, GM84], who proposed the use of "wavelets of constant shape" for the analysis of seismic signals. In [MAFG82, GM84] and subsequent papers [GMP85, GMP86], in which the name was shortened to "wavelets", attention was restricted to what is now known as the continuous wavelet transform where the dilations and translations vary continuously (i.e. $(a,b) \in \mathbb{R} \setminus 0 \times \mathbb{R}$).

Generalization of the concept of bases in Hilbert spaces leads to the notion of what are called *frames* (c.f. [Dau90, DS52]). A review of the key aspects of frame theory is provided in Chapter 2, and is supplemented by material in Appendix C. The most important property of frames is that the sequence of numbers obtained by taking inner products of a vector f, in a Hilbert space $\mathcal{H}$, with the elements of a frame for $\mathcal{H}$, comprise a complete and 'stable' representation of the vector f. In [DGM86] discrete forms of the wavelet transform were considered in which dilations and translations were restricted to discrete lattices so that the resulting translates and dilates of the analyzing wavelet formed frames. This was a first step towards the construction of a number of orthonormal wavelet bases (c.f. [Mey86, Bat87]). The subsequent development of the theory of multiresolution analyses [Mal89a], provided a framework for the study of a class of orthonormal wavelet bases, and led to the construction of families of compactly supported orthonormal wavelet bases by Daubechies [Dau88a]. Most of the activity involving wavelet transforms in signal analysis has since been restricted to orthonormal wavelet bases, partly due to their appealing computational properties and their connections to FIR filters and subband coding (c.f. [Dau88a]). In this dissertation the emphasis is on wavelet frames rather than orthonormal bases.

Perhaps the most useful property of affine wavelet transforms, is the time-frequency localization which arises from the use of dilations and translations together with an 'admissibility' requirement which forces the analyzing wavelet to be approx-

imately a bandpass function. By time-frequency localization, we are referring to the fact that a wavelet transform approximately provides a frequency analysis of signals, locally in time. This should be viewed in analogy with the short time Fourier transform (STFT), where window functions are used to achieve time localization of the frequency analysis. Thus the wavelet transform is well-suited to the analysis of signals with time-varying frequency content. There exist numerous examples in nature of signals with such time-varying frequency content. One interesting example pointed out in [Dau90] is that of music. A musical score (c.f. Figure 1.1) may be regarded as a time-frequency localized representation in which the length of a note is its time duration and the particular note specifies the frequency content. Other examples of

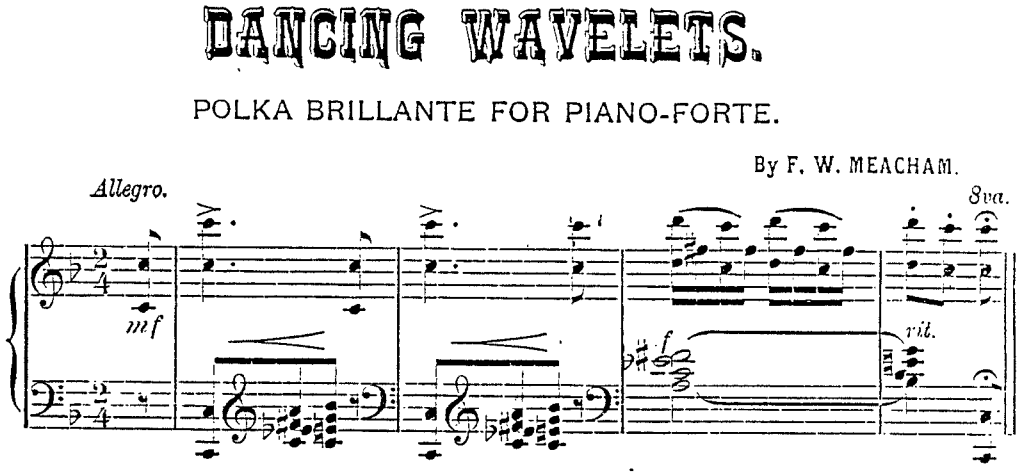

Figure 1.1: "Dancing Wavelets", by F. W. Meacham (Willis Woodward & Co. 1892)

such signals include visual images, where now we have to consider the two-dimensional notion of spatio-spectral localization, for instance, edges in an image may be regarded as a spatially-localized high frequency components. Much of the work described in this dissertation is directly aimed at exploiting the time-frequency localization afforded by affine wavelets.

1.2 Rational Wavelets in Approximation and Identification of Stable Linear Systems

A recurring theme in the study of linear dynamical systems is the approximation of transfer functions by rational functions. It is well-known that given a transfer function $G(s)$, the system described by G has a finite-dimensional state space realization if and only if G is a rational function of s. The problem of rational approximation arises in two contexts associated with linear dynamical systems. First there is the problem of model order reduction where high-order (often infinite-dimensional) systems are to be approximated by lower order systems. In this case it is assumed that the system (transfer function) is known. The second setting in which the problem of rational approximation arises is that of system identification. In this case it is assumed that the true system is not known, and a model of the system is to be constructed based on observations of the input-output behavior.

1.2.1 Rational Wavelet Approximations of Stable Linear Systems

Rational approximation of infinite-dimensional systems is a topic which has received considerable attention. The problem is that of approximating (nonrational) transfer functions of infinite-dimensional systems by a low-order rational approximants. A variety of rational approximation techniques, have been proposed and studied over the years. Among these are methods based on Hankel singular values, truncations of balanced realizations, Pade approximations, and truncations of Fourier representations with respect to specific orthonormal bases (c.f. [GLP90, GLP91a]). Among the issues which are addressed in this area are: (i) the rate of convergence of approximation as model order is increased, (ii) optimally convergent methods, (iii) ease of computation, (iv) the class or classes of problems well-suited to a given method.

In Chapter 3, we propose a new method for use in the problem of rational approximation of a class of stable transfer functions. The transfer functions of interest here are contained in the Hardy space $H^2(\Pi^+)$ where Π^+, denotes the right-half com-

plex plane $\Re e\ s > 0$. Our approach utilizes decompositions of $H^2(\Pi^+)$, via frames constructed from dilations and complex translations of a single real-rational analyzing wavelet. The considerable freedom in the choice of rational analyzing wavelets is demonstrated via a characterization of all rational analyzing wavelets for $H^2(\Pi^+)$ in Theorem 3.4. One of the main results of Chapter 3 is Theorem 3.3 which shows that for functions in $H^2(\Pi^+)$ which are Laplace transforms of real-valued functions in $L^2(0,\infty)$, it is possible to regroup terms in wavelet series based on rational analyzing wavelets, such that each term in the new series is a real-rational function. We refer to the series obtained via such regroupings as a *wavelet system (WS) decomposition.* A wavelet system decomposition may be viewed as a parallel decomposition of systems, via time-frequency localized finite-dimensional systems. The method we propose for rational approximation of transfer functions is based on particular truncations of WS decompositions. For certain classes of time-frequency localized systems, such truncations can lead to fairly low order approximants. Our approach was in part motivated by the observation that transfer functions arising from physical systems often lend themselves to reasonably compact time-frequency localized representations. We also examine some of the properties of WS decompositions including minimal state space realizations of truncated WS representations, and establish coarse bounds on the approximation error for the truncated series.

1.2.2 Rational Wavelet Models in System Identification

System identification is a process of using observed data to determine usable descriptions of unknown dynamical systems. Here we are concerned with systems with the explicit assumptions of linearity, time-invariance, and causality. System identification plays a crucial role in any design process involving physical systems, and thus is deserving of the extensive attention which it has received. For a thorough treatment and survey of much of the work in the area of system identification we refer to [Eyk74, Lju87, UR90, Str81, Wel81, You81]. Descriptions of systems obtained via the identification process may be either in parametric or nonparametric form. In this dis-

sertation attention is largely restricted to parametric descriptions. Methods leading to parametric descriptions of systems are termed parametric identification methods.

The essential steps in the process of parametric identification are: (i) experiment design for the collection of data, (ii) selection of a parametric model set, and (iii) selection of an identification scheme to fit the model to the data via estimation of the parameters. It has often been noted that the most important as well as difficult step in this process, is the selection of a suitable parametric model set. It is important that any *a priori* knowledge or engineering intuition about the unknown system be incorporated into the formal properties of the parametric model set. The types of parametric models we consider here are typically called 'black-box' models, and are characterized by the fact that the parameters in the models have no physical significance.

In Chapter 4, we show that truncations of WS representations, may be used as linear-in-parameters black-box models for the purpose of identification. It is also shown that the time-frequency localization of the component systems of a WS model, offer a convenient means of incorporating time and frequency domain *a priori* information into the model. The forms of prior knowledge considered are time constants, delays, and frequency weighting. An important feature of WS models is that both time and frequency domain information may be treated simultaneously, as opposed to the separate treatment encountered in most schemes.

We make comparisons of WS models with methods based on the classical Laguerre filters. Laguerre filters, which form orthonormal bases for $H^2(\Pi^+)$, have been extensively studied in the context of system identification and rational approximation. The use of Laguerre filters in system identification apparently dates back to Wiener [Wie56]. There has recently been considerable renewed interest in Laguerre methods due to computational simplicity of these techniques relative other (optimal) approximation schemes such as Hankel norm optimal methods. More recent work on Laguerre filters may be found in [Mak90a, Wah91, Par91, Mak90b, DZP90] and the references contained therein. We demonstrate by means of examples, that for certain important classes of systems, the performance of the WS approximation may be far

superior to that of Laguerre methods.

1.3 Wavelet Analysis and Synthesis of Feedforward Neural Networks

Over the past few years there has been a great deal of interest in the study and applications of neural networks. Neural networks are a class of computational architectures characterized by large numbers of simple processing elements which are interconnected in a weighted manner. The term *neural* reflects the initial biological inspiration for such networks. Feedforward neural networks, which comprise an important subclass of neural networks, are characterized by a well defined (forward) direction of signal flow, and have found applications in the approximation of (static) mappings from discrete data.

Problems of approximation of static mappings arise within a variety of contexts. Examples of static map learning problems to which feedforward networks have been applied may be found in areas such as speech recognition [LZ89], control and identification of dynamical systems [NP90] and robot motion control [Kup88] [KW90], among others. There of course exist numerous methods from mathematical approximation theory which may also be considered for application to these problems. The appeal of the feedforward network methodology derives from empirically demonstrated success in problems involving mappings where the domain or range, or both are of high dimension. For such high-dimensional problems, the more structured approaches of classical approximation theory often prove to be computationally intractable.

The empirical success of feedforward networks in approximation problems prompted questions regarding the class or classes of mappings which may be approximated within these architectures. In answer to these questions, a number of rigorous mathematical descriptions of the approximating properties of feedforward networks (c.f. [Cyb89, Cyb88, HSW89, HSW90]) were put forth. Most of these descriptions rely on arguments of density, of the class of maps that can be implemented within a

feedforward network, in various function spaces. Thus these results should be viewed as theoretical justification for the use of feedforward networks in certain classes of approximation problems. However, a unknown entity in these formulations was the exact feedforward network implementation of a given mapping from a suitable class. In this sense the above results are nonconstructive and provide no further insight into the problem of synthesis of feedforward networks. The problem of feedforward network synthesis is that of designing a network suited to solve the approximation problem at hand. Thus arises the question: is it possible to construct a theoretical framework for feedforward networks which first of all provides a constructive analysis of the approximation properties of feedforward networks, and secondly, is amenable to the development of synthesis algorithms.

In Chapter 5 we utilize the theory of frames and affine wavelets to develop a formal mathematical framework suitable for both analysis and synthesis of feedforward neural networks. Our approach was initially motivated by the observations that (i) there exists an inherent translation and dilation structure in feedforward networks, and (ii) the flexibility of frame theory permits considerable freedom in the selection of analyzing wavelets. It is shown that the commonly-used 'sigmoidal activation functions' may be combined in a manner so as to form admissible analyzing wavelets, and thereby frames for L^2, within the standard architecture of feedforward networks. In this manner we obtain a constructive analysis result for the approximation of square integrable functions by feedforward networks. We also show that time-frequency localization properties of affine wavelets can form the basis for the development of systematic network synthesis methods.

Chapter 2

Background on Wavelet Transforms and Frames

2.1 Preliminaries

Given the wide range of conventions used in the fields of engineering, mathematics, and physics, this section covers the various definitions which will be used throughout this dissertation.

Most of this dissertation deals with the Hilbert space $L^2(\mathbb{R})$, the space of all measurable *finite energy* functions, i.e all measurable functions defined on the real line such that

$$\int_{\mathbb{R}} |f(x)|^2 \, dx \; < \; \infty.$$

This space is equipped with a standard inner product, denoted by $\langle \cdot, \cdot \rangle$.

$$\langle f, g \rangle = \int_{\mathbb{R}} f(x)\overline{g(x)}dx.$$

2.1.1 Fourier and Laplace Transforms

Fourier Transforms on $L^2(\mathbb{R})$

The definition of Fourier transform which is used here is according to the convention commonly used in engineering literature.

Given a function $f \in L^2(\mathbb{R})$ its Fourier transform $\widehat{f}$ is defined as,

$$\widehat{f(\omega)} = \int_{\mathbb{R}} f(x) e^{-i\omega x} dx,$$

where convergence of the integral is taken in the L^2 sense. The corresponding inversion formula is,

$$f(x) = \frac{1}{2\pi} \int_{\mathbb{R}} \widehat{f(\omega)} e^{i\omega x} dx.$$

The unitary nature of the Fourier Transform is expressed in Parseval's theorem.

Theorem 2.1 (Parseval) *Given $f \in L^2(\mathbb{R})$ with Fourier transform $\widehat{f}$,*

$$\int_{\mathbb{R}} |f(x)|^2 \, dx = \frac{1}{2\pi} \int_{\mathbb{R}} \left|\widehat{f}(\omega)\right|^2 d\omega.$$

A generalization of Parseval's theorem which is attributed to Plancheral is, the fact that,

$$\langle f, g \rangle = \frac{1}{2\pi} \left\langle \widehat{f}, \widehat{g} \right\rangle.$$

Laplace Transforms

For functions defined on the positive half-line $\mathbb{R}_+$ the (unilateral) Laplace transform is defined by,

$$F(s) = \int_0^\infty f(x) e^{-sx} dx,$$

where the integral converges on a half-plane $\Re e\, s > \sigma$, σ being the *abscissa of convergence*. Inversion of the Laplace transform is accomplished by the inversion formula,

$$f(x) = \frac{1}{2\pi i} \int_{\gamma - i\infty}^{\gamma + i\infty} F(s) e^{st} ds,$$

where γ is taken larger than the abscissa of convergence.

2.1.2 Time-Frequency Localization

The notion of localization in joint time-frequency space is important in many areas of signal analysis and is crucial to the utility of wavelet transforms. In this section we introduce, and to some extent formalize the concept of time-frequency localization.

In the context of time-frequency localization, we are interested in functions which are *essentially time-limited* to some interval $[-T, T]$ and *essentially band-limited* to some frequency range $[\Omega_0, \Omega_1] \bigcup [-\Omega_0, -\Omega_1]$. One measure of how well a function is localized in either the time or frequency domains is given in terms of the second moments (or variances) of the squared magnitude functions. There is however a limit to the extent of joint time-frequency localization attainable, which is specified by Heisenberg's inequality. Heisenberg's inequality states that both for the second moment of $|f|^2$ and the second moment of $|\widehat{f}|^2$ cannot simultaneously be made arbitrarily small, and in fact the the product of these two second moments is bounded below away from zero. More precisely, we have the following classical result (c.f. [DM72]).

Theorem 2.2 *(Heisenberg's inequality) For* $f \in \mathrm{L}^2(\mathbb{R})$,

$$\int_{\mathbb{R}} x^2 \, |f(x)| \, dx \;\times\; \int_{\mathbb{R}} \omega^2 \left|\widehat{f}(\omega)\right|^2 d\omega \geq \frac{1}{4}\|f\|^4. \tag{2.1.1}$$

Equality in (2.1.1) is achieved only by functions which are constant multiples of the Gaussian function. Thus Gaussian functions are optimally concentrated in joint time-frequency space.

Let us make the following definitions for the *centers of concentration* of functions f, whose Fourier transforms have even magnitude $|\widehat{f}(-\omega)| = |\widehat{f}(\omega)|$.

Definition 2.1 *Given a function* $f \in \mathrm{L}^2(\mathbb{R})$, *with Fourier transform* $\widehat{f}$, *such that* $|\widehat{f}(-\omega)| = |\widehat{f}(\omega)|$;

(1) The center of concentration, $x_c(f)$, *of* f, *is defined as*

$$x_c(f) = \frac{1}{\|f\|^2} \int_{\mathbb{R}} x|f(x)|^2 dx.$$

(2) the center of concentration, $\omega_c(|\widehat{f}|^2)$, *of* $|\widehat{f}|^2$, *(or center frequency of* f*) is defined as*

$$\omega_c(\widehat{f}) = \frac{1}{\pi\|f\|^2} \int_0^\infty \omega|\widehat{f}(\omega)|^2 d\omega.$$

Note that this definition also applies to functions whose Fourier transforms are supported strictly on $\mathbb{R}^+$. If we now define the second moments,

$$\begin{aligned}\sigma(f) &= \frac{1}{\|f\|^2}\int_{\mathbb{R}}(x-x_c(f))^2|f(x)|^2dx \\ \sigma(\widehat{f}) &= \frac{1}{\pi\|f\|^2}\int_0^\infty(\omega-\omega_c(\widehat{f})^2|\widehat{f}(\omega)|^2d\omega,\end{aligned}$$

Thus $\sigma(f)$ and $\sigma(\widehat{f})$ may be respectively used as measures of time and frequency localization.

A second related view of time-frequency localization may be stated in terms of regions which contain most of the 'energy' in the signal. Let us define two projection operators P_Ω and Q_T on $\mathrm{L}^2(\mathbb{R})$ by,

$$\begin{aligned}(\widehat{P_\Omega f})(\omega) &= \chi_{[-\Omega,\Omega]}(\omega)\widehat{f}(\omega) \\ (Q_T f)(x) &= \chi_{[-T,T]}(x)f(x),\end{aligned}$$

where χ_I denotes the indicator function of the interval I. Using these definitions we assume that the functions f of interest to us are such that,

$$\|(\mathbb{1}-Q_T)f\|<\epsilon \text{ and } \|(\mathbb{1}-(P_{\Omega_1}-P_{\Omega_0}))f\|<\epsilon. \tag{2.1.2}$$

To relate Ω_0, Ω_1 and T to a function $f\in\mathrm{L}^2(\mathbb{R})$ in a more precise manner, we make the following definitions.

Definition 2.2 *Given $f\in\mathrm{L}^2(\mathbb{R})$, $f:\mathbb{R}\to\mathbb{R}$, with Fourier transform $\widehat{f}$, and centers of concentration $x_c(f)$ and $\omega_c(|\widehat{f}|^2)$,*

$$\mathcal{P}(f;\epsilon)=\left\{[x_0,x_1]:\ |x_c(f)-x_0|=|x_c(f)-x_1| \text{ and } \int_{x\in\mathbb{R}\setminus[x_0,x_1]}|f(x)|^2dx\le\epsilon\|f\|^2\right\},$$

and,

$$\begin{aligned}\widehat{\mathcal{P}}(f;\widehat{\epsilon}) = \Big\{&[\omega_0,\omega_1]:\ \omega_0=\max(0,\widetilde{\omega_0}),\ |\omega_c(|\widehat{f}|^2)-\widetilde{\omega_0}|=|\omega_c(|\widehat{f}|^2)-\omega_1|\,, \\ &\text{and } \int_{\omega\in\mathbb{R}\setminus[\omega_0,\omega_1]}|\widehat{f}(\omega)|^2d\omega\le\widehat{\epsilon}\|f\|^2\Big\}.\end{aligned}$$

(1) The epsilon support (or time concentration) of f, denoted ϵ-supp(f,ϵ) is the set $[x_o(f), x_1(f)] \in \mathcal{P}(f;\epsilon)$ such that,

$$|x_0(f) - x_1(f)| = \inf_{[x_0,x_1]\in\mathcal{P}} |x_0 - x_1|.$$

(2) The epsilon support of $|\widehat{f}|^2$ (or frequency concentration of f) denoted ϵ-supp$(|\widehat{f}|^2,\widehat{\epsilon})$ is the set $[\omega_0(f),\omega_1(f)] \in \widehat{\mathcal{P}}(f;\widehat{\epsilon})$ such that

$$|\omega_1(f) - \omega_0(f)| = \inf_{[\omega_0,\omega_1]\in\widehat{\mathcal{P}}} |\omega_1 - \omega_0|.$$

Remark: The ϵ-support of f is the smallest (symmetric about $x_c(f)$) interval containing $(1-\epsilon)\times$ the total signal energy. Note that when $x_c(f) = 0$, taking $x_0(f) = -x_1(f) = -T$, $\Omega_0 = \omega_0(f)$, $\Omega_1 = \omega_1(f)$, and $\epsilon = \widehat{\epsilon}$, Equation 2.1.2 is satisfied.

2.1.3 Time-Frequency Localized Representations and Windowed Fourier Transforms

In a variety of applications of signal processing one often encounters problems where it is desirable to analyze the frequency content of a signal locally in time. Examples of applications where joint time-frequency localized representations are desirable can be found for instance in image processing [Mal89c] [Mal89b] [Dau83] [PZ88], and analysis of acoustic signals [KMMG87]. To illustrate this point, consider the function f defined on $[-\pi,\pi]$ shown in Figure 2.1. Since the trigonometric system $\left\{\left(\sqrt{2\pi}\right)^{-1} e^{int}\right\}$, is an orthonormal basis for the Hilbert space $L^2[-\pi,\pi]$, we can represent f by its Fourier expansion

$$f(t) = \sum_{n\in\mathbb{Z}} c_n \frac{1}{\sqrt{2\pi}} e^{int}, \tag{2.1.3}$$

where the Fourier coefficients c_n's are computed via the inner products,

$$c_n = \frac{1}{\sqrt{2\pi}} \int_{-\pi}^{\pi} f e^{-int} dt.$$

The representation in (2.1.3) gives a precise frequency analysis of the signal f, in the sense that since each basis function is exactly localized in the frequency domain at $\omega =$

n, the coefficients c_n readily reveal the presence or absence of these frequencies in the signal. However, since each basis element has constant magnitude $\left(= \left(\sqrt{2\pi}\right)^{-1}\right)$ over the entire interval $[-\pi, \pi]$, the coefficients are obtained by integrating contributions of the corresponding frequencies with equal weighting over the entire time span. Hence the c_n's cannot readily reveal the fact that the signal is mostly flat and that high frequency components are localized to a short time interval. It is the need to analyze

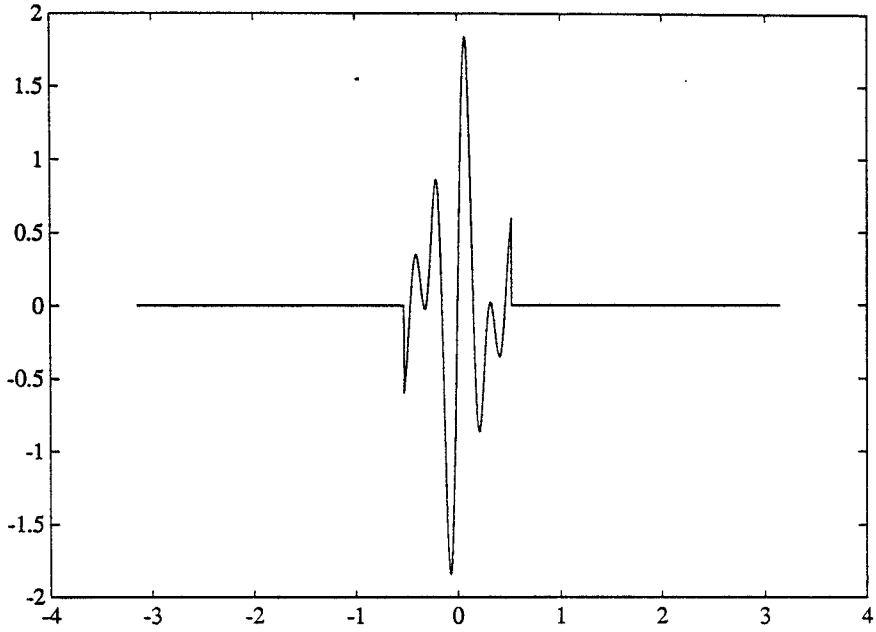

Figure 2.1: Example of signal with time-varying frequency content.

such signals with time-varying frequency content which has led to the study of function decompositions which naturally capture this behavior. Such decompositions call for 'basis' functions which are themselves well-localized in both time and frequency. We refer to such decompositions as *time-frequency localized representations.*

The short-time (or windowed) Fourier transform (STFT) was developed as one means of obtaining such a time-frequency localized representation. The STFT involves multiplying a signal f by a window function g and then computing the Fourier coefficients of the resulting product fg. Usually the window function g is chosen to be either compactly supported or at least rapidly decaying. Hence if the window function g is centered at $x = 0$, the Fourier coefficients of fg give a picture of the frequency content of f locally in time near $x = 0$. Further analysis of the signal may then be per-

formed by shifting the window function in time and once again computing the Fourier coefficients of f multiplied by the shifted window function $g(x - x_0)$. Repeating this process, results in a doubly indexed set of coefficients,

$$c_{m,n}(f) = \int_{\mathbb{R}} f(x)g(x - nx_0)e^{-im\omega_0 x}dx, \quad m, n \in \mathbb{Z}. \tag{2.1.4}$$

which provide a frequency analysis of f over different (localized) regions of time. A question that naturally arises regarding the STFT is; do the coefficients $\{c_{m,n}(f)\}$ provide a complete and 'stable' representation of the original signal f. As we will see in Section 2.2.4, this question may be addressed using the theory of *frames*. Gabor in [Gab46] proposed a transform of the form in (2.1.4) for use in data transmission using a Gaussian window function g. Gabor originally proposed this transform with $x_0\omega_0 = 2\pi$, which in fact results in unstable reconstructions (c.f. [Dau90]).

Remark: Here we refer to the coefficient sequence $\{c_{m,n}(f)\}$, as a *complete* representation of f, if f, can be reconstructed from the sequence. If furthermore, the reconstruction of f, is via a bounded operator, we refer to the representation as *stable*.

2.2 Wavelet Transforms

2.2.1 Weyl-Heisenberg Wavelets and the Windowed Fourier Transform

From another viewpoint, the coefficients $\{c_{m,n}\}$ in the windowed Fourier transform (2.1.4), are obtained via the $L^2(\mathbb{R})$ inner products of f with a sequence of functions $\{g_{m,n}\}$ which are generated via modulations and translations of a single function g. If we define the modulation and translation operators E_a and T_b on $L^2(\mathbb{R})$ respectively by,

$$\begin{aligned}(E_a f)(x) &= e^{iax} f(x) \\ (T_b f)(x) &= f(x - b),\end{aligned}$$

then we have

$$g_{m,n}(x) = (E_{m\omega_0} T_{nx_0} \overline{g})(x) = e^{im\omega_0} \overline{g(x - nx_0)}.$$

The sequence $g_{m,n}$ thus defined can be regarded as samples on a discrete sublattice of time-frequency space of the functions

$$g^{(p,q)} = (E_p T_q \overline{g})(x) = e^{ipx} \overline{g(x - q)},$$

where p and q are now continuous variables in $\mathbb{R}$. An important property of the functions $g^{(p,q)}$ is the *resolution of the identity* expressed in

$$\int \int \left| \left\langle f, g^{(p,q)} \right\rangle \right|^2 dpdq = 2\pi \|g\|^2 \|f\|^2.$$

The resolution of the identity implies that given the function,

$$(\Phi f)(p,q) = \left\langle f, g^{(p,q)} \right\rangle \in \mathrm{L}^2(\mathbb{R}^2) \ , \tag{2.2.5}$$

we can recover f via the reconstruction formula,

$$f = \frac{1}{2\pi} \int \int \left\langle f, g^{(p,q)} \right\rangle g^{(p,q)} dpdq. \tag{2.2.6}$$

The mapping $\Phi : \mathrm{L}^2(\mathbb{R}) \rightarrow \mathrm{L}^2(\mathbb{R}^2)$ as defined in (2.2.5) is often referred to as the continuous *Weyl-Heisenberg wavelet transform.* The resolution of the identity tells us that Φ is an isometric mapping up to a constant factor from $\mathrm{L}^2(\mathbb{R})$ to $\mathrm{L}^2(\mathbb{R}^2)$. And the reconstruction formula (2.2.6) defines for us the inverse transform.

Remark: The name Weyl-Heisenberg is used in reference to the fact that the operations of modulation and translation arise via the action of the left-regular representation of the Weyl-Heisenberg group on $\mathrm{L}^2(\mathbb{R})$. Affine wavelet transforms which we introduce in the next section are also associated with the representation of a Lie group on $\mathrm{L}^2(\mathbb{R})$, namely the affine (or $ax + b$) group.

Clearly the continuous Weyl-Heisenberg wavelet transform $(\Phi f)(p,q) = \left\langle f, g^{(p,q)} \right\rangle$ is a complete and 'stable' representation of any function $f \in \mathrm{L}^2(\mathbb{R})$. Consider now

the case where instead of allowing p and q to vary continuously, we select a discrete lattice $\{(p_n, q_n)\}$, and define the mapping Φ_d on $\mathrm{L}^2(\mathbb{R})$ by

$$\Phi_d f = \left\{ \left\langle f, g^{(p_n,q_n)} \right\rangle \right\}. \tag{2.2.7}$$

In this case the mapping Φ_d is known as the *discrete Weyl-Heisenberg wavelet transform.* Thus the STFT can now be viewed as a discrete Weyl-Heisenberg wavelet transform. Of course there remains the question of whether knowledge of the sequence $\left\{ \left\langle f, g^{(p_n,q_n)} \right\rangle \right\}$ is sufficient to recover the function f in a stable manner. As we will see in Section 2.2.3 the answer to these questions rely on selection of the discrete lattice $\{(p_n, q_n)\}$ such that the sequence of functions $\{g^{p_n,q_n}\}$ forms a *frame* for $\mathrm{L}^2(\mathbb{R})$.

2.2.2 Affine Wavelet Transforms

Modulations and translations as described in the last section are not the only means of generating a family of time-frequency localized functions from a single suitable *analyzing* function. Let us consider instead the actions of dilation and translation provided by the left-regular representation of the affine $(ax+b)$ group on $\mathrm{L}^2(\mathbb{R})$. Let D_a denote the dilation operator on $\mathrm{L}^2(\mathbb{R})$ defined by ,

$$(D_a f)(x) = a^{1/2} f(ax), \quad a \neq 0,$$

and define

$$h^{(a,b)}(x) = (D_a T_b h)(x) = a^{1/2} h(ax - b).$$

In the Weyl-Heisenberg case, there were no restrictions placed on the analyzing function in deriving the resolution of the identity. In the affine case however, we are forced to consider only analyzing functions h, which satisfy the following *admissibility* condition,

$$C_h = \int_{\mathbb{R}} \frac{\left|\widehat{h}(\omega)\right|^2}{|\omega|} d\omega < \infty. \tag{2.2.8}$$

Any $h \in \mathrm{L}^2(\mathbb{R})$ satisfying the admissibility condition (2.2.8), is called an *admissible analyzing wavelet* (c.f. [HW89, Dau90]).

Remark: Note that for any function h with sufficient decay at ∞, the admissibility condition is equivalent to requiring that $\int h(x)dx = 0$.

Given an admissible analyzing wavelet $h \in \mathrm{L}^2(\mathbb{R})$, there exists once again a resolution of the identity which may be expressed as

$$\langle f, g\rangle = \frac{1}{C_h}\int\int \left\langle f, h^{(a,b)}\right\rangle \left\langle h^{(a,b)}, g\right\rangle \frac{dadb}{a^2},$$

for all $f, g \in \mathrm{L}^2(\mathbb{R})$. Analogous to the Weyl-Heisenberg case, we can define an operator $W : \mathrm{L}^2(\mathbb{R}) \rightarrow \mathrm{L}^2(\mathbb{R}^2)$ by,

$$(Wf)(a,b) = \left\langle f, h^{(a,b)}\right\rangle. \tag{2.2.9}$$

The mapping W defined in (2.2.9) is called the *continuous (affine) wavelet transform*, and furthermore the resolution of the identity in this case gives the following reconstruction formula,

$$f = \frac{1}{C_h}\int\int \left\langle f, h^{(a,b)}\right\rangle h^{(a,b)} \frac{dadb}{a^2}. \tag{2.2.10}$$

Remark: Note that in Equation (2.2.10) the measure used for integration is now $a^{-2}dadb$.

Once again as in the Weyl-Heisenberg case we can consider a discrete lattice $\{a_n, b_n\}$ and define the corresponding *discrete wavelet transform* W_d on $\mathrm{L}^2(\mathbb{R})$ by,

$$W_d f = \left\{\left\langle f, h^{(a_n,b_n)}\right\rangle\right\}. \tag{2.2.11}$$

Here also we need to ask the questions regarding completeness and stability of the sequence $\left\{\left\langle f, h^{(a_n,b_n)}\right\rangle\right\}$.

2.2.3 Bases and Frames in Hilbert Spaces

By definition, an orthonormal basis for a separable Hilbert space $\mathcal{H}$ is a sequence $\{h_n\} \subset \mathcal{H}$ of normalized ($\|\cdot\| = 1$) vectors, which is complete in the sense that the closed linear span of $\{h_n\}$ is dense in $\mathcal{H}$, and furthermore the vectors are mutually orthogonal, i.e.

$$\langle h_n, h_m\rangle = \delta_{m,n}.$$

A key property of an orthonormal basis, known as Parseval's identity, is that the sequence of (Fourier) coefficients obtained via inner-products of $f \in \mathcal{H}$ and the basis elements h_n is such that,

$$\sum_n |\langle f, h_n \rangle|^2 = \|f\|^2_{\mathcal{H}}.$$

Hence the sequence of Fourier coefficients with respect to an orthonormal basis form a square-summable sequence. Furthermore by the Riesz-Fischer theorem we know that every square-summable sequence may be obtained in this manner. Parseval's identity together with the Riesz-Fischer theorem shows that the operator $\Gamma : \mathrm{L}^2(\mathbb{R}) \rightarrow \ell^2(\mathbb{Z}^2)$, $\Gamma : f \mapsto \{\langle f, h_n \rangle\}$ is a unitary operator. Hence, given an orthonormal basis $\{h_n\}$ for a Hilbert space $\mathcal{H}$, we have the following Fourier expansion of any $f \in \mathcal{H}$,

$$f = \sum_n \langle f, h_n \rangle \, h_n. \tag{2.2.12}$$

Thus for an orthonormal basis $\{h_n\}$, the sequence of Fourier coefficients $\{\langle f, h_n \rangle\}$ is a complete and stable representation of f.

Orthonormal bases are not the only sequences with this property. If we relax the requirement of orthogonality and normalization, while retaining the weaker property of linear independence, we can consider sequences which are know as *Riesz bases* (c.f [You80]).

Definition 2.3 *A sequence of vectors $\{h_n\} \subset \mathcal{H}$ is called a Riesz basis if the sequence is complete in $\mathcal{H}$ and there exist two constants $0 < C_1 \leq C_2 < \infty$, such that for arbitrary positive m and arbitrary scalars $\{a_1, \ldots, a_n\}$,*

$$C_1 \sum_{n=1}^{m} |a_n|^2 \leq \| \sum_{n=1}^{m} a_n h_n \|^2 \leq C_2 \sum_{n=1}^{m} |a_n|^2 .$$

Equivalently,

(1) The vectors $\{h_n\}$ are linearly independent and,

(2) There exist constants $0 < A \leq B < \infty$ such that for any $f \in \mathcal{H}$,

$$A\|f\|^2 \leq \sum |\langle f. h_n \rangle|^2 \leq B\|f\|^2.$$

Given a Riesz basis $\{h_n\}$ for a Hilbert space $\mathcal{H}$, the Hahn-Banach theorem asserts the existence of a unique biorthogonal sequence $\{g_n\}$ ($\langle h_n, g_m \rangle = \delta_{m,n}$) such that for every $f \in \mathcal{H}$,

$$f = \sum_n \langle f, h_n \rangle \, g_n = \sum_n \langle f, g_n \rangle \, h_n.$$

Hence in the case of Riesz bases as well, the sequence $\{\langle f, h_n \rangle\}$ is a complete and stable representation of any $f \in \mathcal{H}$.

The notion of *frames* is yet another level of generalization of orthonormal bases where even linear independence can be sacrificed while still retaining the properties of completeness and stability. Note that in sacrificing linear independence, strictly speaking, we will not even have a (Schauder) basis.

Frames, which were first introduced by Duffin and Schaeffer in [DS52], are defined as follows.

Definition 2.4 *Given a Hilbert space $\mathcal{H}$, a sequence of vectors $\{h_n\}_{n=-\infty}^{\infty} \subset \mathcal{H}$, is called a frame if there exist constants $A > 0$ and $B < \infty$ such that*

$$A\|f\|^2 \leq \sum_n | < f, h_n > |^2 \leq B\|f\|^2, \tag{2.2.13}$$

for every $f \in \mathcal{H}$. A and B are called the frame bounds.

Remarks:

(a) A frame $\{h_n\}$ with frame bounds $A = B$ is called a *tight frame.*

(b) A frame $\{h_n\}$, which ceases to be a frame upon removal of a single element, is called an *exact frame.*

(c) Every orthonormal basis is a tight exact frame with $A = B = 1$.

(d) A tight frame of unit-norm vectors for which $A = B = 1$ is an orthonormal basis.

Given a frame $\{h_n\}$ in the Hilbert space $\mathcal{H}$, with frame bounds A and B, define the operator $\Gamma : \mathrm{L}^2(\mathbb{R}) \rightarrow \ell^2$ by

$$\Gamma f = \{\langle f, h_n \rangle\}. \tag{2.2.14}$$

Remark: Note that in general due to the redundancy allowed by not requiring linear independence, the range of the operator Γ will not be all of ℓ^2, but instead a closed proper subspace of ℓ^2. In Section 2.3.1 we describe how this redundancy is useful in providing 'robust' representations. Here robustness refers to the fact that the reconstruction error induced by perturbations of the coefficients $\{\langle f, h_n \rangle\}$, is diminished due to a projection operation onto the range of Γ.

Definition 2.5 *Given a frame $\{h_n\}$ for a Hilbert space $\mathcal{H}$, the frame operator $S : \mathcal{H} \rightarrow \mathcal{H}$ is defined as $S = \Gamma^*\Gamma$, where Γ^* is the adjoint of Γ. Thus for any $f \in \mathcal{H}$,*

$$Sf = \sum_n < f, h_n > h_n. \tag{2.2.15}$$

Some properties of the frame operator which follow from the definition of a frame are collected together in the following theorem.

Theorem 2.3 ([DS52]) *(1) S is a bounded linear operator with $AI \leq S \leq BI$, where I is the identity operator in $\mathcal{H}$.*

(2) S is an invertible operator with $B^{-1}I \leq S^{-1} \leq A^{-1}I$.

(3) Since $AI \leq S \leq BI$ implies that $\|I - \frac{2}{A+B}S\| \leq 1$, S^{-1} can be computed via the Neumann series,

$$S^{-1}g = \frac{2}{A+B} \sum_{k=0}^{\infty} \left(I - \frac{2}{A+B}S\right)^k g. \tag{2.2.16}$$

(4) The sequence $\{S^{-1}h_n\}$ is also a frame, called the dual frame, *with frame bounds B^{-1} and A^{-1}.*

By the above properties of the frame operator, we have the following representation theorem for $\mathcal{H}$ with respect to a frame or associated dual frame.

Theorem 2.4 ([DS52]) *Given any $f \in \mathcal{H}$, f can be decomposed in terms of the frame (or dual frame) elements as*

$$f = \sum < f, S^{-1}h_n > h_n = \sum < f, h_n > S^{-1}h_n. \tag{2.2.17}$$

In general frame representations are not unique, i.e. it is possible that that sequence $\{c_n\} = \{\langle f, S^{-1}h_n \rangle\}$ is not the only sequence of coefficients such that $f = \sum c_n h_n$. However the following theorem shows that any other sequence of expansion coefficients must be related to the sequence $\{\langle f, S^{-1}h_n \rangle\}$ via a *Pythagorean* relation.

Theorem 2.5 ([DS52]) *Given $f \in \mathcal{H}$, if there exists another sequence of coefficients $\{a_n\}$ (other than the sequence $\{< f, S^{-1}h_n >\}$) such that $f = \sum a_n h_n$, then the a_n's are related to the coefficients given in (2.2.17) by the formula,*

$$\sum |a_n|^2 = \sum | < f, S^{-1}h_n > |^2 + \sum | < f, S^{-1}h_n > - a_n|^2. \tag{2.2.18}$$

Remark: Note that by Theorem 2.5, the sequence of coefficients obtained via the inverse frame operator is optimal in the sense of minimum ℓ^2 norm.

2.2.4 Discrete Wavelet Transforms and Frames

Armed with the theory of frames, it is now possible to discuss completeness and stability of the discrete wavelet transforms Φ_d and W_d defined in Section 2.2. Simply stated, it is necessary to select the discrete lattices $\{(p_n, q_n)\}$ and $\{(a_n, b_n)\}$, in such a manner that the sequences $\left\{g^{(p_n,q_n)}\right\}$ and $\left\{h^{(a_n,b_n)}\right\}$ respectively form frames for $\mathrm{L}^2(\mathbb{R})$. As this dissertation deals almost exclusively with affine wavelets, we restrict discussion to the affine case and make some remarks regarding discrete Weyl-Heisenberg

wavelets at the end of this section. In the affine case we restrict attention to regular discrete lattices in which discretization of dilations is treated exponentially. That is, we consider discrete lattices of the form $\{(a_0^m, nb_0)\}_{m,n\in\mathbb{Z}}$ for fixed constants $a_0 > 1$ and $b_0 > 0$. We note that it is not necessary to restrict to lattices of this form and in general even the requirement of regular lattices is not necessary. We refer readers interested in more general discretizations to [FG] in which frames are constructed by utilizing the underlying group structure.

Given $a_0 > 1$, $b_0 > 0$, and an admissible analyzing wavelet $\psi \in \mathrm{L}^2(\mathbb{R})$ define,

$$\psi_{m,n}(x) = (D_{a_0^m} T_{nb_0} \psi)(x) = a_0^{m/2} \psi(a_0^m x - nb_0). \tag{2.2.19}$$

Daubechies in [Dau90] studied the problem of constructing frames of the form $\{\psi_{m,n}\}$. Under very mild additional hypotheses on the analyzing wavelet ψ, it is possible to determine values of the dilation stepsize a_0 and translation stepsize b_0 such that the family of functions $\{\psi_{m,n}\}$ is a frame for $\mathrm{L}^2(\mathbb{R})$. In this case we say that (ψ, a_0, b_0) generates an affine frame for $\mathrm{L}^2(\mathbb{R})$. Given an admissible mother wavelet $\psi \in \mathrm{L}^2(\mathbb{R})$, the following theorem by Daubechies [Dau90] can be used to numerically determine values of the parameters a_0 and b_0 for which (ψ, a_0, b_0) generates an affine frame for $\mathrm{L}^2(\mathbb{R})$.

Theorem 2.6 ([Dau90]) *Let $h \in \mathrm{L}^2(\mathbb{R})$ and $a > 1$ be such that:*

(1)

$$m(h; a) = \operatorname{ess} \inf_{|\omega|\in[1,a]} \sum_m |\widehat{h}(a^m\omega)|^2 > 0 \tag{2.2.20}$$

(2)

$$M(h; a) = \operatorname{ess} \sup_{|\omega|\in[1,a]} \sum_m |\widehat{h}(a^m\omega)|^2 < \infty \tag{2.2.21}$$

(3)

$$\lim_{b\to 0} 2 \sum_{k=1}^{\infty} \beta(2\pi k/b)^{1/2} \beta(-2\pi k/b)^{1/2} = 0, \tag{2.2.22}$$

where

$$\beta(s) = \operatorname{ess} \sup_{|\omega|\in[1,a]} \sum_m |\widehat{h}(a^m\omega)||\widehat{h}(a^m\omega - s)|.$$

Then there exists $B_c > 0$ such that (h, a, b) generates an affine frame for each $0 < b < B_c$.

Proof: See Appendix A

The following is a useful corollary of the above theorem.

Corollary 2.1 ([Dau90]) *If $h \in \mathrm{L}^2(\mathbb{R})$ and $a > 1$ satisfy the hypotheses of Theorem 2.6 then,*

$$B_c \geq b_c = \inf\{b|\ m(h;a) - 2\sum_{k=1}^{\infty} \beta(2\pi k/b)^{1/2}\beta(-2\pi k/b)^{1/2} \leq 0\} \tag{2.2.23}$$

and for $0 < b < b_c$, the frame bounds A and B can be estimated as,

$$\begin{aligned} A &\geq b^{-1}\left(m(h;a) - 2\sum_{k=1}^{\infty} \beta(2\pi k/b)^{1/2}\beta(-2\pi k/b)^{1/2}\right) \\ B &\leq b^{-1}\left(M(h;a) + 2\sum_{k=1}^{\infty} \beta(2\pi k/b)^{1/2}\beta(-2\pi k/b)^{1/2}\right) \end{aligned} \tag{2.2.24}$$

Given an affine frame $\{\psi_{m,n}\}$ for $\mathrm{L}^2(\mathbb{R})$, it is clear that the operator Γ defined in Section 2.2.3 is precisely the discrete wavelet transform operator W_d (see (2.2.11)). Hence by the frame property, W_d is a bounded operator from $\mathrm{L}^2(\mathbb{R})$ to $\ell^2(\mathbb{Z}^2)$. Furthermore, using the frame operator $S = W_d^* W_d$, we get the following *wavelet decomposition* of $\mathrm{L}^2(\mathbb{R})$:

$$f = \sum_{m\in\mathbb{Z}}\sum_{n\in\mathbb{Z}} \left\langle f, S^{-1}\psi_{m,n}\right\rangle \psi_{m,n}, \tag{2.2.25}$$

and the corresponding *dual frame decomposition*,

$$f = \sum_{m\in\mathbb{Z}}\sum_{n\in\mathbb{Z}} \langle f, \psi_{m,n}\rangle\, S^{-1}\psi_{m,n}. \tag{2.2.26}$$

Since the frame property assures that the frame operator S is bounded and has bounded inverse, we see that in the case where $\psi_{m,n}$ is a frame, $W_d f$ is a complete and stable representation of any $f \in \mathrm{L}^2(\mathbb{R})$.

Remarks: Our discussion in this section has been limited to the general setting of frames of affine wavelets. It is however possible to construct orthonormal bases of affine wavelets (c.f. [Dau88a]) and also biorthogonal systems (Riesz bases) of affine wavelets (c.f [Chu92]). However the constructions of orthogonal or even biorthogonal wavelets are too restrictive for the applications considered in this dissertation.

Remarks on Discrete Weyl-Heisenberg Wavelets

In the Weyl-Heisenberg case as well, a theorem similar to Theorem 2.6 is given in [Dau90]. The regular discrete lattices for the Weyl-Heisenberg wavelets are such that both modulations and translations are treated linearly; i.e. lattices of the form $\{(mp_0, nq_0)\}$. A point to be made regarding Weyl-Heisenberg wavelets is that it is natural to define the time-frequency density in terms of the product p_0q_0. Furthermore, there exists in this case a critical density, such that the family of functions $\left\{g^{(mp_0,nq_0)}\right\}$ can only form a frame if the product p_0q_0, is less than or equal to this critical density. For p_0q_0 greater than the critical density, $\left\{g^{(mp_0,nq_0)}\right\}$, will be incomplete. In contrast to this, there exists no such critical density in the affine case, and in fact it is not possible to define an equivalent notion of density (c.f [Dau90]).

2.2.5 Time-Frequency Localization Properties of Wavelets

Perhaps the most useful property of wavelet decompositions, is the property of time-frequency localization. To illustrate the manner in which time-frequency localization arises in affine wavelets, recall the admissibility condition (2.2.8) which the analyzing wavelet must satisfy. Satisfying (2.2.8) imposes the requirement that the Fourier transform of the analyzing wavelet ψ must have a zero at $\omega = 0$, i.e. $\widehat{\psi}(0) = 0$. Furthermore, the admissibility condition requires that $\left|\widehat{\psi}(\omega)\right|^2 \to 0$, faster than ω. In addition, given smoothness assumptions on $\psi \in \mathrm{L}^2(\mathbb{R})$, we know that $\widehat{\psi}(\omega) \to 0$ as $\omega \to \infty$. Thus, an admissible analyzing wavelet must approximately mimic the behavior of a 'bandpass' function. The required decay in the time domain approximately localizes the analyzing wavelet in time. In general of course there are only moderate

constraints on the decay at infinity in both the time and frequency domains. However, within the constraints imposed by Heisenberg's inequality, there is still a great deal of freedom in the choice of analyzing wavelets with reasonably fast decay in both time and frequency. Since an affine frame is constructed via translations and dilations of the analyzing wavelet ψ, we need to look at how these operations affect the time-frequency concentration of ψ . Assume the analyzing wavelet ψ is concentrated on the rectangle of time-frequency defined by,

$$\begin{aligned} \mathcal{Q}_{0,0}(\psi) &= [x_0(\psi), x_1(\psi)] \times [\omega_0(\psi), \omega_1(\psi)] \\ &= R(\psi) \times \Omega(\psi). \end{aligned}$$

Recalling the dilation property of the Fourier transform,

$$f(ax) \xrightarrow{\mathcal{F}} a^{-1} \widehat{f}(a^{-1}\omega),$$

we see that the translates and dilates $\psi_{m,n}$ are concentrated on time-frequency rectangles defined by,

$$\begin{aligned} \mathcal{Q}_{m,n}(\psi) &= [a_0^{-m}(x_0(\psi) + nb_0), a_0^{-m}(x_1(\psi) + nb_0)] \times [a_0^m \omega_0(\psi), a^m \omega_1(\psi)] \\ &= R(\psi_{m,n}) \times \Omega(\psi_{m,n}). \end{aligned}$$

Thus dilation shifts the frequency concentration of the wavelets on a logarithmic scale. For large values of m the frequency concentration is shifted to the higher frequencies and as m decreases, the frequency concentration shifts towards zero. This is illustrated by Figure 2.2, where we see that as m gets large, the function ψ gets narrower and thereby includes higher frequency components. Translation simply shifts the time concentration by steps proportional to $a_0^{-m} b_0$. The factor a_0^{-m}, appearing in the translation stepsize accommodates the dilations by keeping the translation steps small for large m (narrow functions), and larger for large m (wide functions).

Windowed Fourier Transforms vs. Affine Wavelets

There is an important distinction between the type of time-frequency localization arising in the Weyl-Heisenberg case and the type of time-frequency localization afforded

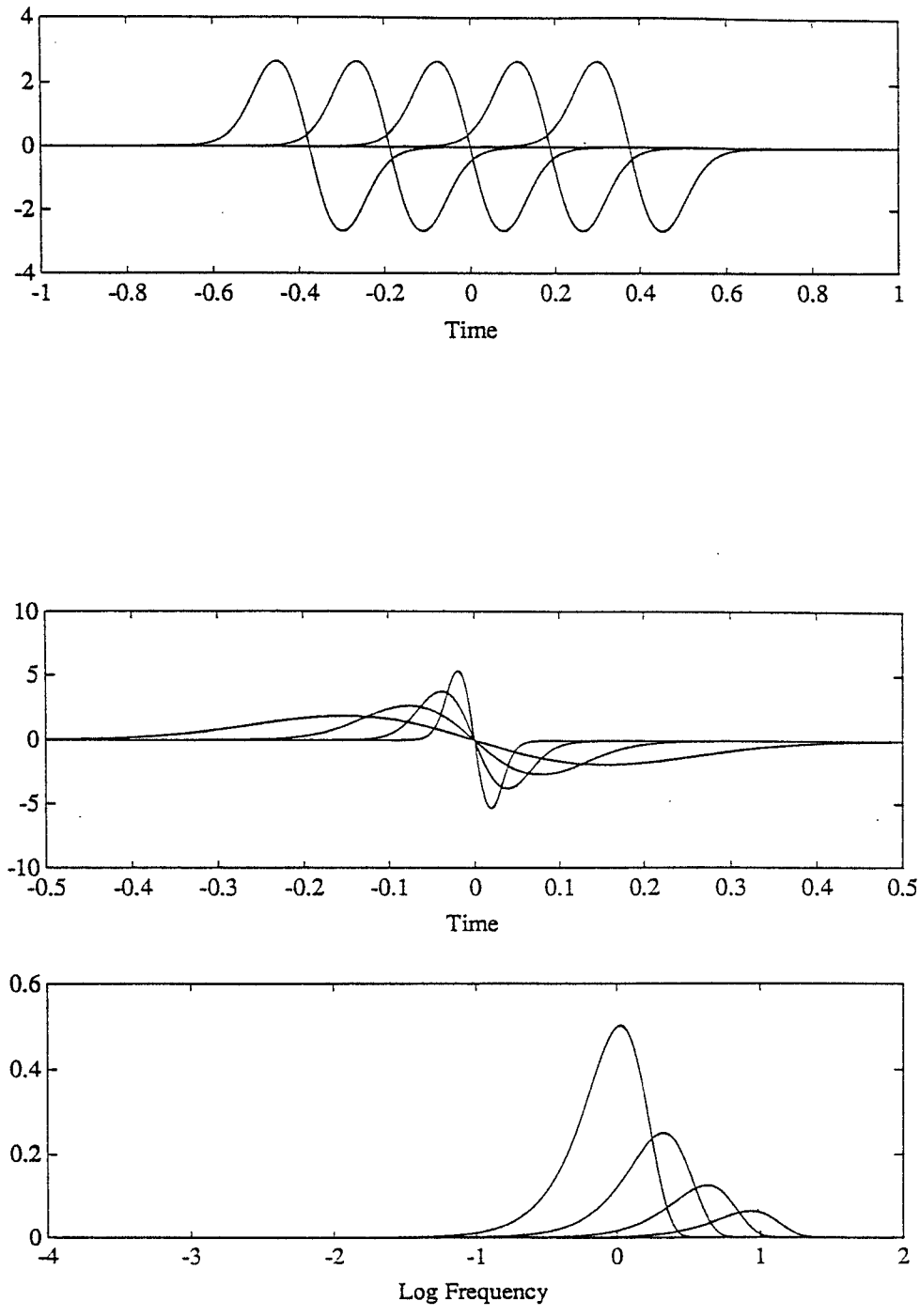

Figure 2.2: (a) Translations in the time domain. (b) The effect of dilations in the time domain (c) The effect of dilations in the frequency domain

by affine wavelets. In the Weyl-Heisenberg case the 'width' of the window function remains constant, and it is via the exponential modulation that higher frequencies are analyzed. Exponential modulation corresponds to a linear shift of the frequency concentration. Thus in the Weyl-Heisenberg case the extent of localization in time (and frequency) remains constant. In the affine case higher frequencies are analyzed using narrower functions. More precisely, the time concentration of the wavelet shrinks in size as m gets large. This feature is useful in 'zooming in ' on details of a signal. For instance in image analysis if one were trying to identify the location of an edge, it is necessary to be able to identify a high frequency component which is sharply localized in time. The trade-off is that in the frequency domain, the frequency concentration gets wider at higher frequencies. Simply stated affine wavelets allow us to resolve lower frequencies with greater accuracy than higher frequencies. In many applications this is a very natural phenomena. For example, processing of acoustic signals by the human cochlea can be modeled in this manner (see [YWS92]).

2.3 Finite Wavelet Approximations

In practice it is necessary to consider only finitely many terms in the wavelet decomposition. This leads to the question of how well a given function can be represented by truncations of a wavelet decomposition. In general, arbitrary truncations can result in arbitrarily large errors. However in the case where the functions of interest are well-localized in time-frequency, it is possible to bound the approximation error associated with particular types of truncations. Daubechies in [Dau90] examined this problem, and derived upper bounds on the approximation error for a particularly important class of truncations. Suppose we are interested in functions f which are essentially time-limited to $[-T,T]$ and essentially band-limited to the frequency range $[\Omega_0,\Omega_1]\bigcup[-\Omega_0,-\Omega_1]$. That is, we assume that the functions f of interest to us are such that,

$$\|(\mathbb{1}-Q_T)f\|<\epsilon \quad \text{and} \quad \|(\mathbb{1}-(P_{\Omega_1}-P_{\Omega_0}))f\|<\epsilon. \tag{2.3.27}$$

Given an affine frame $\{\psi_{m,n}\}$ where the analyzing wavelet is itself well localized in time-frequency, we can ask the following question: for any given $\epsilon > 0$, is there a finite subset $B_\epsilon(T, \Omega_0, \Omega_1) \subset \mathbb{Z}^2$ such that the error in approximating f by

$$\tilde{f} = \sum_{(m,n)\in B_\epsilon(T,\Omega_0,\Omega_1)} \langle f, \psi_{m,n}\rangle \, S^{-1}\psi_{m,n} \tag{2.3.28}$$

is less than $\epsilon\|f\|$. The answer to this question was provided by Daubechies in [Dau90]. For a function f which is essentially concentrated (as defined by Equation (2.3.27)) on the rectangle

$$\mathcal{Q}_f = [-T, T] \times [\Omega_0, \Omega_1],$$

in time-frequency, it is possible to construct an enlarged box containing $\mathcal{Q}_f$ such that by including in $B_\epsilon(T, \Omega_0, \Omega_1)$ all indices (m, n) corresponding to wavelets $\psi_{m,n}$ with concentration centers in this enlarged box, the error in approximating f by $\tilde{f}$ (2.3.28) is bounded above by ϵ. A precise statement of this result is in the following theorem.

Theorem 2.7 ([Dau90]) *Let $\{h_{m,n}\}$ be a frame for $\mathrm{L}^2(\mathbb{R})$ with frame bounds A and B, and associated dual frame $\{S^{-1}h_{m,n}\}$. Assume that*

$$\left|\widehat{h}(\omega)\right| \leq C\,|\omega|^{\beta}\,(1+\omega^2)^{-(\alpha+\beta)/2},$$

with $\beta > 0$ and $\alpha > 1$. Also assume that for some $\gamma > 1/2$,

$$\int (1+x^2)^{\gamma}\,|h(x)|^2 < \infty.$$

Now if we choose $T > 0$, and $0 < \Omega_0 < \Omega_1$, then for any $\epsilon > 0$, there exists a finite subset $B_\epsilon(T, \Omega_0, \Omega_1) \subset \mathbb{Z}^2$, such that for all $f \in \mathrm{L}^2(\mathbb{R})$,

$$\begin{aligned} &\|f - \sum_{(m,n)\in B_\epsilon(T,\Omega_0,\Omega_1)} \langle f, h_{m,n}\rangle \, S^{-1}h_{m,n}\| \\ &\quad \leq \left(\frac{B}{A}\right)^{1/2} [\|(\mathbb{I} - Q_T)f\| + \|(\mathbb{I} - P_{\Omega_1} + P_{\Omega_0})f\| + \epsilon\|f\|] \end{aligned}$$

Remarks: The error bounds of Theorem 2.7, are derived using the dual frame reconstruction formula and cannot trivially be extended to the frame reconstruction formula. This is primarily because in general the dual frame elements will not be generated as translates and dilates of a single function and may have localization properties different from those of the original wavelets. However we note that in the case where the frame is tight ($A = B$), Theorem 2.7 as stated above is also applicable for the frame reconstruction formula since in this case, the frame operator is a multiple of the identity. In particular, for a tight frame $\langle f, S^{-1}h_{m,n}\rangle = A^{-1}\langle f, h_{m,n}\rangle$.

2.3.1 Robustness of Frame Representations

As noted in [Dau90], time-frequency localized frame representations are in general quite robust against perturbations of the coefficient values. This insensitivity can be attributed to both time-frequency localization and the redundancy of frames. Time-frequency localization helps by localizing errors due to particular coefficients; i.e. in any given region of time-frequency, errors in the coefficient values cannot all contribute equally to errors in the frame representation.

Robustness due to redundancy of the frame can be best described in terms of the range of the operator Γ defined in Section 2.2.3. As noted earlier (c.f. remark following Equation 2.2.14), the closed range of Γ, for a frame whose elements are not linearly independent, is a proper subspace of $\ell^2(\mathbb{Z})$. Therefore if the frame reconstruction formula (Theorem 2.4) is applied to vectors $c \in \ell^2$, which are not necessarily in the range of Γ, i.e. if we consider the formula,

$$\sum_n c_n S^{-1}h_n,$$

then this consists of: (1) a projection of ℓ^2onto Ran Γ, and (2) inverting Γ on its range. Since errors in the coefficients will in general 'live' on all of ℓ^2, application of the reconstruction formula will reduce the norm of error component due to the projection onto Ran Γ. The greater the redundancy of the frame, the smaller the range of Γ. Hence for very redundant frames, this reduction in the effects of errors is

more pronounced.

The robustness of redundant frame representations is a very useful property when dealing with numerical computation of wavelet decompositions, as the effects of numerical errors are thus reduced.

2.4 Computing Wavelet Frame Decompositions

In principle, given an affine frame $\{\psi_{m,n}\}$, and a function $f \in \mathrm{L}^2(\mathbb{R})$, the coefficients,

$$c_{m,n}(f) = \left\langle f, S^{-1}\psi_{m,n} \right\rangle$$

may be computed by first computing the elements of the dual frame $\{S^{-1}\psi_{m,n}\}$ using the Neumann series expansion for the inverse frame operator S^{-1} and then computing the inner products of f with elements of the dual frame. However in practice, this may prove to be an extremely cumbersome computation, especially in cases where the frame is not close to being a tight frame ($B/A = 1$). By the frame property, we know that

$$\|\mathbb{I} - \frac{2}{A+B}S\| \leq \frac{B/A-1}{B/A+1}.$$

Hence the rate of convergence of the Neumann series (2.2.16), is governed by how 'snug' the frame is (i.e. by how close B/A is to 1).

Computation via Sampled Convolutions

In the case of a tight frame, the computation is greatly simplified since in this case $S^{-1}\psi_{m,n} = A^{-1}\psi_{m,n}$. Furthermore the inner products $\langle f, \psi_{m,n}\rangle$ are easily computed by noting that these are simply regular samples of convolutions. More precisely,

$$\begin{aligned} \langle f, \psi_{m,n}\rangle &= \int_{\mathbb{R}} f(x) a_0^{m/2} \overline{\psi(a_0^m x - nb_0)} dx \\ &= \left(f * \overline{\psi_{m,0}^-}\right)(nb_0), \end{aligned}$$

where $\psi_{m,0}^-$ denotes the reflection of $\psi_{m,0}$ about the origin, i.e. $\psi_{m,0}^-(x) = \psi_{m,0}(-x)$. Hence using the convolution theorem for Fourier transforms, $\{\langle f, \psi_{m,n}\rangle\}$ is easily computed.

The above formulation may also be used to simplify computation in the case of frames which are not tight. This can be done by using the fact that the frame operator S (and therefore S^{-1}) is self-adjoint, to write,

$$\left\langle f, S^{-1}\psi_{m,n}\right\rangle = \left\langle S^{-1}f, \psi_{m,n}\right\rangle.$$

Thus the inverse frame operator series need only be applied once to compute $S^{-1}f$, and then the coefficients may be computed as samples of convolutions as described above.

Normal Equations

Expansions with respect to frames are in general not unique due to the lack of linear independence. It can be seen however, from Theorem 2.5 that among all possible expansion coefficients for a given function f, the coefficient sequence $c(f) = \{\langle f, S^{-1}\psi_{m,n}\rangle\}$ is optimal in the sense of minimum $\ell^2(\mathbb{Z}^2)$ norm. That is, if $\{\alpha_{m,n}\}$ is such that

$$f = \sum_m \sum_n \alpha_{m,n}\psi_{m,n}$$

then,

$$\sum_m \sum_n \left|\left\langle f, S^{-1}\psi_{m,n}\right\rangle\right|^2 \leq \sum_m \sum_n |\alpha_{m,n}|^2.$$

This property may be utilized to formulate the coefficient computation problem as a constrained optimization problem. Namely,

$$\begin{aligned} &\text{minimize } \sum_m \sum_n |\alpha_{m,n}|^2 \\ &\text{such that } f = \sum_m \sum_n \alpha_{m,n}\psi_{m,n}. \end{aligned}$$

Consider now the case of a finite wavelet approximation to f,

$$f \approx \tilde{f} = \sum_{(m,n)\in\mathcal{I}} \alpha_{m,n}\psi_{m,n}. \tag{2.4.29}$$

Let $\text{Span}\{h_n\}$ denote the closed linear span of the vectors $\{h_n\}$. It is clear that f can be represented exactly by the expansion in (2.4.29) *if and only if* $f \in$

Span$\{\psi_{mn},\ (m,n) \in \mathcal{I}\}$, where Span$\{h_n\}$, denotes the closed linear span of the vectors $\{h_n\}$. If $f \notin$ Span$\{\psi_{mn},\ (m,n) \in \mathcal{I}\}$ then the 'best'[1] approximation to f in terms of the finite subset of frame elements with indices in $\mathcal{I}$ is the projection of f onto Span$\{\psi_{mn},\ (m,n) \in \mathcal{I}\}$. In this case, we would like to compute the coefficients of expansion of the projection of f onto Span$\{\psi_{mn},\ (m,n) \in \mathcal{I}\}$. It can easily be shown that any finite number of vectors form a frame for their span (c.f. [Pat91]). In this case we can reformulate the optimization problem stated above as,

$$\begin{aligned} &\text{minimize} \sum_{(m,n)\in\mathcal{I}} |\alpha_{m,n}|^2 \\ &\text{such that} \\ &\|f - \sum_{(m,n)\in\mathcal{I}} \alpha_{m,n}\psi_{m,n}\|^2 = \min \|f - \sum_{(m,n)\in\mathcal{I}} \alpha_{m,n}\psi_{m,n}\|^2. \end{aligned} \tag{2.4.30}$$

The optimization problem defined by (2.4.30) is convex. Hence, one means of solving (2.4.30) is by direct optimization.

Consider now the *normal equations* associated with the problem of minimizing $\|f - \sum_{k=1}^{N} c_k h_k\|^2$. The normal equations are obtained via the first-order optimality condition,

$$\frac{\partial}{\partial c_k}\|f - \sum_{k=1}^{N} c_k h_k\|^2 = 0, \quad k = 1, \ldots, N,$$

and may be written as,

$$P\ C \ = \ W \tag{2.4.31}$$

where, P is the $N \times N$ matrix defined by,

$$P = [P_{kj}] = [\langle h_k, h_j \rangle], \tag{2.4.32}$$

$$W = [\langle f, h_1 \rangle, \ldots, \langle f, h_N \rangle]^T, \tag{2.4.33}$$

and $C = [c_1, \ldots, c_N]$ is the vector of coefficients.

[1] With respect to the $L^2(\mathbb{R})$ norm.

Suppose now that we are searching for the minimum norm solution to the normal equations (2.4.31). It is well-know that the Moore-Penrose generalized inverse $P^\dagger = (P^*P)^{-1}P^*$, generates the minimum norm solution to (2.4.31), as

$$C = P^\dagger W,$$

whenever the $(P^*P)^{-1}$, exists. In cases where the problem is very ill-conditioned, stabilizing techniques such as singular value decomposition may be used to compute the generalized inverse.

Thus the solution to the normal equations via the generalized inverse provide another means of computing the frame decomposition coefficients. For numerical solutions where we are dealing with discrete samples of the functions the inner products in the definition of the normal equations may be approximated by sums.

Remarks: In searching for the minimum norm sequence of coefficients as above, where only a finite number of coefficients are involved, technically we are no longer computing the coefficients $c_{m,n} = \langle f, S^{-1}\psi_{m,n}\rangle$ with respect to the original frame $\{\psi_{m,n}\}_{m,n\in\mathbb{Z}}$. In fact what we are doing is computing the frame expansion of the orthogonal projection of f onto $H = \text{Span}\{\psi_{mn},\ (m,n)\in\mathcal{I}\}$, with respect to the frame $\{\psi_{mn},\ (m,n)\in\mathcal{I}\}$, for H. Hence, in general the set of coefficients $\{c_k\}_{k=1}^N$ will not agree with the corresponding coefficients computed with respect to the infinite frame. In cases where the index set $\mathcal{I}$, is large and such that $\{\psi_{mn},\ (m,n)\in\mathcal{I}\}$, covers 'most' of the time-frequency concentration of f, the error between the two sets of coefficients will be small. The advantage to computing the coefficients with respect to the new (finite) frame is that in general the quality of approximation will be better than if a truncation of the infinite frame expansion were used (see Appendix C).

Chapter 3

Rational Wavelet Decompositions of Stable Linear Systems

In this chapter we study wavelet decompositions of the Hardy space $H^2(\Pi^+)$, (where Π^+ denotes the half-plane $\Re e\ s > 0$) via real-rational analyzing wavelets. The restriction of rationality of the analyzing wavelet leads us to consider affine frames for $H^2(\Pi^+)$. The space H^2 was in fact considered among the first investigations of continuous wavelet transforms [GM84]. With the recent development of multiresolution analyses and the resulting orthonormal bases of wavelets for $L^2(\mathbb{R})$, attention has shifted primarily to the study of wavelet transforms on $L^2(\mathbb{R})$. Our use of frames rather than orthonormal systems, is further motivated by recent results which have shown that there do not exist any 'nice' orthonormal wavelet bases for $H^2(\Pi^+)$ associated with a mutiresolution analysis. This result is discussed in further detail in Section 3.6.

Of particular interest here, are functions in $H^2(\Pi^+)$ arising as Laplace transforms of real-valued functions in $L^2(0,\infty)$, as these include transfer functions of stable, causal, linear time-invariant systems. We use the notation $H^2_{\mathbb{R}}(\Pi^+)$ for this class of

functions. In Section 3.3, it is shown that by starting with a real-rational analyzing wavelet and appropriately grouping terms in a wavelet decomposition, functions in $H^2_{\mathbb{R}}(\Pi^+)$ may be represented as infinite sums of time-frequency localized, real-rational functions of bounded McMillan degree. We refer to such representations as , *wavelet system* (WS) *decompositions* of $H^2_{\mathbb{R}}(\Pi^+)$. One of the main results of this chapter is Theorem 3.3, which shows the existence of such real-rational (WS) decompositions. A real-rational function in $H^2(\Pi^+)$ can of course be viewed as the transfer function of a stable, finite-dimensional, causal, linear time invariant system. Thus wavelet system decompositions are representations of (possibly infinite-dimensional) systems, as infinite parallel connections of time-frequency localized finite-dimensional systems. Such representations are useful in constructing finite-dimensional approximations to systems. In Section 3.5 we consider the problem of constructing a causal rational approximation to a causal nonrational transfer function by selecting a finite number of terms from the WS expansion. For dynamical systems with transfer functions which are well-localized in time-frequency, this approach can generate low-order approximants. Some aspect of WS decompositions, including minimal state-space realizations are investigated in 3.3.

3.1 Background on Hardy Spaces

In this section we review some basic properties of the Hardy spaces $H^p(\Pi^+)$ where $\Pi^+$is the right-half complex plane $\Re e\ \ s > 0$. For a more complete exposition of the properties of these spaces see [Hof88, Dur70, Gar81].

Definition 3.1 *Given a function F which is analytic in Π^+, F is said to belong to the class $H^p(\Pi^+)$, $0 < p < \infty$ if*

$$\sup_{x>0} \int_{-\infty}^{\infty} |F(x+iy)|^p \, dy < \infty. \tag{3.1.1}$$

A function F which is analytic in Π^+, is said to belong to class $H^\infty(\Pi^+)$if,

$$\sup_{x>0} |F(x+iy)| < \infty. \tag{3.1.2}$$

For $1 \leq p \leq \infty$, $\mathrm{H}^p(\Pi^+)$ is a Banach space with norm defined by (3.1.1) for $p < \infty$ and by (3.1.2) for $p = \infty$.

Some of the most basic properties of $\mathrm{H}^p(\Pi^+)$ are captured by the following theorem (c.f. [Hof88]).

Theorem 3.1 *Given $F \in \mathrm{H}^p(\Pi^+)$, the following are true:*

(1) The nontangential limit of F exists at almost every point on the imaginary axis.

(2) The boundary value function of F is in $L^p(\mathbb{R})$ and,

$$F(x+iy) = \frac{1}{\pi}\int_{\mathbb{R}} F(i\omega)\frac{x}{x^2+(y-\omega)^2}d\omega, \quad x > 0$$

(3) The functions $F_x(y) = F(x+iy)$ converge in L^p norm to $F(iy)$ as $x \to 0$.

Note: The boundary value function (c.f. [Gar81]) of $F \in \mathrm{H}^p(\Pi^+)$ is defined via the limit $F^*(i\omega)$, of $F(s)$ as $s \to i\omega$, nontangentially i.e.

$$F^*(i\omega) = \lim_{\Lambda_\alpha(i\omega)\ni s \to i\omega} F(s), \ \alpha > 0,$$

where for $\alpha > 0$, $\Lambda_\alpha(i\omega)$ is the cone defined by,

$$\Lambda_\alpha(i\omega) = \{s = x + iy \in \Pi^+ : |y-\omega| < \alpha x\}.$$

Of particular interest in the context this dissertation is the space $\mathrm{H}^2(\Pi^+)$. The space $\mathrm{H}^2(\Pi^+)$ is a Hilbert space with the inner product defined by,

$$\langle F, G\rangle_{H^2} = \int_{-\infty}^{\infty} F(i\omega)\overline{G(i\omega)}d\omega.$$

One can view $\mathrm{H}^2(\Pi^+)$ as a space whose elements are transfer functions of causal input-output stable linear systems. This statement is precisely captured by the following classical result of Paley and Wiener.

Theorem 3.2 (Paley-Wiener) *A complex-valued function F is in $H^2(\Pi^+)$ if and only if,*

$$F(s) = \int_0^\infty f(t)e^{-st}dt,$$

for some $f \in L^2(0,\infty)$. Furthermore this representation is unique.

Thus by the above theorem, $H^2(\Pi^+)$ arises as the Laplace transform of square-integrable functions on the half-line $[0,\infty)$. For any $F \in H^2(\Pi^+)$ define the restriction of F to vertical lines in the right half-plane by,

$$F_x(y) = F(x+iy), \qquad x > 0.$$

Also define the Fourier transform along vertical lines in $\Pi^+$by,

$$\widehat{F}_x(u) = \frac{1}{2\pi}\int_{\mathbb{R}} F(x+iy)e^{iuy}dy$$

for $F \in H^2(\Pi^+)$. Note that this definition of the Fourier transform on $H^2(\Pi^+)$ actually corresponds to our previous definition of the inverse Fourier transform. By Theorem 3.1, we know that boundary values of functions in $H^2(\Pi^+)$ are in $L^2(\mathbb{R})$. However, since by the Paley-Wiener

$$\frac{1}{2\pi}\int_{\mathbb{R}} F(i\omega)e^{i\omega t}d\omega = 0 \quad \text{for} \quad t < 0, \tag{3.1.3}$$

boundary values of functions in $H^2(\Pi^+)$ comprise a subspace, denoted $H^2_+(\mathbb{R})$, of $L^2(\mathbb{R})$ characterized by the Fourier transform vanishing on the negative half-line (3.1.3). It can also be shown that $H^2_+(\mathbb{R})$ is a closed subspace of $L^2(\mathbb{R})$. The orthogonal complement of $H^2_+(\mathbb{R})$ in $L^2(\mathbb{R})$, denoted $H^2_-(\mathbb{R})$, consists of functions whose Fourier transforms vanish on the positive half-line. Elements of $H^2_-(\mathbb{R})$ are boundary values of functions in $H^2(\Pi^-)$ where Π^- is the half-plane $\Re e\ s < 0$. Functions in $H^2(\Pi^+)$ are completely characterized by their boundary values since by Theorem 3.1, the boundary value function $F(i\omega)$, can be analytically continued to recover F on the right-half complex plane via the Poisson integral. By the maximum principle, we also know that $\|F\|_{H^2} = \|\widetilde{F}\|_{L^2}$ where $\widetilde{F}$ is the nontangential limit of F.

Remarks: In what follows, we take the liberty of identifying $H^2(\Pi^+)$ with $H^2_+(\mathbb{R})$, keeping in mind that element of the latter are boundary values of functions in $H^2(\Pi^+)$. We use ω to denote the real frequency variable and write $F(\omega)$ to denote the boundary value function $F(i\omega)$. The complex frequency variable will be denoted by $s = x + iy$. We also adopt the following notation in the remainder of this dissertation:

$RH^2(\Pi^+)$: Real-rational functions in $H^2(\Pi^+)$, that is rational functions in $H^2(\Pi^+)$ with real coefficients.

$H^2_{\mathbb{R}}(\Pi^+)$: Functions in $H^2(\Pi^+)$ which are Laplace transforms of *real-valued* functions in $L^2(0,\infty)$.

Note that $RH^2(\Pi^+) \subset H^2_{\mathbb{R}}(\Pi^+)$.

3.2 Wavelet Transforms on $H^2(\Pi^+)$

When $H^2(\Pi^+)$ is considered as a closed subspace of $L^2(\mathbb{R})$, it is easy to see how wavelet theory developed for $L^2(\mathbb{R})$ may be applied to $H^2(\Pi^+)$. Let $\Psi \in H^2(\Pi^+)$ be an admissible analyzing wavelet for $H^2(\Pi^+)$, where admissibility is now defined by applying the admissibility condition (2.2.8) to the restriction of Ψ to vertical lines in Π^+, i.e.

$$C_{\Psi_x} = \int_{\mathbb{R}} \frac{\left|\widehat{\Psi}_x(u)\right|^2}{|u|} du < \infty, \qquad x > 0. \tag{3.2.4}$$

As in the case of $L^2(\mathbb{R})$ it is possible to define a continuous wavelet transform on $H^2(\Pi^+)$ with respect to Ψ as follows. Let,

$$\Psi^{(a,b)}(s) = (T_{ib} D_a)\Psi(s) = |a|^{1/2}\, \Psi(as - ib), \qquad a, b \in \mathbb{R}, \quad a > 0.$$

Then for any $F \in H^2(\Pi^+)$ define the continuous wavelet transform on the line $\Re e\, s = x$ by,

$$W^x F(a,b) = \left\langle f, \Psi^{(a,b)} \right\rangle = \int_{\mathbb{R}} F_x(y) \overline{\Psi_x^{(a,b)}(y)} dy. \tag{3.2.5}$$

Inversion of this transform is accomplished by the inversion formula,

$$F_x(y) = \frac{1}{C_{\Psi_x}} \int_{\mathbb{R}} \int_{\mathbb{R}} W_x F(a,b) \Psi_x^{(a,b)}(y) \frac{da\, db}{a^2}.$$

To define a discrete wavelet transform with respect to Ψ, let

$$\Psi_{m,n}(s) = a_0^{m/2}\Psi(a_0^m s - inb_0) \qquad a_0 > 0, \quad \Re e\ s = x.$$

Assume Ψ satisfies the admissibility condition and let $a_0 > 0$ and b_0 be such that the family $\{\Psi_{m,n}\}_{m,n\in\mathbb{Z}}$, is a *frame* for $\mathcal{D}$ which is a closed subspace of $L^2(\mathbb{R})$. Thus for any $F \in H^2(\Pi^+)$ we have that

$$F_x(y) = \sum_m \sum_n \left\langle F, S^{-1}\Psi_{m,n} \right\rangle \Psi_{m,n},$$

where S is the *frame operator* associated with the frame $\{\Psi_{m,n}\}$.

3.3 Wavelet System Transfer Functions

Here we restrict discussion to affine frames constructed on the imaginary axis. Hence we require admissibility of the analyzing wavelet $\Psi(s)$ for $\Re e\ s = 0$ and consider the boundary values of $H^2(\Pi^+)$.

Let $\Psi(\omega)$ denote the nontangential limit of an admissible analyzing wavelet $\Psi(s)$ and let (a_0, b_0) be such that (Ψ, a_0, b_0) generates an affine frame for $H^2(\Pi^+)$. Then any $F \in H^2(\Pi^+)$ can be represented as

$$F(\omega) = \sum_m \sum_n c_{m,n}\Psi_{m,n}(\omega), \tag{3.3.6}$$

where as before $\Psi_{m,n}(\omega) = a_0^{m/2}\Psi(a_0^m\omega - nb_0)$, and one set of suitable coefficients may be computed using the inverse of the frame operator (see (2.2.17)). Assuming that $F \in H^2(\Pi^+)$ is the Laplace transform of a real-valued weighting pattern in $L^2(0,\infty)$, (i.e $F \in H^2_{\mathbb{R}}(\Pi^+)$), and Ψ is a real-rational analyzing wavelet ($\Psi \in RH^2(\Pi^+)$), we can ask the question; is an arbitrary truncation of the frame expansion (3.3.6) the transfer function of a *real* weighting pattern? Since $RH^2(\Pi^+)$ arises as the image under the Laplace transform of a class of *real-valued* weighting patterns, if the analyzing wavelet $\Psi \in RH^2(\Pi^+)$ then $\Psi_{m,n}(-\omega) = \Psi^*_{m,n}(\omega)$ for $n = 0$ and $m \in \mathbb{Z}$. However, this symmetry is violated for $n \neq 0$. Hence arbitrary truncations of the series (3.3.6), will

not in general result in real-rational functions, i.e.

$$\sum_{n\in\mathcal{J}} c_{m,n}\Psi_{m,n} \notin \mathrm{RH}^2(\Pi^+),$$

for arbitrary finite index sets $\mathcal{J}$. This observation motivates the following definition of a *wavelet system* transfer function.

Definition 3.2 *Given* $\Psi \in \mathrm{RH}^2(\Pi^+) \subset \mathrm{H}^2(\Pi^+)$ *a wavelet system transfer function is defined as a function of the form,*

$$G^{m,n}(s) = \alpha\Psi_{m,n}(s) + \overline{\alpha}\Psi_{m,-n}(s)$$

where $\overline{\alpha}$ *denotes the complex conjugate of* α.

Proposition 3.1 *Let* $F(s)$ *be a real-rational function in* $\mathrm{H}^2(\Pi^+)$. *Then, the wavelet system transfer function defined by*

$$G^{m,n}(s) = \alpha F_{m,n}(s) + \overline{\alpha}F_{m,-n}(s),$$

is also a real-rational function in $\mathrm{H}^2(\Pi^+)$.

Proof: Since $\mathrm{H}^2(\Pi^+)$ is a closed linear space, it is clear that $G^{m,n}(s) \in \mathrm{H}^2(\Pi^+)$. It is also clear that $G^{m,n}(s)$ is rational. To show that $G^{m,n}(s)$ is real-rational we only need to show that

$$G^{m,n}(-\omega) = \overline{G}^{m,n}(\omega).$$

Now,

$$\begin{aligned}
G^{m,n}(-\omega) &= \alpha F_{m,n}(-\omega) + \overline{\alpha}F_{m,-n}(-\omega) \\
&= \alpha a_0^{m/2}F(-a_0^m\omega - nb_0) + \overline{\alpha}a_0^{m/2}F(-a_0^m\omega + nb_0) \\
&= \alpha a_0^{m/2}F(-(a_0^m\omega + nb_0)) + \overline{\alpha}a_0^{m/2}F(-(a_0^m\omega - nb_0)) \\
&= \alpha a_0^{m/2}\overline{F}(a_0^m\omega + nb_0) + \overline{\alpha}a_0^{m/2}\overline{F}(a_0^m\omega - nb_0) \\
&= \alpha\overline{F}_{m,-n}(\omega) + \overline{\alpha}\overline{F}_{m,n}(\omega) \\
&= \overline{G}^{m,n}(\omega). \quad \blacksquare
\end{aligned}$$

One set of suitable coefficients in the wavelet decomposition (3.3.6), is given by $c_{m,n} = \langle F, S^{-1}\Psi_{m,n}\rangle$. The utility of the notion of wavelet system transfer functions hinges on the requirement that

$$c_{m,n} = \left\langle F, S^{-1}\Psi_{m,n}\right\rangle = \overline{\langle F, S^{-1}\Psi_{m,-n}\rangle} = \overline{c_{m,-n}}. \tag{3.3.7}$$

However, in general there is no reason to expect these coefficients to satisfy this kind of symmetry condition. We now show that this symmetry is satisfied for a sufficiently interesting class of functions in $\mathrm{H}^2(\Pi^+)$, namely the class $\mathrm{H}^2_{\mathbb{R}}(\Pi^+)$.

As a first step, in verifying condition (3.3.7), consider the following proposition.

Proposition 3.2 *Let f and g be boundary values of functions in $\mathrm{H}^2(\Pi^+)$. Also let f and g be such that $f(-\omega) = \overline{f(\omega)}$, and $g(-\omega) = \overline{g(\omega)}$. then,*

$$\langle f, g_{m,n}\rangle = \overline{\langle f, g_{m,-n}\rangle}.$$

Proof: (See Appendix B)

Remark: Note that if we were to consider only tight frames, Proposition 3.2 is sufficient to guarantee that (3.3.7) is satisfied for all $F \in \mathrm{H}^2_{\mathbb{R}}(\Pi^+)$, since in the case of a tight frame the frame operator is a multiple of the identity.

The following lemma states that for general affine frames, (3.3.7) is satisfied for all $F \in \mathrm{H}^2_{\mathbb{R}}(\Pi^+)$.

Lemma 3.1 *Let f and g be boundary values of functions in $\mathrm{H}^2(\Pi^+)$ such that $f(-\omega) = \overline{f(\omega)}$, and $g(-\omega) = \overline{g(\omega)}$. Let $a_0 > 0$ and b_0 be such that $\{g_{m,n}\}_{m,n\in\mathbb{Z}}$ is a frame and let S be the associated frame operator. Then,*

$$c_{m,n} = \left\langle f, S^{-1}g_{m,n}\right\rangle = \overline{\langle f, S^{-1}g_{m,-n}\rangle} = \overline{c_{m,-n}}.$$

Proof: Since the frame operator S is self-adjoint,

$$\left\langle f, S^{-1}g_{m,n}\right\rangle = \left\langle S^{-1}f, g_{m,n}\right\rangle.$$

Therefore by Proposition 3.2 we need only check that if $f(-\omega) = \overline{f(\omega)}$ then $S^{-1}f(-\omega) = \overline{S^{-1}f(\omega)}$. Now,

$$(S^{-1}f)(-\omega) = \frac{2}{A+B}\sum_{k=0}^{\infty}\left(I - \frac{2}{A+B}S\right)^k f(-\omega). \tag{3.3.8}$$

Let

$$\begin{aligned} G^{m,n}(\omega) &= \langle f, g_{m,n}\rangle\, g_{m,n}(\omega) + \langle f, g_{m,-n}\rangle\, g_{m,-n}(\omega) \quad m \in \mathbb{Z}\,, n \in \mathbb{Z}^+, \;\; n \neq 0 \\ G^{m,0}(\omega) &= \langle f, g_{m,0}\rangle\, g_{m,0}(\omega) \quad m \in \mathbb{Z}\,. \end{aligned}$$

Then

$$\begin{aligned} (Sf)(-\omega) &= \sum_m \left[G^{m,0}(-\omega) + \sum_{n=1}^{\infty} G^{m,n}(-\omega)\right] \\ &= \sum_m \left[\overline{G^{m,0}}(\omega) + \sum_{n=1}^{\infty} \overline{G^{m,n}}(\omega)\right] \\ &= \overline{(Sf)}(\omega). \end{aligned}$$

Thus,

$$\left[\left(I - \frac{2}{A+B}S\right) f\right](-\omega) = \overline{\left(I - \frac{2}{A+B}S\right) f(\omega)}$$

and together with (3.3.8), we get $(S^{-1}f)(-\omega) = \overline{(S^{-1}f)}(\omega)$, which completes the proof. ■

As a step in formalizing later discussion, let us define a transform operator which may be associated with the grouping suggested by the definition of WS transfer functions. We refer to this transform as a *wavelet system transform* on $\mathrm{H}^2_{\mathbb{R}}(\Pi^+)$. We begin by defining the space which contains the image of $\mathrm{H}^2_{\mathbb{R}}(\Pi^+)$ under the WS transform operator.

Definition 3.3 *Define $\mathcal{R}(J)$ as the space of sequences of functions $\{F_k\}_{k\in\mathcal{J}}$ such that $F_k \in \mathrm{RH}^2(\Pi^+) \subset \mathrm{H}^2(\Pi^+)$ for all $k \in \mathcal{J}$, and*

$$\|\sum_{k\in\mathcal{J}} F_k\|^2_{H^2} < \infty, \tag{3.3.9}$$

where $\mathcal{J}$, is a countable (index) set.

Definition 3.4 (Wavelet System Transform) *Let $\Psi \in \mathrm{H}^2(\Pi^+)$ be an admissible real-rational analyzing wavelet and $a_0 > 0$, b_0 such that (Ψ, a_0, b_0) generates an affine frame for $\mathrm{H}^2(\Pi^+)$. Let S be the associated frame operator. The Wavelet System transform is defined by the operator $H_\Psi : \mathrm{H}^2_{\mathbb{R}}(\Pi^+) \longrightarrow \mathcal{R}(\mathbb{Z} \times \mathbb{Z}^+)$,*

$$H_\Psi F = \{F^{m,n}\}_{m\in\mathbb{Z},\ n\in\mathbb{Z}^+},$$

where for any $F \in \mathrm{H}^2_{\mathbb{R}}(\Pi^+)$, $F^{m,n}$ is given by,

$$\begin{aligned} F^{m,n}(\omega) &= \left\langle F, S^{-1}\Psi_{m,n}\right\rangle \Psi_{m,n}(\omega) + \left\langle F, S^{-1}\Psi_{m,-n}\right\rangle \Psi_{m,-n}(\omega) \\ &\qquad m \in \mathbb{Z}, n \in \mathbb{Z}^+ \setminus \{0\}, \\ F^{m,0}(\omega) &= \left\langle F, S^{-1}\Psi_{m,0}\right\rangle \Psi_{m,0}(\omega) \qquad m \in \mathbb{Z}. \end{aligned} \tag{3.3.10}$$

The operator H_Ψ defines an invertible isometry from $\mathrm{H}^2(\Pi^+)$ to $\mathcal{R}(\mathbb{Z} \times \mathbb{Z}^+)$, (where (3.3.9) defines the norm on $\mathcal{R}(\mathcal{J})$).

Remark: A second definition could be used for the space containing Ran H_Ψ. We could define $\mathcal{R}(\mathrm{J})$ as in Definition 3.3, with (3.3.9) replaced by the requirement that

$$\sum_{k\in\mathcal{J}} \|F_k\|^2_{H^2} < \infty.$$

This is possible using the knowledge that $\{\Psi_{m,n}\}$ is a frame and that $\|\Psi_{m,n}\| = C$ for all $(m,n) \in \mathbb{Z}^2$ and some finite constant C. To explicitly see how this works, let $F \in \mathrm{H}^2_{\mathbb{R}}(\Pi^+)$, (thus (3.3.7) is satisfied), and let A and B be the upper and lower frame bounds associated with the frame $\{\Psi_{m,n}\}$. Thus,

$$\begin{aligned} \sum_{m\in\mathbb{Z},n\in\mathbb{Z}^+} \|F^{m,n}\|^2 &= \sum_{m\in\mathbb{Z}} \|c_{m,0}\Psi_{m,0}\|^2 + \sum_{n\in\mathbb{Z}^+\setminus\{0\}} \|c_{m,n}\Psi_{m,n} + c_{m,-n}\Psi_{m,n}\|^2 \\ &\le \sum_{m\in\mathbb{Z}} \|c_{m,0}\Psi_{m,0}\|^2 + \sum_{n\in\mathbb{Z}^+\setminus\{0\}} (\|c_{m,n}\Psi_{m,n}\| + \|c_{m,-n}\Psi_{m,n}\|)^2 \\ &\le C^2 \sum_{m\in\mathbb{Z}} |c_{m,0}|^2 + \sum_{n\in\mathbb{Z}^+\setminus\{0\}} (|c_{m,n}| + |c_{m,-n}|)^2 \end{aligned}$$

$$
\begin{aligned}
&\leq C^2 \sum_{m\in\mathbb{Z}} |c_{m,0}|^2 + 4 \sum_{n\in\mathbb{Z}^+\setminus\{0\}} |c_{m,n}|^2 \\
&\leq C^2 \sum_{m\in\mathbb{Z}} 2\,|c_{m,0}|^2 + 4 \sum_{n\in\mathbb{Z}^+\setminus\{0\}} |c_{m,n}|^2 \\
&= 2C^2 \sum_{m,n\in\mathbb{Z}} |c_{m,n}|^2 \leq 2C^2 B\|F\|^2 < \infty
\end{aligned}
$$

However, in this case H_Ψ would no longer be an isometry.

Inversion of H_Ψ involves a simple summation of terms in the sequence $\{F^{m,n}\}$, and together with Proposition 3.1 and Lemma 3.1, gives us the following decomposition theorem for $\mathrm{H}^2_{\mathbb{R}}(\Pi^+)$.

Theorem 3.3 (Wavelet System Decomposition of $\mathrm{H}^2_{\mathbb{R}}(\Pi^+)$) *Let $\Psi \in \mathrm{RH}^2(\Pi^+)$ be an admissible analyzing wavelet, and let $a_0 > 0$, b_0 be such that (Ψ, a_0, b_0) generates an affine frame for $\mathrm{H}^2(\Pi^+)$. Then, any F in $\mathrm{H}^2_{\mathbb{R}}(\Pi^+)$ may be represented as,*

$$
F = \sum_m \sum_{n=0}^{\infty} F^{m,n}, \tag{3.3.11}
$$

where, each $F^{m,n}$ $(\in \mathrm{RH}^2(\Pi^+))$ is a wavelet system transfer function defined by,

$$
\begin{aligned}
F^{m,n} &= \left\langle F, S^{-1}\Psi_{m,n} \right\rangle \Psi_{m,n} + \overline{\langle F, S^{-1}\Psi_{m,n}\rangle}\Psi_{m,-n}, \quad m \in \mathbb{Z}, \quad n \in \mathbb{Z}^+\setminus\{0\} \\
F^{m,0} &= \left\langle F, S^{-1}\Psi_{m,0} \right\rangle \Psi_{m,0} \qquad m \in \mathbb{Z}.
\end{aligned} \tag{3.3.12}
$$

Remark: Of subsequent significance is the fact that if the analyzing wavelet Ψ is of degree N, then the degree of each wavelet system transfer function $F^{m,n}$, is bounded by $2N$.

3.3.1 Examples: Rational Analyzing Wavelets for $\mathrm{H}^2(\Pi^+)$

Example 1

As an example of a rational analyzing wavelet for $\mathrm{H}^2(\Pi^+)$, consider the function

$$
\Psi(s) = \frac{1}{(s+\gamma)^2 + \xi^2}, \qquad \gamma, \xi > 0.
$$

It is easily verified that $\Psi(s)$ is in $H^2(\Pi^+)$ and furthermore Ψ is an admissible analyzing wavelet i.e.,

$$\int_{\mathbb{R}} \Psi(x+iy)dy = 0 \quad \text{for } x > 0.$$

Taking the inverse Laplace transform of Ψ, the weighting pattern $\psi(t)$ corresponding to Ψ is given by,

$$\psi(t) = \begin{cases} \xi^{-1}e^{-\gamma t}\sin(\xi t) & \text{for } t \geq 0 \\ 0 & \text{for } t < 0 \end{cases}$$

The $H^2(\Pi^+)$ norm of Ψ can also be found to be,

$$\|\Psi\|_{H^2}^2 = \frac{2\pi}{4\xi^2}\left(\frac{1}{\gamma} - \frac{\cos(\arctan(\xi/\gamma))}{\sqrt{\xi^2+\gamma^2}}\right)$$

Figures 3.1 and 3.2 show this analyzing wavelet Ψ, evaluated on the imaginary axis, and the corresponding weighting pattern ψ for different values of ξ and γ.

Constructing an Affine Frame for $H^2(\Pi^+)$ from Ψ: For the purpose of numerically determining values of the dilation stepsize a_0 and translation stepsize b_0 such that (Ψ, a_0, b_0) generates an affine frame for $H^2(\Pi^+)$ we can utilize Theorem 2.6 and Corollary 2.1. Figures 3.3–3.4 show the results of applying Theorem 2.6 and Corollary 2.1 for the case where $a_0 = 2.0$. Hence for $a_0 = 2.0$ and $0 < b_0 \leq 17$ the sequence $\{\Psi_{m,n}\}$ forms an affine frame for $H^2(\Pi^+)$.

Example 2

For a second family of rational analyzing wavelets for $H^2(\Pi^+)$, consider the functions,

$$\Psi^k(s) = \frac{1}{(s+p)^k}; \quad p > 0; \quad k = 2, 3, \ldots.$$

The corresponding weighting patterns are,

$$\psi^k(t) = \frac{1}{(k-1)!}t^{k-1}e^{-pt}.$$

Admissibility is easily verified since,

$$\begin{aligned} \int_0^\infty \frac{|\psi^k(t)|^2}{t}dt &= \left(\frac{1}{(k-1)!}\right)^2 \int_0^\infty t^{2k-3}e^{-2pt}dt \\ &= \left(\frac{1}{(k-1)!}\right)^2 (2k-3)!(2a)^{-2m+2} < \infty. \end{aligned}$$

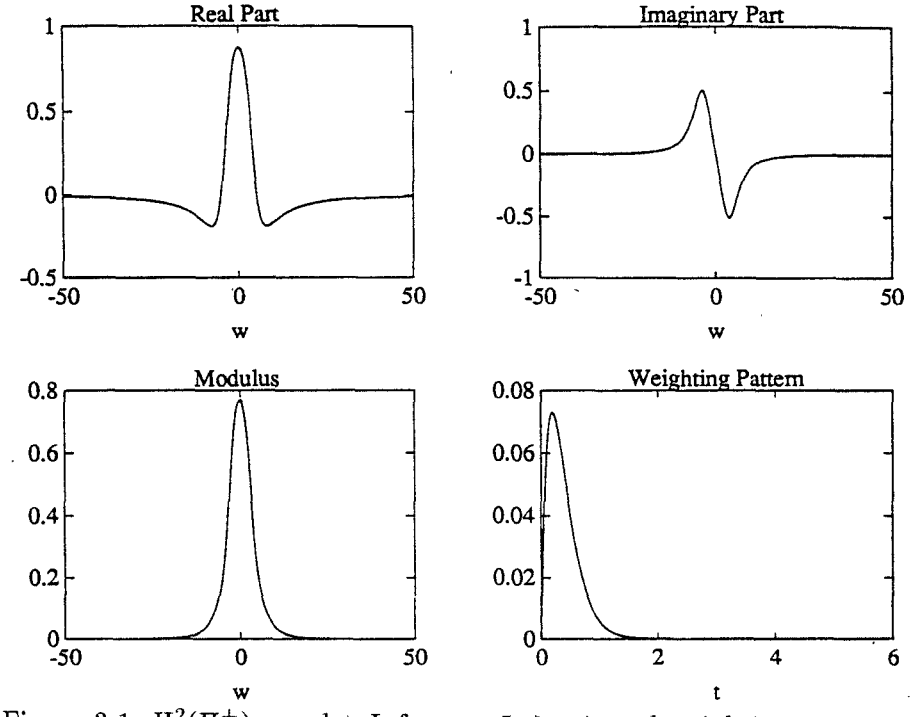

Figure 3.1: $H^2(\Pi^+)$ wavelet Ψ for $\gamma = 5, \xi = 1$, and weighting pattern ψ.

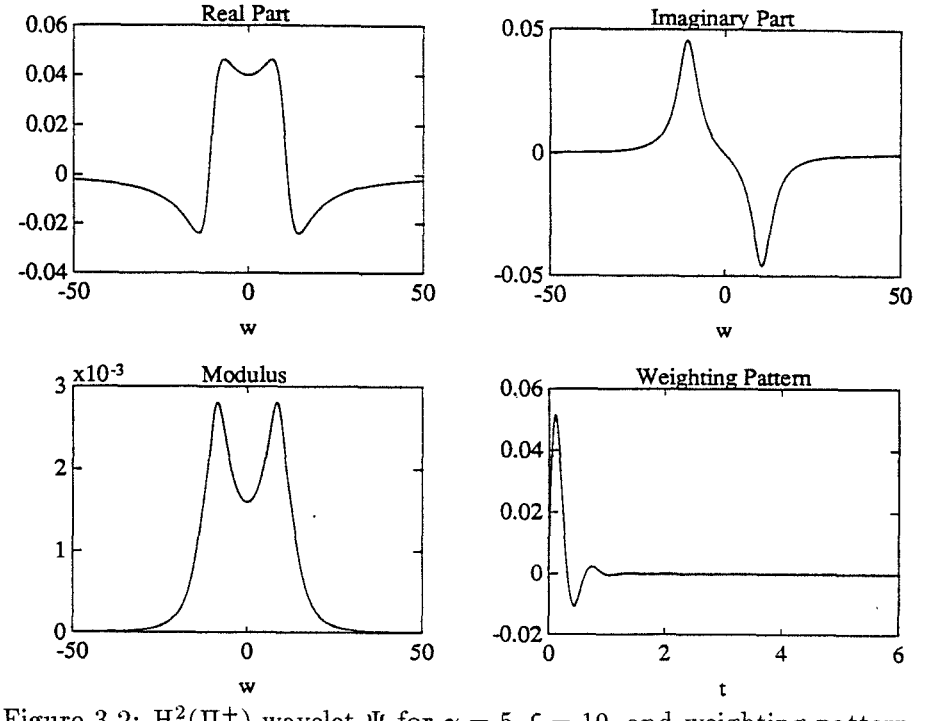

Figure 3.2: $H^2(\Pi^+)$ wavelet Ψ for $\gamma = 5, \xi = 10$, and weighting pattern ψ.

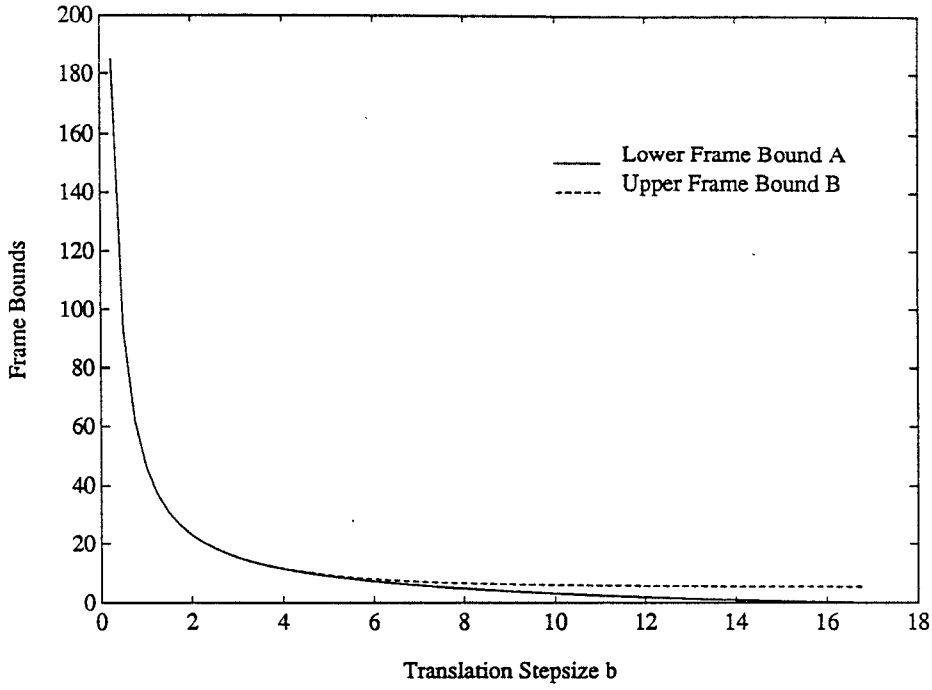

Figure 3.3: Estimates of frame bounds, using $H^2(\Pi^+)$ analyzing wavelet Ψ of Example 1, with $\gamma = 5.0$, $\xi = 1.0$ and $a_0 = 2$, as translation stepsize b_0 is varied. Solid curve: lower frame bound A; Dashed curve:upper frame bound B.

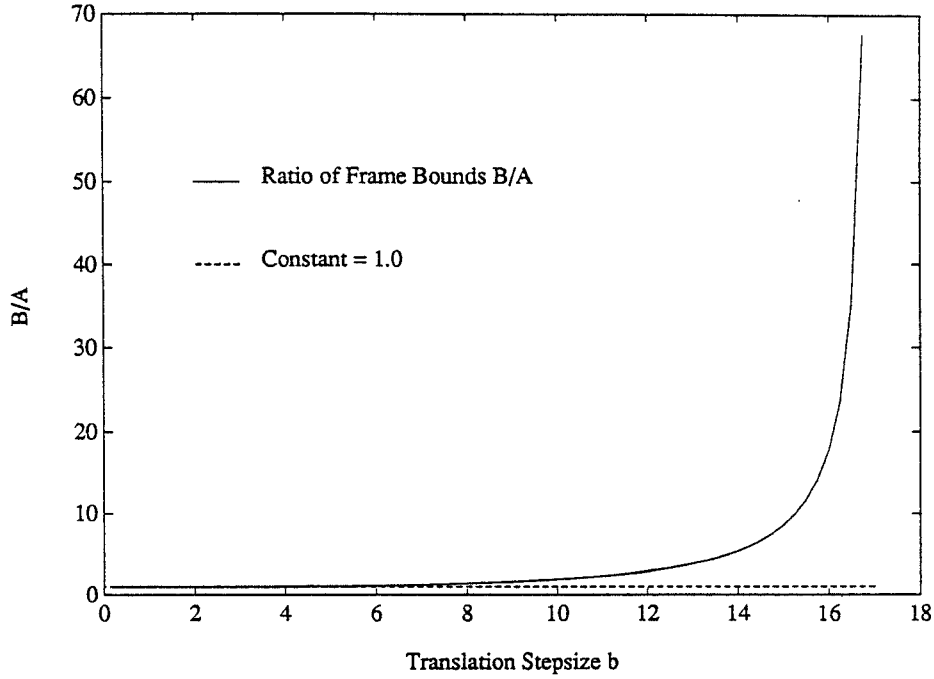

Figure 3.4: Ratio (B/A) of estimated frame bounds, using $H^2(\Pi^+)$ analyzing wavelet Ψ of Example 1, with $\gamma = 5.0$, $\xi = 1.0$ and $a_0 = 2$, as translation stepsize b_0 is varied. Solid curve: B/A; Dashed line: constant=1.0.

Figure 3.5 shows this wavelet and the corresponding weighting pattern for $p = 5.0, k = 2.0$. As in the last example the frame parameters can be numerically determined with

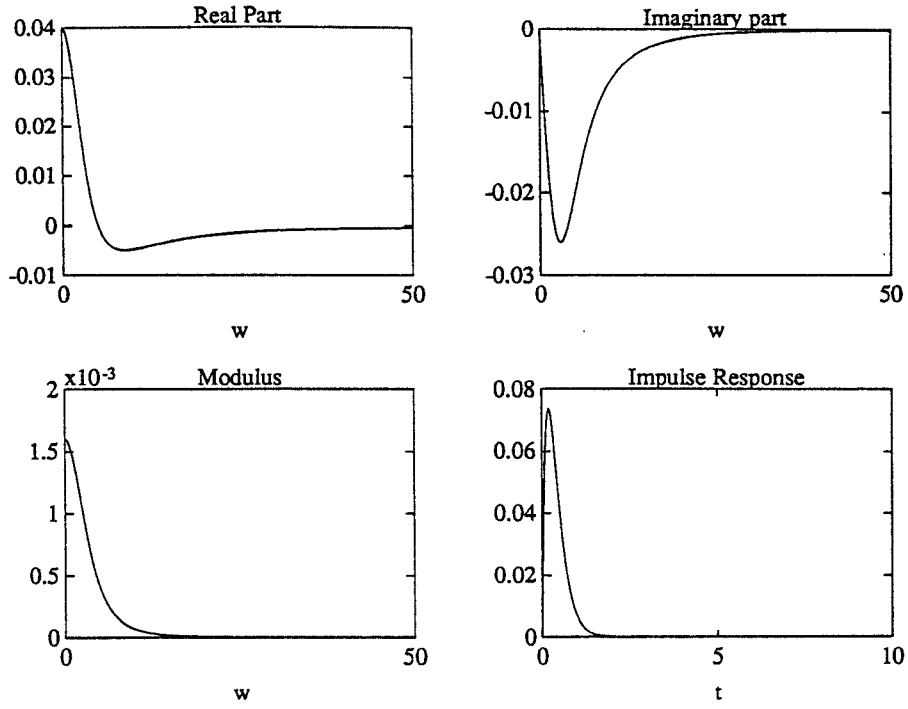

Figure 3.5: $H^2(\Pi^+)$ analyzing wavelet Ψ for $p = 5.0$, $k = 2$ and corresponding weighting pattern

the help of Theorem 2.6. Figures 3.6–3.7 show the results of this exercise for the case where $a_0 = 2.0$ and $k = 2$, and $p = 5.0$. Hence for $a_0 = 2.0$ and $0 < b_0 \leq 17$ the sequence $\{\Psi_{m,n}\}$ forms an affine frame for $H^2(\Pi^+)$.

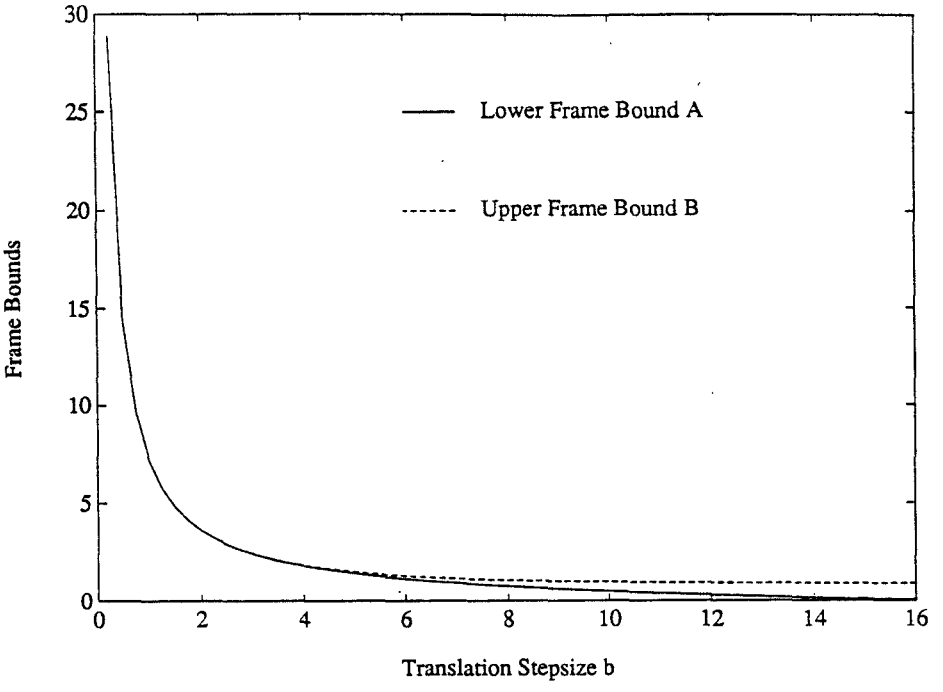

Figure 3.6: Estimates of frame bounds, using $\mathrm{H}^2(\Pi^+)$ analyzing wavelet Ψ of Example 2, with $p = 5.0$, $k = 2.0$ and $a_0 = 2$, as translation stepsize b_0 is varied. Solid curve: lower frame bound A; Dashed curve:upper frame bound B.

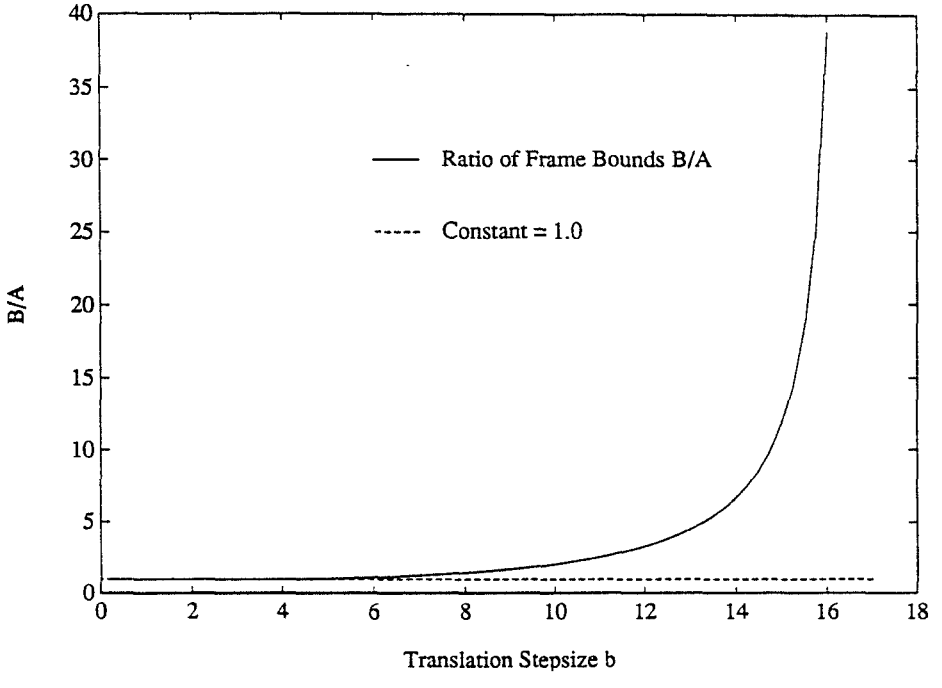

Figure 3.7: Ratio (B/A) of estimated frame bounds, using $\mathrm{H}^2(\Pi^+)$ analyzing wavelet Ψ of Example 2, with $p = 5.0$, $k = 2$ and $a_0 = 2$, as translation stepsize b_0 is varied. Solid curve: B/A; Dashed line: constant=1.0.

Aside from the examples of the last section we can ask for a characterization of all admissible rational $H^2(\Pi^+)$ analyzing wavelets. The following theorem provides such a characterization.

Theorem 3.4 *Let $\Psi \in RH^2(\Pi^+)$, and let (A, B, C) be a state space realization of Ψ. Then the following are equivalent:*

(1) Ψ is an admissible $H^2(\Pi^+)$ analyzing wavelet.

(2) $s\Psi(s) \to 0$, as $s \to \infty$.

(3) $CB = 0$.

Proof: Recall that,

$$\left(\frac{d^n f}{dt^n})\right)_{t=0} = \frac{1}{2\pi i}\int_{-i\infty}^{i\infty} s^n F(s)ds.$$

Thus if $f(t)$, has a zero of order $k+1$, at $t = 0$, i.e.

$$f(0) = \left(\frac{df}{dt}\right)_{t=0} = \cdots = \left(\frac{d^k f}{dt^k}\right)_{t=0} = 0,$$

then

$$\int_{-i\infty}^{i\infty} s^n F(s)ds = 0, \quad n = 0, 1, \ldots, k. \tag{3.3.13}$$

This requires that $F(s)$ goes to zero faster than $1/s^{k+1}$, as $s \to \infty$. For rational $F(s)$, this means,

$$F(s) \to \frac{1}{s^{k+2}}, \quad \text{for} \quad s \to \infty.$$

Conversely for $F(s)$ with this asymptotic behavior, we can deduce that $f(t)$ has a zero of order $k+1$, at $t = 0$, (c.f. [Gui63]). Therefore $sF(s) \to 0$, as $s \to \infty$, if and only if $f(t)$ has a first order zero at $t = 0$. This gives $|f(t)|^2$, a second order zero at $t = 0$, and therefore admissibility of F.

Thus $s\Psi(s) \to 0$, for $s \to \infty$, if and only if Ψ, is admissible. Equivalence of $sF(s) \to 0$, to $CB = 0$, is easily seen from the Laurent series expansion of F;

$$F(s) = \sum_{k=1}^{\infty} h_k s^{-k},$$

where the Markov parameters h_k are given by,

$$h_k = CA^{k-1}B. \qquad \blacksquare$$

3.4 Properties of Wavelet System Decompositions

3.4.1 Time-Frequency Localization

As noted earlier, time-frequency localization is perhaps the most beneficial property of affine wavelet representations. Wavelet system transfer functions inherit the time-frequency localization properties of the underlying (rational) wavelets. As in Section 2.2.5, let $\Omega(\Psi) = [\omega_0(\Psi), \omega_1(\Psi)]$ denote the frequency concentration of Ψ and $R(\Psi) = [t_0(\Psi), t_1(\Psi)]$ $(t_0 \geq 0)$ denote the time concentration of Ψ (computed via the inverse Laplace transform). Then Ψ is a function which is concentrated in the time frequency plane on the rectangle $\mathcal{Q} = \Omega(\Psi) \times R(\Psi)$ and each of the WS transfer functions are concentrated on rectangles

$$\begin{aligned} \mathcal{Q}_{mn} &= [a_0^{-m}(\omega_0(\Psi) + nb_0), a_0^{-m}(\omega_1(\Psi) + nb_0)] \times [a_0^m t_0(\Psi), a^m t_1(\Psi)] \\ &= \Omega(\Psi_{m,n}) \times R(\Psi_{m,n}). \end{aligned} \tag{3.4.14}$$

Figure 3.8, shows the distribution of the rectangles $\mathcal{Q}_{mn}$ in the time-frequency plane. Since the wavelets for $H^2(\Pi^+)$ are constructed in the frequency domain, the time and frequency axes are interchanged when compared with the corresponding picture for wavelets constructed in the time-domain, i.e. it is now the time axis which is treated logarithmically. In some sense, this interchange of the localization in time and frequency is more natural for the decomposition of linear systems than the localization arising from wavelets constructed in the time-domain. To see this, note that:

- Near $t = 0$, while time localization is good, the frequency concentration of each wavelet system encompasses a large band of frequencies.

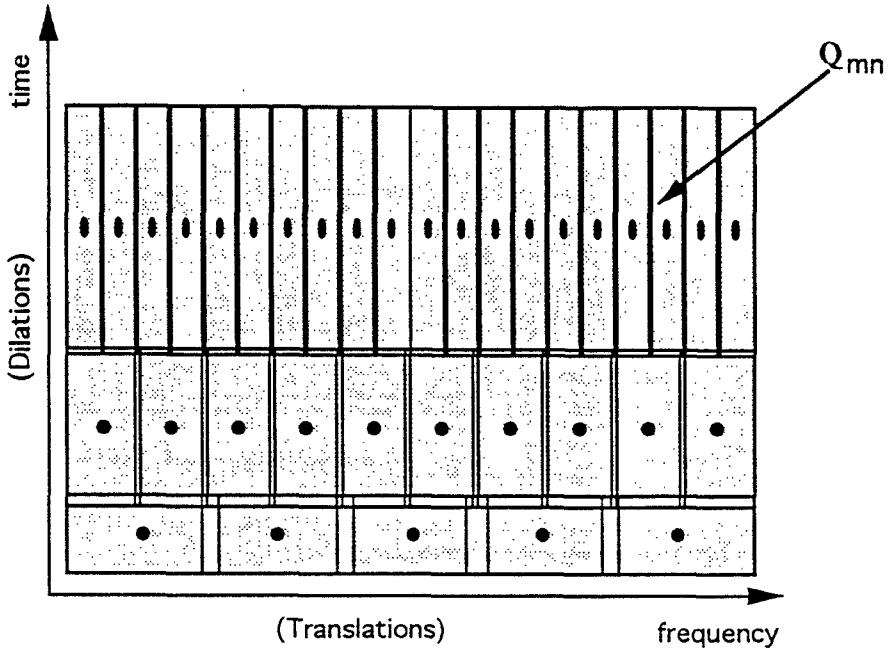

Figure 3.8: Time-frequency concentrations of wavelet systems.

- For $t \gg 0$, frequency localization is very good so that it is possible to 'zoom' in on narrow frequency bands, whereas localization in time is poor.

Often, in the case of physical systems, high-frequency components of the impulse response are localized near the time-origin (c.f. Figure 4.4). Furthermore away from the origin, the impulse response decays 'smoothly'. The form of time-frequency concentration arising in WS transfer functions allows us to capture this behavior efficiently, since relatively few terms are required near the time-origin to capture a broad range of frequency components. Moreover, away from the time-origin, the narrower localization in frequency allows us for example to represent a narrow band of low frequencies.

3.4.2 Poles and Zeros

Often a great deal of insight into the behavior of a system may be derived from a description of the poles and zeros. Given the poles and zeros of the analyzing wavelet

Ψ, we may examine the manner in which the poles and zeros of the WS transfer functions are influenced by the translations and dilations. Assume first of all that Ψ has no real axis poles and that Ψ is a degree N real-rational function in $\mathrm{H}^2(\Pi^+)$. Let $\{p_k, \overline{p_k}\}_{k=1}^{N/2}$ be the set set of poles of $\Psi(s)$, and $\{z_j, \overline{z_j}\}_{j=1}^{J}$ be the set of zeros of Ψ. Since Ψ is real-rational, Ψ can be written as

$$\Psi(s) = \frac{P(s)}{Q(s)} = \frac{\prod_j (s - z_j)(s - \overline{z_j})}{\prod_k (s - p_k)(s - \overline{p_k})},$$

where, $P(s)$ and $Q(s)$ are coprime. Thus,

$$\begin{aligned} \Psi_{m,n}(s) &= \frac{a_0^{m/2} \prod_j (a_0^m s - z_j - inb_0)(a_0^m s - \overline{z_j} - inb_0)}{\prod_k (a_0^m s - p_k - inb_0)(a_0^m s - \overline{p_k} - inb_0)} \\ &= \frac{a_0^{m/2} \prod_j (s - \beta_j(m,n))(s - \gamma_j(m,n))}{\prod_k (s - \eta_k(m,n))(s - \nu_k(m,n))} = \frac{P_{m,n}(s)}{Q_{m,n}(s)}, \end{aligned} \tag{3.4.15}$$

where,

$$\beta_k(m,n) = a_0^{-m}(z_j + inb_0) \qquad \gamma_k(m,n) = a_0^{-m}(\overline{z_j} + inb_0) \tag{3.4.16}$$

$$\eta_k(m,n) = a_0^{-m}(p_k + inb_0) \qquad \nu_k(m,n) = a_0^{-m}(\overline{p_k} + inb_0). \tag{3.4.17}$$

Note that $\eta_k(m,-n) = \overline{\nu_k}(m,n)$ and $\nu_k(m,-n) = \overline{\eta_k}(m,n)$ and $\beta_k(m,-n) = \overline{\gamma_k}(m,n)$ and $\gamma_k(m,-n) = \overline{\beta_k}(m,n)$. Therefore the poles of $G^{m,n}(s) = \alpha\Psi_{m,n}(s) + \overline{\alpha}\Psi_{m,-n}(s)$ are

$$\{\eta_k(m,n), \overline{\eta_k}(m,n), \nu_k(m,n), \overline{\nu_k}(m,n)\}. \tag{3.4.18}$$

Thus the effect of dilations and translations upon poles is,

- Dilations move the poles of $G^{m,n}$ radially away from and towards zero. As the dilation index m increases, the poles move towards zero and as m decreases the poles move away from zero. However, the poles remain in the closed left half-plane which is crucial since otherwise the $G^{m,n}$ would not remain in $\mathrm{H}^2(\Pi^+)$.

- The complex translations simply translate the poles along vertical lines in the left half-plane.

Figure 3.9 illustrates the behavior of the poles of $G^{m,n}$.

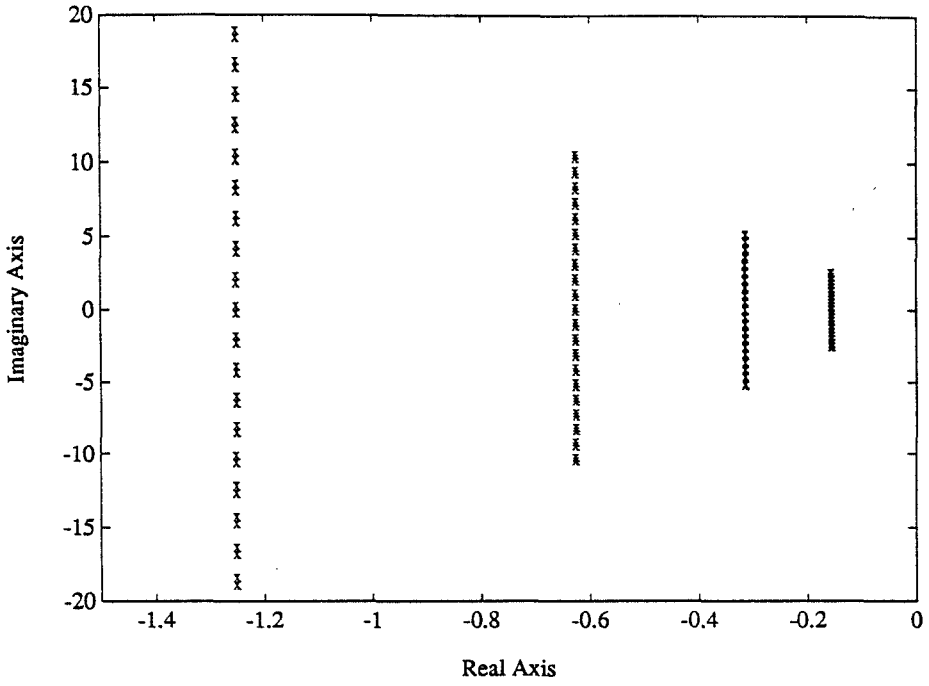

Figure 3.9: Behavior of poles of WS transfer functions

If we write $G^{m,n}(s) = N_{m,n}(s)/D_{m,n}(s)$, then the zeros of $G^{m,n}(s)$ are the roots of

$$\begin{aligned} N_{m,n}(s) &= \alpha P_{m,n}(s)D_{m,-n}(s) + \overline{\alpha} P_{m,-n}(s)D_{m,n}(s) \\ &= \alpha \prod_j (s - \beta_j(m,n))(s - \gamma_j(m,n)) \prod_k (s - \overline{\eta_k}(m,n))(s - \overline{\nu_k}(m,n)) \\ &\quad + \overline{\alpha} \prod_j (s - \overline{\beta_j}(m,n))(s - \overline{\gamma_j}(m,n)) \prod_k (s - \eta_k(m,n))(s - \nu_k(m,n)). \end{aligned}$$

Without actually deriving expressions for the zeros of $G^{m,n}(s)$ we make the following observations:

- The zeros of $G^{m,n}(s)$ occur in complex conjugate pairs.
- For $n \neq 0$, if $G^{m,n}$ has no real-axis poles, then $N_{m,n}(s)$ and $D_{m,n}$ are coprime, and therefore $G^{m,n}(s)$ is a strictly proper rational function of order $2N$.
- For $n = 0$ pole-zero cancellation results in $G^{m,n}(s)$ of order N.
- If $l(n)$ is the number of poles of $G^{m,n}$ on the real axis then the order of $G^{m,n}(s)$ is $2N - l(n)$.

3.4.3 State Space Realizations of Wavelet System Transfer Functions

Let $\psi(t)$ be the weighting pattern (i.e. inverse Laplace transform) corresponding to the real rational $\mathrm{H}^2(\Pi^+)$-wavelet Ψ and define the triplet (A, B, C) to be a minimal realization of Ψ. In this section we examine the question of realizations of the WS transfer function $G^{m,n}(s) = \alpha\Psi_{m,n}(s)+\overline{\alpha}\Psi_{m,-n}(s)$. Let α_R and α_I denote respectively the real and imaginary parts of α. Since (A, B, C) is a realization of Ψ,

$$\psi(t) = C\exp(At)B.$$

Taking the inverse Laplace transform, the weighting pattern corresponding to $G^{m,n}(s)$ is,

$$\begin{aligned}
g_{m,n}(t) &= \alpha a_0^{-m/2}\psi(a_0^{-m}t)e^{ina_0^{-m}b_0t} + \overline{\alpha}a_0^{-m/2}\psi(a_0^{-m}t)e^{-ina_0^{-m}b_0t} \\
&= a_0^{-m/2}\psi(a_0^{-m}t)2\left[\alpha_R\cos(na_0^{-m}b_0t) - \alpha_I\sin(na_0^{-m}b_0t)\right] \qquad (3.4.19) \\
&= \alpha a_0^{-m/2}C\exp(a_0^{-m}At)Be^{ina_0^{-m}b_0t} + \overline{\alpha}a_0^{-m/2}C\exp(a_0^{-m}At)Be^{-ina_0^{-m}b_0t} \\
&= \alpha a_0^{-m/2}C\exp((a_0^{-m}A + ina_0^{-m}b_0I)t)B \\
&\qquad +\overline{\alpha}a_0^{-m/2}C\exp((a_0^{-m}A - ia_0^{-m}nb_0I)t)B. \qquad (3.4.20)
\end{aligned}$$

Equation (3.4.20) immediately provides a *complex* realization of $G^{m,n}(s)$ which is

$$\begin{aligned}
A_{mn} &= \begin{bmatrix} a_0^{-m}A + ina_0^{-m}b_0I & 0 \\ 0 & a_0^{-m}A - ina_0^{-m}b_0I \end{bmatrix} \qquad (3.4.21) \\
B_{mn} &= [B \quad B]^T \qquad (3.4.22) \\
C_{mn} &= \left[a_0^{-m/2}\alpha C \quad a_0^{-m/2}\overline{\alpha}C\right]. \qquad (3.4.23)
\end{aligned}$$

However, since $\psi_{m,n}(t)$ is a real weighting pattern, we need a change of basis to give us a real realization. The differential equations corresponding to (3.4.23) are

$$\begin{aligned}
\dot{x_1} &= (a_0^{-m}A + ina_0^{-m}b_0I)x_1 + Bu \\
\dot{x_2} &= (a_0^{-m}A - ina_0^{-m}b_0I)x_2 + Bu \qquad (3.4.24)
\end{aligned}$$

and the output map is given by

$$y = a_0^{-m/2}\alpha Cx_1 + a_0^{-m/2}\overline{\alpha}Cx_2. \qquad (3.4.25)$$

Let, $z_1 = (x_1 + x_2)$ and $z_2 = i(x_1 - x_2)$. Then we get

$$\begin{aligned} \dot{z_1} &= a_0^{-m} A z_1 + n a_0^{-m} b_0 z_2 + 2Bu \\ \dot{z_2} &= a_0^{-m} A z_2 - n a_0^{-m} b_0 z_1. \end{aligned} \tag{3.4.26}$$

Under this transformation the output map becomes

$$\begin{aligned} y &= a_0^{-m/2} \left(\alpha_R C(x_1 + x_2) + i\alpha_I C(x_1 - x_2) \right) \\ &= a_0^{-m/2} \left(\alpha_R C z_1 + i\alpha_I C z_2 \right). \end{aligned} \tag{3.4.27}$$

From (3.4.26) and (3.4.26) we get the following *real* realization of $G^{m,n}(s)$,

$$A_{mn} = \begin{bmatrix} a_0^{-m} A & n a_0^{-m} b_0 I \\ -n a_0^{-m} b_0 I & a_0^{-m} A \end{bmatrix}, \quad n \neq 0 \tag{3.4.28}$$

$$B_{mn} = \begin{bmatrix} 2B & 0 \end{bmatrix}^T, \quad n \neq 0 \tag{3.4.29}$$

$$C_{mn} = \begin{bmatrix} a_0^{-m/2} \alpha_R C & a_0^{-m/2} \alpha_I C \end{bmatrix}, \quad n \neq 0 \tag{3.4.30}$$

$$(A_{m,0}, B_{m,0}, C_{m,0}) = (a_0^{-m} A, B, a_0^{-m/2} \alpha C) \tag{3.4.31}$$

It is interesting to note that, in this form (3.4.28–3.4.30), the dilations and translations which appear in the WS transfer function $G_{m,n}(s)$ affect the state space realization via dilations and translations as well, i.e.

$$A_{m,n} = a_0^{-m} \left(\begin{bmatrix} A & 0 \\ 0 & A \end{bmatrix} - n b_0 \begin{bmatrix} 0 & -I \\ I & 0 \end{bmatrix} \right), \quad n \neq 0.$$

3.4.4 Parallel Connections of WS Transfer Functions

In constructing rational approximations (see Section 3.5), we will be considering parallel connections of WS transfer functions of the form,

$$G_{\mathcal{J}}(s) = \sum_{(m,n) \in \mathcal{J}} G^{m,n}(s), \tag{3.4.32}$$

where $\mathcal{J}$ is a *finite* index set. Given Equations (3.4.28–3.4.30) defining the realization $(A_{m,n}, B_{m,n}, C_{m,n})$ of $G^{m,n}(s)$, a state space realization of $G_{\mathcal{J}}(s)$ is readily obtained.

$$A_{\mathcal{J}} = \begin{bmatrix} \begin{bmatrix} A_{m_1,n_1^1} & & 0 \\ & A_{m_1,n_2^1} & \\ 0 & & \ddots \end{bmatrix} & & 0 & \\ & \begin{bmatrix} A_{m_2,n_1^2} & & 0 \\ & A_{m_1,n_2^2} & \\ 0 & & \ddots \end{bmatrix} & & \\ 0 & & 0 & \ddots \end{bmatrix} \tag{3.4.33}$$

$$B_{\mathcal{J}} = \left[B_{m_1,n_1^1},\ B_{m_1,n_2^1},\cdots\right]^T \tag{3.4.34}$$

$$C_{\mathcal{J}} = \left[C_{m_1,n_1^1},\ C_{m_1,n_2^1},\cdots\right] \tag{3.4.35}$$

3.4.5 Minimality of State Space Realizations

An obvious question that can be asked regarding the realization (3.4.33–3.4.35) of $G_{\mathcal{J}}(s)$ is whether such a realization is minimal in the sense of being both controllable and observable. We have the following result,

Theorem 3.5 *Let $\Psi \in \mathrm{H}^2(\Pi^+)$ be an admissible rational analyzing wavelet, let $\{p_j\}$ denote the poles of Ψ and let (A, B, C) be a minimal realization of Ψ (of dimension N). Also let $\mathcal{J}$ be a finite, bounded index set. Then*

(a) *The realization (3.4.28–3.4.30) of $G^{m,n}(s)$ is minimal for all $(m,n) \in \mathcal{J}$ if and only if, for each $j = 1, \ldots, N$, there does not exist a nonzero integer k, such that.*

$$\frac{\mathcal{I}m\ p_j}{b_0} = k. \tag{3.4.36}$$

(b) *The realization (3.4.33–3.4.35) of $G_{\mathcal{J}}(s)$ is minimal if,*

(1) $(A_{m,n}, B_{m,n}, C_{m,n})$ as defined in (3.4.28–3.4.30) is a minimal realization of $G^{m,n}(s)$ for all $(m,n) \in \mathcal{J}$, and

(2) For each pair $(j,l) \in \{1,\ldots,N\} \times \{1,\ldots,N\}$, *there does not exist a nonzero integer* k, *such that.*

$$\frac{1}{\log a_0} \log\left(\frac{-\Re e\ p_j}{-\Re e\ p_l}\right) = k. \tag{3.4.37}$$

Proof: (See Appendix B.1) ■.

Remarks: The proof of the above theorem relies on there being no cancellations of poles by zeros in the required combinations of translates and dilates of the analyzing wavelet. Note also that (3.4.36) implies that the poles of any nonzero translate ($n \neq 0$) of the analyzing wavelet remain away from the real-axis.

3.4.6 Example: Wavelet System Decomposition

Example 1: Heat Equation with Dirichlet Boundary Control

Consider a system defined by the partial differential equation,

$$\begin{cases} \frac{\partial z}{\partial t} &= \frac{\partial^2 z}{\partial x^2}\ ;\ z(0) = 0,\ z(1) = u(t) \\ y(t) &= z(x_0,t) \end{cases} \tag{3.4.38}$$

This system has transfer function [Cur88]

$$G_1(s) = \frac{\sinh\sqrt{s}x_0}{\sinh\sqrt{s}}.$$

By assuming lowpass characteristics of the sensor where the measurement y, is made, we can write the overall transfer function as ,

$$G(s) = \frac{1}{s+\pi}\frac{\sinh\sqrt{s}x_0}{\sinh\sqrt{s}}. \tag{3.4.39}$$

A decomposition of G(s) (with $x_0 = 0.5$) was computed using 12 dilation levels ($m = -5,\ldots,6$) and up to 33 translations at each dilation level. The analyzing wavelet used is that of Example 1, in Section 3.3.1, with $\gamma = 5$ and $\xi = 1$. The results of this decomposition are shown in Figures 3.10–3.12 which are different representations of the magnitude of the wavelet system expansion coefficients. Along the dilation axis,

zero corresponds to the lowest dilation level ($m = -5$), and along the translation axis zero corresponds to $n = 0$. Figures 3.10 and 3.11 are 3D and contour plots respectively of the coefficient magnitudes and Figure 3.12 is a density plot in which each rectangle is shaded according to the corresponding coefficient magnitude. The key feature in

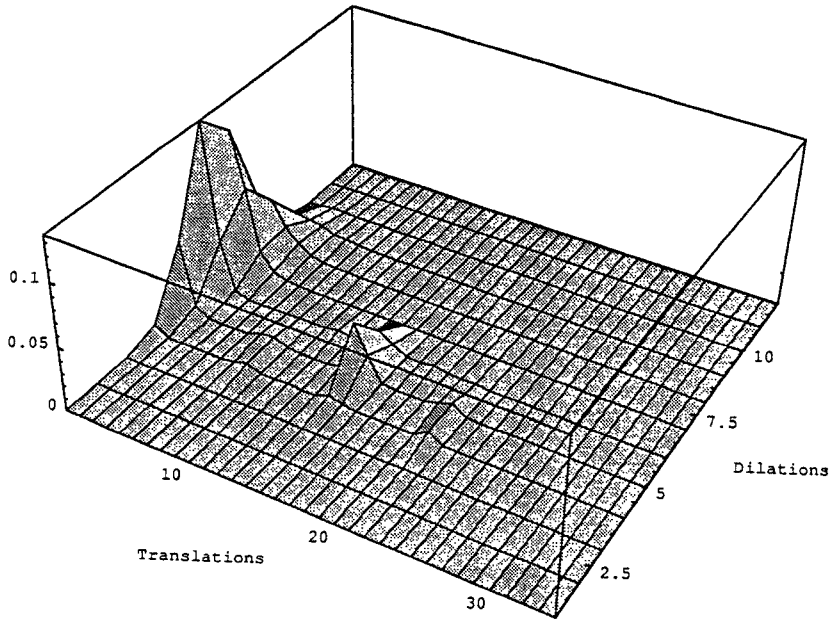

Figure 3.10: Wavelet system decomposition of heat equation transfer function - 3D plot of magnitude of expansion coefficients

this decomposition, which is probably most obvious in the density plot (Figure 3.12) is that the magnitudes of the coefficients are very well concentrated. This feature, which is due to the time-frequency localization properties of affine wavelets, permits us to pick a finite number of 'significant' terms in the wavelet system decomposition. In doing so, a finite-dimensional approximation to the original transfer function is obtained. Using the results of Section 3.4.3, it is also possible to immediately write down a minimal state space realization of the approximating system.

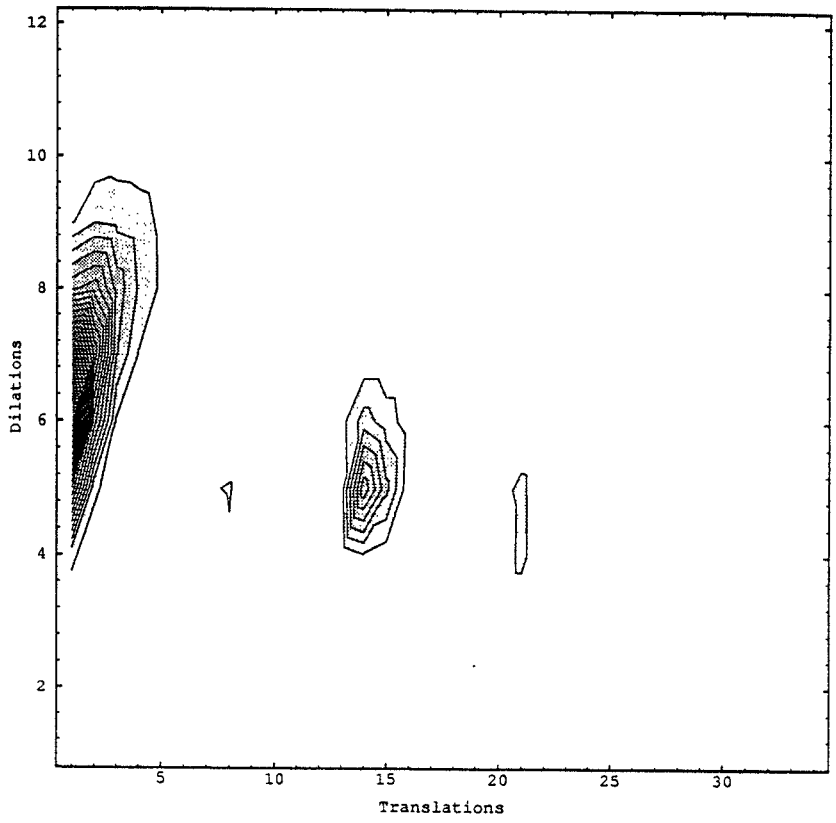

Figure 3.11: Wavelet system decomposition of heat equation transfer function - contour plot of magnitude of expansion coefficients

3.5 Rational Wavelet System Approximations

Wavelet system decompositions as in (3.3.11) provide a means of representing nonrational transfer functions in $H^2(\Pi^+)$ as infinite sums of rational transfer functions[1]. As mentioned earlier, our primary objective in deriving such a decomposition is to devise a systematic method of constructing rational approximations. What is required now is a mechanism which allows for judicious selection of a finite number of terms from the expansion in (3.3.11) which will allow useful approximation of a nonrational transfer function. For this purpose we utilize the localization properties afforded us

[1]Note that causality is preserved due to the property described by Equation (3.1.3)

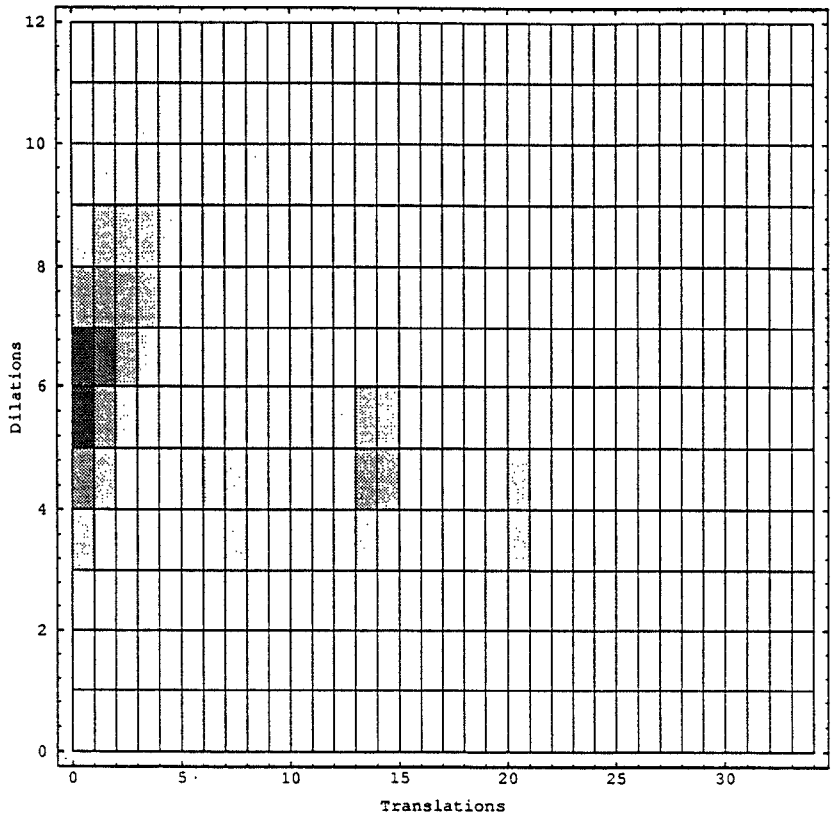

Figure 3.12: Wavelet system decomposition of heat equation transfer function - density plot of magnitude of expansion coefficients

by affine wavelets.

For a significant class of transfer functions arising from physical systems, the WS decomposition will result in a reasonably compact representation in the sense of well localized and rapidly decaying coefficients. This phenomenon can be explained on the basis of the time-frequency localization properties of the WS transfer functions and the observation that $H^2(\Pi^+)$ transfer functions arising from physical systems are often well localized in time-frequency as well. It is possible to devise a variety of schemes, each relying on time-frequency localization properties, for the selection of terms in a WS decomposition for use in a finite-dimensional approximation.

One possible choice for the selection of a finite-dimensional WS approximation can

be based upon knowledge of the time-frequency concentration of the (nonrational) transfer function which is to be approximated. For example given that the time-frequency concentration of a transfer function $f \in \mathrm{H}^2(\Pi^+)$ is $\mathcal{Q}(f)$ we can select a subset of the wavelet system transfer functions based upon the size of $\mathcal{Q}(f) \bigcap \mathcal{Q}_{m,n}$, where $\mathcal{Q}_{m,n}$ is the concentration of the WS transfer function $G^{m,n}(s)$. Daubechies in [Dau90] provides bounds for the error of such approximations in terms of the energy of f outside $\mathcal{Q}(f)$. A second selection scheme could consist of first computing the wavelet expansion coefficients for a large number of terms and then simply discarding those terms with 'small' coefficients. This second method is similar to those used to achieve signal or image compression via wavelet decompositions (c.f. [CMQW90, Wic89]). One such selection criterion, can be based upon the ℓ^2 norm of the coefficients. Assume that the WS decomposition of a transfer function G has been computed, and let $\alpha_{m,n} = \langle G, S^{-1}\Psi_{m,n} \rangle$ denote the coefficients. We choose the K largest coefficients, (whose indices we store in an index set $\mathcal{J}$), where $K = \#(\mathcal{J})$ is the smallest integer such that,

$$\frac{\sum_{(m,n)\in\mathcal{J}} |\alpha_{m,n}|^2}{\sum_{(m,n)} |\alpha_{m,n}|^2} \geq (1-\delta),$$

where $0 \leq \delta < 1$ is some predetermined tolerance. We now define a rational approximation, $G_{\mathcal{J}}$, to G as, $G_{\mathcal{J}}(s) = \sum_{(m,n)\in\mathcal{J}} G^{m,n}(s)$. Note that the results of Section 3.4.3 immediately provide a minimal state space realization of $G_{\mathcal{J}}$.

3.5.1 Approximation Error Bounds

The following lemma provides a bound on the approximation error using the scheme just described.

Lemma 3.2 *Let $\{x_n\}_n \in \mathbb{Z}$ be a frame for a Hilbert space $\mathcal{H}$, with frame bounds A and B. Assume $\|x_n\| = 1$, for all $n \in \mathbb{Z}$. For any $f \in \mathcal{H}$, define an approximation $\tilde{f}$ to f by,*

$$\tilde{f} = \sum_{n\in\mathcal{J}} \left\langle f, S^{-1}x_n \right\rangle x_n,$$

where J is an index set, chosen to satisfy

$$\sum_{n\in\mathcal{J}} \left|\left\langle f, S^{-1}x_n\right\rangle\right|^2 \geq (1-\delta)\sum_{n\in\mathbb{Z}} \left|\left\langle f, S^{-1}x_n\right\rangle\right|^2,$$

for $0 \leq \delta < 1$. Then,

$$\|f-\tilde{f}\|^2 \leq \delta\frac{B}{A}\|f\|^2.$$

Proof: By the frame condition,

$$B^{-1}\|f-\tilde{f}\|^2 \leq \sum_{k\in\mathbb{Z}} \left|\left\langle f-\tilde{f}, S^{-1}x_k\right\rangle\right|^2 \leq A^{-1}\|f-\tilde{f}\|^2.$$

Since, $f-\tilde{f} = \sum_{n\notin\mathcal{J}}\langle f, S^{-1}x_n\rangle x_n$, we have two coefficients sequences representing the expansion of $f-\tilde{f}$ with respect to the frame $\{x_n\}$. Therefore by Theorem 2.5,

$$\sum_{n\notin\mathcal{J}} \left|\left\langle f, S^{-1}x_n\right\rangle\right|^2 \geq \sum_{k\in\mathbb{Z}} \left|\left\langle f-\tilde{f}, S^{-1}x_k\right\rangle\right|^2.$$

Therefore,

$$\begin{aligned} B^{-1}\|f-\tilde{f}\|^2 &\leq \sum_{k\in\mathbb{Z}} \left|\left\langle f-\tilde{f}, S^{-1}x_k\right\rangle\right|^2 \\ &\leq \sum_{n\notin\mathcal{J}} \left|\left\langle f, S^{-1}x_n\right\rangle\right|^2 \\ &\leq \delta\sum_{k\in\mathbb{Z}} \left|\left\langle f, S^{-1}x_k\right\rangle\right|^2 \\ &\leq \delta A^{-1}\|f\|^2 \end{aligned}$$

from which the result follows. ■

Remark: The error bound in Lemma 3.2 is established in the general setting of frames in Hilbert spaces. When applied to the specific case of affine wavelet frames, the bound may prove to be quite conservative. This is because time-frequency localization properties of affine wavelets are not exploited in the lemma.

3.5.2 Example: Rational WS Approximation

As an example, consider the WS decomposition of the heat equation transfer function in Section 3.4.6. Letting $\delta = 0.4$ the above described scheme results in the selection

of 7 terms, with a corresponding normalized L^2 approximation error of 0.109, and an approximating system of dimension 22.

3.6 Some Motivation and Remarks in Retrospect

A point should be made regarding our motivation for constructing affine frames in the frequency (Laplace) domain as opposed to directly decomposing weighting patterns via affine wavelets in the time domain. First of all, our approach naturally preserves causality of the approximating system since each term in the WS expansion is in $H^2(\Pi^+)$ and therefore corresponds to the transfer function of a causal system. If one were to use affine wavelets in the time domain, special 'tricks' need to be applied to preserve causality since (even in the case of compactly supported wavelets), translations would eventually result in a noncausal wavelet. Secondly, there would be no mechanism for retaining rationality of the Laplace transforms of the individual wavelets, since translations (delays) prevent this.

Orthonormal Wavelet Bases for H^2 ?

In the beginning of this chapter, it was mentioned that there are certain difficulties associated with constructing 'well-behaved' orthonormal wavelet bases for $H^2(\Pi^+)$. To fully clarify this statement would require some description of the recently formalized subject of multiresolution analyses [Mal89c]. We forgo such a description and refer to [Dau88a] for a thorough treatment of the subject.

It is well-known that associated with every multiresolution analysis of $L^2(\mathbb{R})$ (or H^2), there exists an orthonormal wavelet basis. In fact, to date, all known examples of orthonormal wavelet bases can be associated with multiresolution analyses. In the case of L^2, it is possible, via multiresolution analyses, to construct orthonormal wavelet bases which are very well-behaved in the sense of the wavelets being arbitrarily smooth and being well-localized in time-frequency. However, if one considers the space $H^2(\Pi^+)$ instead, the situation is quite different. In fact it is not even possible to construct an

orthonormal basis of wavelets in $H^2(\Pi^+)$ with continuous and well localized Fourier transform via multiresolution analyses. More precisely, there is the following theorem of Jaffard [Jaf89, JL92].

Theorem 3.6 *There exists no orthonormal basis of wavelets for* $H^2(\Pi^+)$ *generated via the framework of multiresolution analyses, with an analyzing wavelet* ψ *such that* $\widehat{\psi}$ *is continuous and,*

$$\left|\widehat{\psi(\omega)}\right| \leq C\,|\omega|^{-\alpha} \quad \text{for any } \alpha > 1/2.$$

In particular this rules out smooth and well-localized orthonormal bases of rational wavelets for $H^2(\Pi^+)$. Although it has not been demonstrated that multiresolution analyses are the only means of constructing wavelet orthonormal bases, it remains an open problem to construct an orthonormal wavelet basis (even for $L^2(\mathbb{R})$) which does not arise in this way. The above theorem suggests that if one wishes to use rational analyzing wavelets, it is perhaps necessary to consider the more general setting of frames (including Riesz bases).

3.7 Summary

In this chapter we have introduced a new decomposition (which we refer to as a *wavelet system* (WS) *decomposition*) of the Hardy space $H^2(\Pi^+)$, and examined some properties of this decomposition.

The main result of this chapter is in Theorem 3.3 which states that functions in $H^2_{\mathbb{R}}(\Pi^+)$ may be represented as infinite sums of time-frequency localized, real-rational functions of bounded degree. Construction of the WS representation is based on an appropriate grouping of terms in an affine wavelet frame decomposition of $H^2(\Pi^+)$, where the analyzing wavelet is real-rational. For a real-rational analyzing wavelet of degree N the terms in a WS expansion are either of degree N or $2N$. From a systems viewpoint, WS decompositions are representations of causal LTI systems as infinite parallel connections of causal, time-frequency localized, finite-dimensional systems

of dimension bounded by $2N$. Theorem 3.4 gives a characterization of all rational analyzing wavelets for $H^2(\Pi^+)$, and demonstrates the large amount of freedom offered by frame theory for the selection of 'basis' functions.

WS decomposition naturally leads to methods for constructing rational approximations to nonrational transfer functions in $H^2(\Pi^+)$. Criteria for selecting a finite number of terms from the infinite wavelet system expansion rely on compactness of representation which arises due to time-frequency localization properties of the wavelet systems. Coarse bounds on the L^2 approximation error were established, for one particular selection criterion. It was also shown that state-space realizations of WS approximations are easily generated from a minimal state-space realization of the analyzing wavelet. Furthermore, easily verified conditions for the minimality of such realizations were derived. Much work remains to be done to understand the approach proposed here against the background of prior work on L^2 and H^∞ approximation theory (c.f. [GLP91b, GLP90, GLP91a, Bar87]).

Chapter 4

System Identification Using Wavelet System Models

In this chapter we discuss the use of wavelet system representations for the purpose of identification of an unknown causal linear time-invariant system. The problem of identification may be formulated as the determination of a system model representing the essential aspects of an existing system (or a system to be constructed) and presenting knowledge of that system in usable form [Eyk74]. For a slightly more concrete definition in the present context, consider a linear system of the form shown in Figure 4.1, where $h(\cdot)$ is the weighting pattern (impulse response), $u(\cdot)$ is the input, $y(\cdot)$ is the output, and $v(\cdot)$, is a disturbance (noise). In reference to Figure 4.1, system

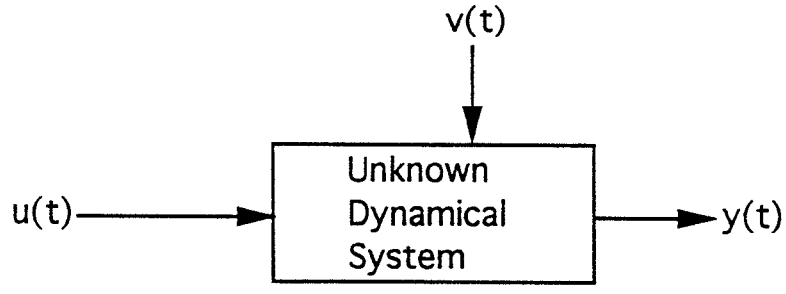

Figure 4.1: Open loop setting for system identification.

identification deals with the problem of constructing usable mathematical models of the system h, based on observed data (u and y). There exists a vast collection of literature devoted to the subject of system identification which we do not attempt to review here. A number of good survey papers and books with extensive references have been written on various aspects of the subject which we refer the reader to for further details (see e.g. [Eyk74, Lju87, UR90, Str81, Wel81, You81]). Here we only review some of the basic philosophy of system identification with particular emphasis on the choice of model sets. We discuss in some detail the role which wavelet system representations can play in system identification and highlight some of the resulting benefits by means of examples. Here we treat truncated WS representations as linear-in-parameters, black-box model sets for system identification. A key feature of WS models, is time-frequency localization which provides a convenient means of incorporating time and frequency domain *a priori* knowledge in the formal properties of a parametric model. Our use of truncated WS representations is close in spirit to the use of truncated Laguerre-Fourier series as rational parametric models. Laguerre filters form a class of orthonormal bases for $H^2(\Pi^+)$, and have received considerable attention in the areas of rational approximation and system identification. We make both qualitative and numerical comparisons of some key properties of WS models and Laguerre models. The two examples considered in the numerical comparisons are: (1) approximation of 'cochlear' filter transfer function and, (2) approximation of a second-order system with delay. Numerical results of these two examples suggest that the performance of WS models may be far superior to that of Laguerre models for an important class of systems.

4.1 Overview of System Identification

Among the various methods for system identification, a clear distinction may be made between parametric and non parametric techniques. We briefly outline some of the essential ideas of both nonparametric and parametric identification identification.

4.1.1 Nonparametric Identification Methods

As opposed to parametric methods which attempt to estimate parameters of some given system structure, nonparametric methods deal with estimating points on an unparameterized system model. In the time-domain, nonparametric identification attempts to estimate the impulse response of an unknown system. The essential relationship on which nonparametric impulse response estimation is based is,

$$R_{uy}(\tau) = (h * R_{uu})(\tau), \tag{4.1.1}$$

where R_{uu} is the autocorrelation function of the input u, and R_{uy}, is the cross-correlation function of the input u, and the output y. Frequency-domain nonparametric identification deals with estimation of the transfer function of an unknown system, and is in general based upon the frequency-domain expression of Equation 4.1.1:

$$S_{uy}(i\omega) = H(i\omega)S_{uu}(i\omega). \tag{4.1.2}$$

In Equation 4.1.2 S_{uu} and S_{uy} are the spectrum and cross-spectrum respectively obtained via the Fourier transform of R_{uu} and R_{uy}, and $H(i\omega)$ is the frequency response of the system.

The methods of nonparametric identification are primarily concerned with the estimation of the functions R_{uu} and R_{uy} (time-domain), or S_{uu} and S_{uy} (frequency-domain). For a survey of some of these techniques see [Wel81].

Due to the current emphasis on control synthesis and design tools which rely on parametric models, it is often necessary to construct a parametric model from the results of nonparametric identification. We will discuss the use of wavelet system representations for the purpose of generating parametric models from nonparametric forms in Section 4.2.2.

4.1.2 Parametric Identification Methods

The basic methodology of parametric identification consists of the following four steps which are depicted in Figure 4.2 (adapted from [Lju87]).

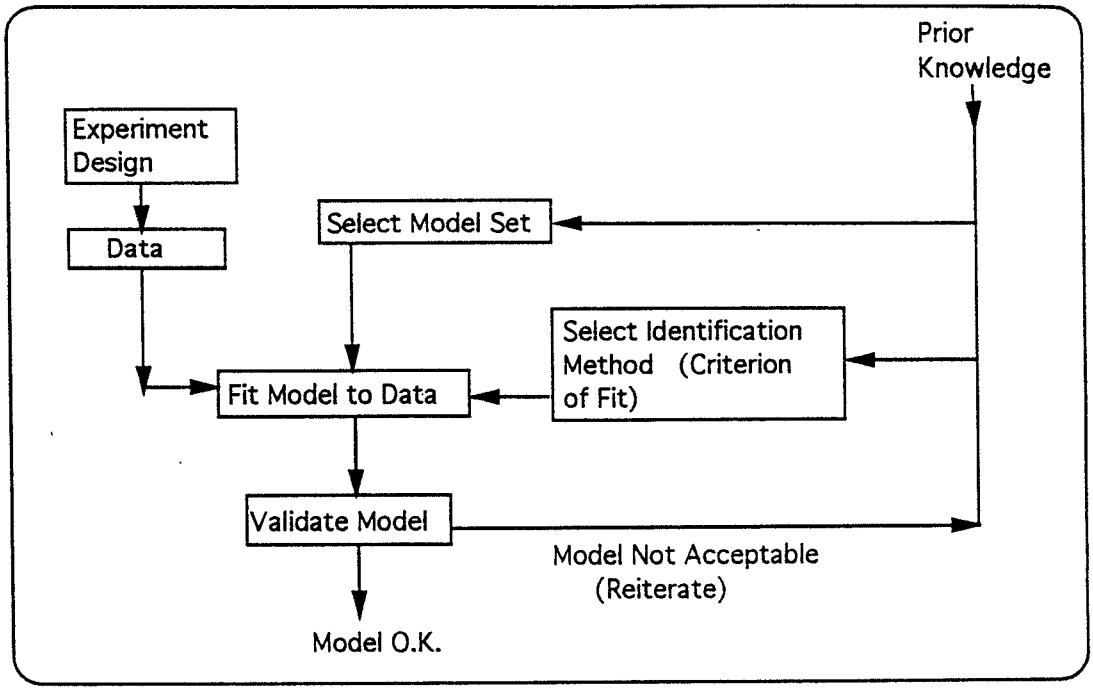

Figure 4.2: Parametric system identification loop.

Experiment design and collection of data. An essential property of data collected for the purpose of identification is that it be 'informative enough' for the construction of a reliable model. The imprecise notion of data which is 'informative enough' may be precisely formulated with respect to a given model set (see [Lju87]). A well designed identification experiment is one which results in the collection of such informative data.

Selection of a (parameterized) model set. For parametric identification, a family of parameterized candidate models must be selected within which the search for a suitable model is to be made. It has often been noted that selection of an appropriate model set is the most important as well as the most difficult step of the identification process. Choosing a good model set for a particular problem involves incorporating a combination of *a priori* knowledge and engineering intuition into the formal properties of the chosen collection of models.

Selection of identification method. A large proportion of the system identification literature has been devoted to design and selection of identification methods. A key feature of every identification method is the particular criterion that is chosen to make precise the notion of which of the models in the model set 'best' represents the data. A very broad categorization of the variety of proposed identification methods would lead us to select between techniques which treat the problem in either the deterministic or the stochastic settings, and also select between time-domain and frequency-domain methods. Once again we give reference to the survey papers [Lju87, UR90, Str81, Wel81, You81] for further detail.

Model validation. Having selected a model from the model set according to the criterion of fit defined by the selected identification method, model validation is the process of determining how well the model describes the unknown system based on further experiments. Following model validation the identified model is either accepted or rejected. If the model is rejected, the identification process may be repeated, possibly with new data, a different model set, and a different identification method.

Here attention is largely restricted to the problem of selecting a suitable model set as this is where wavelet system representation provides a new approach. We shall consider only models of the form commonly known as *black box models.* Parameters of a black box model have no real physical significance in relation to the physical system being modeled. Black box model parameters should be viewed as a means of for approximating the input-output behavior of the system.

4.2 Parametric Identification Using Wavelet System Model Sets

As mentioned above, the importance and difficulty of selecting an appropriate model set has often been noted. The difficulty lies in first developing *a priori* knowledge and engineering insight to recognize what are the relevant aspects of the unknown

system that should be captured by the identified model, and then incorporating this knowledge into the choice of a model set. It is necessary that the model set be 'rich' enough to capture the relevant aspects of the system while, at the same time, it is important that the complexity of the model be kept as low as possible. In this section we discuss how model sets which consist of appropriately truncated wavelet system representations, can be used to incorporate certain forms of *a priori* knowledge, namely joint time-frequency information about the systems' behavior. The manner in which wavelet system representations are used here is very close in spirit to the use of truncated Laguerre representations in system identification (c.f. [Mak90a, Mak90b, Wah91, Par91]. We discuss some of the key similarities and differences in these two approaches.

From Chapter 3, we know that any transfer function $G \in \mathrm{H}^2_{\mathbb{R}}(\Pi^+)$ may be represented by its WS decomposition,

$$G(s) = \sum_{m\in\mathbb{Z}} \sum_{n=0}^{\infty} G^{m,n}(s), \tag{4.2.3}$$

where $G^{m,n}(s)$ are the wavelet system transfer functions obtained via the wavelet decomposition of G with respect to a real-rational analyzing wavelet $\Psi \in \mathrm{RH}^2(\Pi^+)$. If we rewrite Equation 4.2.3 as,

$$\begin{aligned} G(s) &= \sum_{m\in\mathbb{Z}} \alpha_{m,0}\Psi_{m,0}(s) + \sum_{n=1}^{\infty} [\alpha_{m,n}\Psi_{m,n}(s) + \overline{\alpha_{m,n}}\Psi_{m,-n}(s)] \\ &= \sum_{m\in\mathbb{Z}} \sum_{n=0}^{\infty} G^{m,n}(s;\alpha), \end{aligned} \tag{4.2.4}$$

we see that this is precisely a parametric model for transfer functions in $\mathrm{H}^2_{\mathbb{R}}(\Pi^+)$, where the parameters are the wavelet expansion coefficients $\{\alpha_{m,n}\}_{m\in\mathbb{Z},\ n\in\mathbb{Z}^+}$. From a computational point of view, it is perhaps easier to separate the real and imaginary parts of each WS transfer function $G^{m,n}(s)$, and write,

$$\begin{aligned} \Re e\ G^{m,n} &= \Re e\ \alpha\ \Re e\ (\Psi_{m,n} + \Psi_{m,-n}) - \mathcal{I}m\ \alpha\ \mathcal{I}m\ (\Psi_{m,n} - \Psi_{m,-n}) \\ \mathcal{I}m\ G^{m,n} &= \Re e\ \alpha\ \mathcal{I}m\ (\Psi_{m,n} + \Psi_{m,-n}) + \mathcal{I}m\ \alpha\ \Re e\ (\Psi_{m,n} - \Psi_{m,-n}), \end{aligned}$$

since the coefficients and functions appearing in the expressions are then real-valued.

In practice of course it is necessary to select a truncation of the model in (4.2.4) for use as a model set for identification purposes. That is, we consider model sets of the form

$$\mathcal{M}^* = \left\{ \mathcal{M}(\alpha) = \sum_{m,n \in \mathcal{J}} G^{m,n}(s;\alpha) \ : \ \alpha \in \mathcal{D} \subset \ell^2(\mathbb{Z}^2) \right\} \tag{4.2.5}$$

and then select an appropriate parameter estimation technique to estimate the parameters α based on observed data. We will not discuss any of the possible choices for parameter estimation using wavelet system models. It should be noted however that since the parameters in the WS model appear linearly, it is possible to use least-squares techniques (see [Lju87] for a treatment of many of the available choices). Models such as this are often referred to as *linear-in -parameters* models.

As we shall see below, it is in the selection of this truncation, that certain forms of *a priori* knowledge and engineering intuition may be incorporated.

4.2.1 Incorporating A Priori Knowledge in WS Model Sets

Here we consider two forms of *a priori* knowledge which are commonly used in system identification: (1) knowledge of important frequency bands (frequency-domain), (2) knowledge of delays and time constants present in the system (time-domain). These two forms of *a priori* information are often treated separately in choosing model sets for identification. However, in the case of time-frequency localized model sets, such as given by WS representations, there is a natural mechanism for treating time-domain and frequency-domain information simultaneously.

It is common practice in system identification to estimate parameters using some form of frequency weighting. That is, given some *a priori* knowledge or intuition regarding the frequencies which are important in the particular application, identification methods are designed so as to emphasize good models over these frequencies or frequency bands. One method of doing so involves the use of a frequency weighting function in the cost function associated with the particular identification method. For

example a scaler cost function of the form,

$$J(\theta) = \int_{\mathbb{R}} \left(\widetilde{G}(\omega;\theta) - G(\omega)\right) C(\omega) \overline{\left(\widetilde{G}(\omega;\theta) - G(\omega)\right)} d\omega,$$

may be used, where $C(\omega)$ is a frequency weighting function used to emphasize particular frequency bands. Other schemes for emphasizing good modeling in particular frequency bands involve e.g prefiltering of the data (see [Lju87]).

Another problem of some significance in system-identification, is the approximation of delays in the system. Systems with delays are of course infinite-dimensional systems (with nonrational transfer functions). In such cases finite-dimensional (rational) approximations are required. A priori knowledge of time-delays can be incorporated into certain rational model structures such as Laguerre models which we discuss in Section 4.3, and WS models as will be discussed later.

The most important property of wavelet system representations in the context of black box models, is that they provide a straightforward means of capturing time-varying frequency behavior. Since each wavelet system transfer function $G^{m,n}$ is localized in time-frequency on rectangles $\mathcal{Q}_{m,n}$, we can define regions of time-frequency on which we would like to concentrate our model set. Figure 4.3 graphically illustrates the various ways in which *a priori* time-frequency information can be incorporated into a model.

In this section we discuss the use of *a priori* knowledge in WS models from the point of view of time-frequency localization. This point of view is useful in developing an intuitive understanding. In Section 4.5, *a priori* knowledge in WS models is discussed from the slightly more concrete point of view of pole-placement.

Time-Domain Information

Delays: Consider a system with impulse response $h(\cdot) \in \mathrm{L}^2(0,\infty)$ which includes a delay τ; i.e.

$$h(t) = 0, \quad \text{for} \quad t < \tau.$$

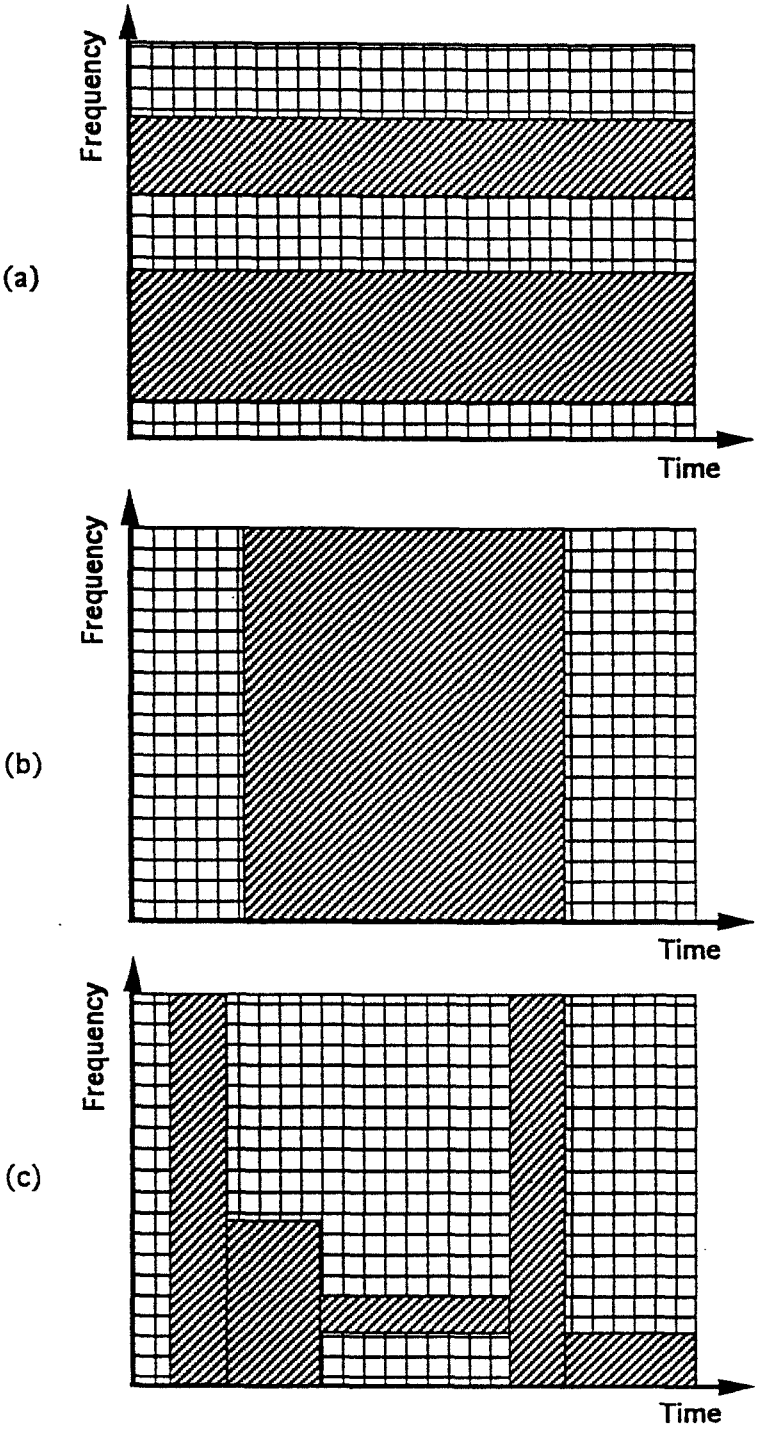

Figure 4.3: Time-Frequency weighting schemes: (a) Frequency weighting, (b) Time weighting: Delays and time constants, (c) Joint time-frequency weighting.

Assuming we have some *a priori* knowledge or estimate of τ, this knowledge can be incorporated in a WS model by only including dilation indices m such that $R(\Psi_{m,n}) \bigcap [0,\tau] = \emptyset$, where $R(\Psi_{m,n})$ is the time concentration of the wavelet $\Psi_{m,n}$ (c.f. (3.4.14)). Such a choice concentrates the model outside the time interval $[0,\tau]$.

Time Constants: Knowledge of dominant time constants of the system to be approximated is approximately the knowledge of the time-concentration of the impulse response. A priori information regarding time-constants may also be used in the selection of dilation indices m, to include in the WS model.

Remark: Note that since dilations are used to represent both delays and time constants, it is reasonable to expect that there may arise situations where these two goals are conflicting. This is in fact the case, as will be shown in Section 4.5. A similar situation arises in the case of Laguerre models as well.

Frequency-Domain

Knowledge of important frequency bands is easily utilized in a WS model by simply choosing translation indices n such that the frequency concentrations $\Omega(\Psi_{m,n})$, 'cover' the frequencies of intertest.

Joint Time-Frequency Space

In the case of physical dynamical systems, the impulse response in often best described in terms of its *time-varying frequency content.* This point is best illustrated by means of the "typical" impulse response shown in Figure 4.4 (a). It is clear that high-frequency components of this impulse response are localized near the origin. Also away from the origin, we see primarily low-frequency behavior, i.e high frequency components are associated with short time constants and longer time constants are associated with low frequency behavior. This is in fact the form of time-frequency localization that arises in WS models (see Figure 3.8). Once again this can be used

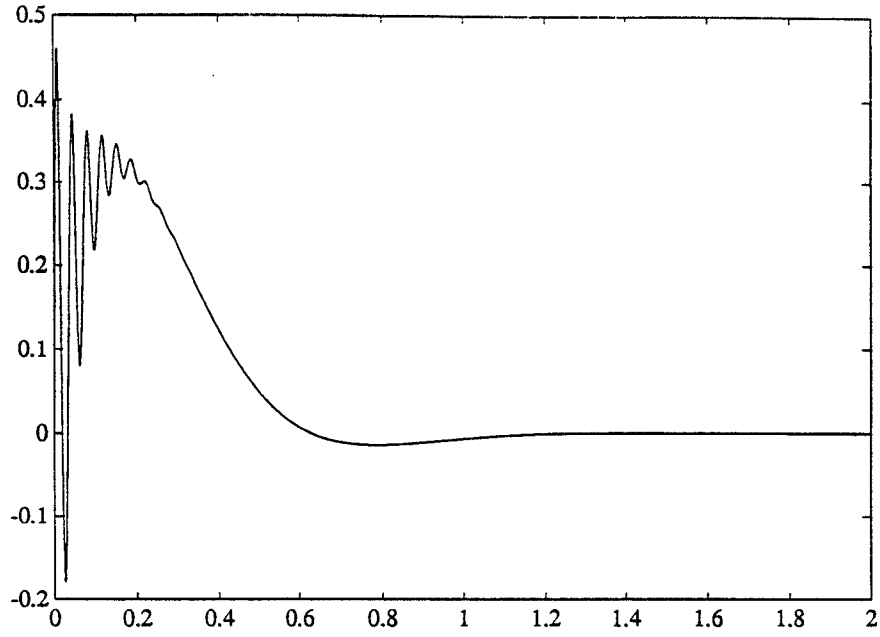

Figure 4.4: Impulse response exhibiting time-varying frequency content.

to explicitly determine the choice of dilations and translations (indices (m, n)) to be included in the model.

4.2.2 Fitting WS Models to Nonparametric Models

Wavelet system models can also be used to construct parametric models based on the results of a nonparametric identification procedure. In particular, given a nonparametric transfer function estimate $\widetilde{G}_{NP}$, we can 'fit' a parametric WS model to $\widetilde{G}_{NP}$ by computing the decomposition,

$$\widetilde{G}_{WS} = \sum_{(m,n)\in\mathcal{J}} \widetilde{G}_{NP}^{m,n}.$$

In fact, the nonparametric model $\widetilde{G}_{NP}$, can provide precisely the type of *a priori* knowledge about the time-frequency content of system, that is required to make a sensible choice of the index set $\mathcal{J}$, as discussed in Section 4.2.1. We will illustrate the use of this technique by example in Section 4.7.1.

4.3 Laguerre Decompositions

Laguerre functions have been studied extensively in the contexts of system identification and approximation of infinite-dimensional systems. The use of Laguerre decompositions in this context is very close to the spirit of our work using wavelet system decompositions and it is worthwhile to make an assessment of some of the key similarities and differences.

We begin by reviewing some of the basic properties of Laguerre polynomials the associated orthonormal bases of $L^2(0,\infty)$ (and consequently $H^2(\Pi^+)$). A thorough treatment of this subject may be found for instance in the book of Szego [Sze39].

4.3.1 Laguerre Polynomials and Orthonormal Bases

The classical Laguerre polynomials $L_m(t)$ are defined by,

$$L_m(t) = \frac{e^t}{m!}\frac{d^m}{dt^m}(t^m e^{-t}), \quad m = 0, 1, \ldots \tag{4.3.6}$$

If we define,

$$\phi_m(t) = e^{-t/2} L_m(t),$$

we have the following well known results.

Theorem 4.1 (Szego[Sze39])

(1) The Laguerre functions $\{\phi_m\}_{m=0}^{\infty}$ *form an orthonormal basis for* $L^2(0,\infty)$.

(2) The Laguerre functions $\{\phi_m\}_{m=0}^{\infty}$ *are dense in* $L^1(0,\infty)$.

(3) For all $t \geq 0$,

$$|\phi_m(t)| \leq 1, \quad m = 0, 1, 2, \ldots \tag{4.3.7}$$

(4) For any fixed $t_0 > 0$,

$$\max_{t \geq t_0} |\phi_m(t)| = O(m^{-1/4}).$$

As a natural modification of the classical Laguerre functions, let,

$$\phi_m^p(t) = \sqrt{2p}e^{-pt}L_m(2pt), \quad p > 0; \quad m = 0, 1, 2, \ldots$$

Then it follows from Theorem 4.1 that the sequence $\{\phi_m^p\}_{m=0}^{\infty}$ is an orthonormal basis for $\mathrm{L}^2(0,\infty)$, and that properties analogous to those listed in the Theorem 4.1 can be derived. The constant $p > 0$ is known as the *Laguerre shift parameter*, for reasons which will be clarified in Section 4.6.2.

Remark: Note that ϕ_m^p is simply a dilation of ϕ_m by a factor of $2p$.

Hence we have the Fourier decomposition of $g \in \mathrm{L}^2(0,\infty)$ with respect to the Laguerre basis $\{\phi_m^p\}_{m=0}^{\infty}$,

$$g = \sum_{m=0}^{\infty} \langle g, \phi_m^p \rangle \, \phi_m^p. \tag{4.3.8}$$

Remark: Although convergence of the series (4.3.8) is in general only guaranteed in the L^2 sense, convergence in other norms (e.g. $\|\cdot\|_1$, $\|\cdot\|_\infty$) can be established under suitable hypotheses on g, as will be mentioned later.

Laguerre Function Bases for $\mathrm{H}^2(\Pi^+)$

Taking the Laplace transform of ϕ_m^p, let

$$\Phi_m^p(s) = (\mathcal{L}\phi_m^p)(s) = \frac{\sqrt{2p}}{s+p}\left(\frac{s-p}{s+p}\right)^m, \quad m = 0, 1, 2, \ldots. \tag{4.3.9}$$

By the Paley-Wiener theorem and Parseval's theorem, $\{\Phi_m^p\}_{m=0}^{\infty}$, is an orthonormal basis for $\mathrm{H}^2(\Pi^+)$. Hence for any $G \in \mathrm{H}^2(\Pi^+)$,

$$G = \sum_{m=0}^{\infty} c_m^p(G)\frac{\sqrt{2p}}{s+p}\left(\frac{s-p}{s+p}\right)^m, \tag{4.3.10}$$

where the coefficients $c_m^p(G)$, are given by the appropriate inner-products.

Remark: The Laguerre series representation (4.3.10) is a decomposition of any transfer function in $\mathrm{H}^2(\Pi^+)$ via rational transfer functions with a *single real pole* $-p < 0$, with increasing multiplicity. This fact may cause slow convergence of the series (4.3.10) for certain classes of transfer functions as described in the next section.

4.4 A Priori Knowledge in Laguerre Models

We briefly review the mechanisms available for the incorporation of *a priori* information in Laguerre models. The essential forms of prior information that may be used in Laguerre models are: (1)knowledge of time delays, and (2) knowledge of dominant time-constants.

4.4.1 Representation of Delays in Laguerre Models

It has often been noted that Laguerre models are suitable for representing delays (c.f. [Mak90a, Par91, DZP90]). To understand how time delay information may be incorporated in a Laguerre model, let us introduce the following equivalent definition of the Laguerre basis which is given in terms of a time-domain shift operator (c.f. [Mak90a]).

Define $\mathbf{T}$

$$\mathbf{T} = (V - p\mathbb{I})(V + p\mathbb{I})^{-1},$$

where $p > 0$, and V is the infinitesimal generator of the semigroup $\{T_\tau\}_{\tau \geq 0}$ of all right shifts on $\mathrm{L}^2(0, \infty)$, i.e.

$$(T_\tau f)(t) = \begin{cases} 0 & \text{for } t < \tau \\ f(t-\tau) & \text{for } t \geq \tau \end{cases}$$

and V, is defined by,

$$Vf = \lim_{\tau \downarrow 0} \frac{1}{\tau}(T_\tau - \mathbb{I})f,$$

where the limit is in the strong sense. Thus if f is absolutely continuous with $f(0) = 0$, $Vf = -df/dt$. The operator $\mathbf{T}$ is called the cogenerator of the semigroup $\{T_\tau\}_{\tau \geq 0}$. $\mathbf{T}$ is a shift operator in the sense that,

$$\mathbf{T} \quad \text{is an isometry,}$$

$$\text{and} \quad (\mathbf{T}^*)^n \to 0, \text{ strongly as } n \to \infty.$$

$\mathbf{T}$ is called the *Laguerre shift* on $\mathrm{L}^2(0, \infty)$, and $\mathbf{T}$ and $\mathbf{T}^*$ are given explicitly by,

$$(\mathbf{T}f)(t) = f(t) - 2p \int_0^t e^{-p(t-\tau)} f(\tau) d\tau$$

$$(\mathbf{T}^* f)(t) \;=\; f(t) - 2p\int_t^\infty e^{-p(t-\tau)} f(\tau) d\tau$$

Now a second equivalent definition of the Laguerre functions ϕ_m^p may be made in terms of the Laguerre shift operator $\mathbf{T}$,

$$\phi_m^p(t) = \sqrt{2p}\mathbf{T}^m e^{-pt}. \tag{4.4.11}$$

Hence, the Laguerre functions are generated by right shifts of a single function, where the shift is defined by the Laguerre shift operator.

To see the effect of the Laguerre shift operator from a slightly different viewpoint [DZP90], note that

$$e^{-s\tau} = \lim_{N\to\infty}\left(\frac{1 - s\tau/2N}{1 + s\tau/2N}\right)^N. \tag{4.4.12}$$

Thus, the all-pass factors of degree m in the Laguerre filters $\Phi_m^p(s)$, can provide a good representation of a time delay τ. From (4.4.12), we see that the pole location p of the Laguerre model should be interpreted as $p = 2N/\tau$ for a good representation of a time delay τ by a N^{th} order Laguerre model. This is precisely the mechanism available for the incorporation of *a priori* knowledge of time-delays in a Laguerre model. Namely the pole location p and model order N may be selected so as to provide a good representation of the delay τ.

4.4.2 Use of Time Constant Information in Laguerre Models

As noted earlier a Laguerre model has only a single real left half plane pole at $-p$. Thus in representing transfer function G with a single dominant pole, it is reasonable to expect that knowledge of the dominant pole of G can be incorporated into a Laguerre model via the selection of the Laguerre pole $-p$. It is also reasonable to expect slow convergence of the series (4.3.10) if G has a highly resonant dominating pole.

To make the above statements more precise, consider the linear fractional transformation,

$$z = \frac{s+p}{s-p} \Longleftrightarrow s = p\frac{z+1}{z-1},$$

which is a conformal mapping of the left half-plane Π^-, onto the open unit disk. Let G be a finite-dimensional transfer function with poles $\{\gamma_k\}$. It can be shown (see e.g. [Wah91]) that in this case, the rate of convergence of the Laguerre series (4.3.10) is governed by the magnitude of the z-plane poles,

$$\frac{\gamma_k + p}{\gamma_k - p}, \tag{4.4.13}$$

of the discrete-time system $G\left(p(z+1)/(z-1)\right)$. In particular convergence will be slow for z-plane poles close to the unit circle. For any given pole γ_k of $G(s)$,

$$p^* = |\gamma_k| = \arg\min \frac{\gamma_k + p}{\gamma_k - p}.$$

The minimum value is determined by,

$$\begin{aligned} \left|\frac{\gamma_k + |\gamma_k|}{\gamma_k - |\gamma_k|}\right|^2 &= \frac{|\gamma_k| + \Re e\ \gamma_k}{|\gamma_k| - \Re e\ \gamma_k} \\ &= \frac{1 + \cos(\theta)}{1 - \cos(\theta)} = \cot^2(\theta/2), \end{aligned}$$

where $\gamma_k = |\gamma_k|\, e^{i\theta}$. Hence, the minimum value is given by,

$$\left|\frac{\gamma_k + p^*}{\gamma_k - p^*}\right| = \left|\cot\left(\arg(\gamma_k)/2\right)\right|. \tag{4.4.14}$$

Thus there exists a notion of an 'optimal' choice of the Laguerre shift parameter p to capture the effect of dominant poles. Consequently, we may make the following observations regarding the the choice of p.

(1) For a high rate of convergence of the Laguerre series, p should be chosen such that $1/p$ is close to the dominating time-constants of the system to be approximated.

(2) If the system to be approximated possesses highly resonant dominant poles, i.e. poorly damped complex poles, convergence of the series will be slow, since the Laguerre pole is on the real-axis. This can also be seen from (4.4.14), noting that for a highly resonant pole γ_k, $\arg(\gamma_k) \approx \pi/2$.

(3) If the system G has a wide range of time-constants, resulting in the poles being scattered, convergence will be slow. This is because in this case, for any choice

of p, $|\gamma_k - p|$ will be large for some k, and consequently there will be z-plane poles close to the unit circle.

Thus knowledge of dominant time-constants may be incorporated in a Laguerre model via the choice of the Laguerre shift parameter p. Clearly difficulties with the rate of convergence arise when there is more than one time-constant involved and these are widely separated.

Extended Laguerre Series and Frames

It has been suggested [Wah91] that for systems with m, dispersed time-constants, the rate of convergence may be improved by considering models of the form,

$$G(s) \approx \sum_{j=1}^{m} \sum_{k=0}^{n_j-1} c_k^{p_j}(G) \frac{\sqrt{2p_j}}{s+p_j} \left(\frac{s-p_j}{s+p_j} \right)^k, \tag{4.4.15}$$

where the *a priori* knowledge of time constants has been incorporated in the choice of the m parameters p_j. It was also suggested in [Wah91] that improved convergence rates for systems with highly resonant poles may be obtained by replacing the Laguerre filters with the so-called Kautz filters which have a single pair of complex poles.

The improved Laguerre model (4.4.15), must be treated as an *ad hoc* formulation if one is restricted to the setting of orthonormal bases. However it is possible to make sense of such a formulation using frame theory as is stated in the following theorem.

Theorem 4.2 *Let $\{p_1, \ldots, p_K\}$, be a finite collection of positive constants, and let $\Phi_m^{p_j}$, denote the mth order Laguerre function with Laguerre shift parameter p_j. Then the doubly-indexed sequence of functions $\left\{\Phi_m^{p_j};\ j = 1, \ldots, K;\ m = 0, 1, 2, \ldots\right\}$, is a tight frame for $\mathrm{H}^2(\Pi^+)$ with frame bounds $A = B = K$.*

Proof: Since for any fixed j, $\left\{\Phi_m^{p_j}\right\}_{m=0}^{\infty}$, is an orthonormal basis for $\mathrm{H}^2(\Pi^+)$,

$$\sum_{m=0}^{\infty} \left| \left\langle F, \Phi_m^{p_j} \right\rangle \right|^2 = \|F\|^2,\ \forall F \in \mathrm{H}^2(\Pi^+), j = 1, \ldots, K.$$

Thus

$$\sum_{j=1}^{K} \sum_{m=0}^{\infty} \left| \left\langle F, \Phi_m^{p_j} \right\rangle \right|^2 = K\|F\|^2. \quad \blacksquare$$

Hence any $F \in \mathrm{H}^2(\Pi^+)$, has the representation,

$$\begin{aligned} F &= \sum_{j=1}^{K} \sum_{m=0}^{\infty} \left\langle F, S^{-1}\Phi_m^{p_j} \right\rangle \Phi_m^{p_j} \\ &= K^{-1} \sum_{j=1}^{K} \sum_{m=0}^{\infty} \left\langle F, \Phi_m^{p_j} \right\rangle \Phi_m^{p_j}. \end{aligned} \tag{4.4.16}$$

We shall refer to the representation (4.4.16) as an *extended Laguerre series (ELS) representation.* Clearly the ELS representation is not unique.

Remark: It is convenient at this point to note an important similarity between the extended Laguerre sedries (4.4.16) and wavelet system representations. As noted earlier Φ_m^p (see (4.3.9)) is simply a dilation of the function Φ_m^1 by a factor of $2p$. Furthermore in the last section it was shown that the Laguerre basis may be viewed as being generated via right shifts of a single function, where the shift is defined by the Laguerre shift operator. Consequently the extended Laguerre series (4.4.16) is a representation via dilates and shifts of a single function, where the dilation operator is as defined in Chapter 2, but the shift operator is now the Laguerre shift.

For Laguerre models, all *a priori* knowledge must be used in selection of the single parameter p. In particular for representation of a delay τ , we would like to choose $p = 2N/\tau$, where N is the order of the Laguerre model, and knowledge of a dominant time-constant T, leads us to choose $p = 1/T$. Clearly there may arise situations where these two goals are conflicting, for example in the case of a long time-delay τ, and a small time constant T, or vice-versa. Furthermore, it is clear that there is no direct mechanism for the use of frequency information in Laguerre models.

4.5 A Priori Knowledge in WS Models Revisited

In light of the description of *a priori* knowledge in Laguerre models, let us re-examine the use of *a priori* knowledge in WS models from the somewhat more concrete point of view of the poles of the model. Note that selection of the Laguerre shift parameter p, is actually a process of modifying the basis functions to suit the problem at hand.

A similar technique may be used in the case of WS models, as is discussed in Section 4.5.3.

4.5.1 Time Delays and Time Constants

As mentioned in Section 4.2.1, the effects of a time-delay τ, can be captured in a wavelet system model via the dilations. To make this statement more precise, consider the dilation operator D_a, on $\mathrm{L}^2(0,\infty)$, as defined in Section 2.2. In particular, for WS models, the appropriate dilations in the time domain are of the form $D_{a_0^{-m}}$. The adjoint $D^*_{a_0^{-m}}$, of this operator is simply $D_{a_0^m}$, since

$$\begin{aligned}\left\langle D_{a_0^{-m}} f, g \right\rangle &= \int_0^\infty a_0^{-m/2} f(a_0^{-m}t)\overline{g(t)}dt \\ &= \int_0^\infty f(t) a_0^{m/2}\overline{g(a_0^m t)}dt = \left\langle f, D_{a_0^m} g \right\rangle .\end{aligned}$$

Therefore the dilation operator is not a shift operator in the same sense as the Laguerre shift operator $\mathbf{T}$, since both $D_{a_0^{-m}}$ and $D^*_{a_0^{-m}}$ are ($\mathrm{L}^2(0,\infty)$) isometries. However, we can still view $D_{a_0^{-m}}$ as a shift operator in the following sense

$$\begin{aligned}\left(D_{a_0^{-m}}\psi\right)(t) &\longrightarrow 0 \text{ as } m \to \infty \qquad \forall t \in [0, t_1],\ t_1 > 0, \\ \left(D^*_{a_0^{-m}}\psi\right)(t) &\longrightarrow 0 \text{ as } m \to \infty \qquad \forall t \in [t_1, \infty],\ t_1 > \epsilon > 0,\end{aligned}$$

where ψ is the inverse Laplace transform of an admissible $\mathrm{H}^2(\Pi^+)$ analyzing wavelet. This shifting effect of the dilation operator is perhaps clearer if we look at time on a logarithmic scale since

$$a_0^{-m/2}\psi(\log a_0^{-m}t) = a_0^{-m/2}\psi(\log t - m\log a_0),$$

and we know that $\psi(0) = 0$, by admissibility.

For a given delay τ, the dead-time can be approximated arbitrarily well by a WS model. To see this let m, be the smallest integer such that $a_0^{-m}\tau < 1$. We can assume without loss of generality that $|\psi(t)|^2 < \epsilon t$, for $t < 1$, and $\epsilon > 0$. Recall that by the admissibility condition, $|\psi(t)|^2$, must decay at least as fast as t, near $t = 0$. Thus,

$$\int_0^\tau \left|a_0^{-m/2}\psi(a_0^{-m}t)\right|^2 dt = \int_0^{a_0^{-m}\tau} |\psi(t)|^2\, dt$$

$$\leq \epsilon \int_0^{a_0^{-m}\tau} t^2 dt = \frac{\epsilon}{2}\left(a_0^{-m}\tau\right)^2 \longrightarrow 0 \text{ as } m \to \infty.$$

So for good representations of the delay τ, we may select dilation indices m, such that

$$m \geq \frac{\log \tau}{\log a_0}.$$

As in the case of Laguerre models, there is a tradeoff between the representation of long delays and small time constants. The manner in which this tradeoff arises is precisely the same in the WS case as it was in the Laguerre case. This follows from the observation in Section 4.3.1 that the Laguerre function Φ_m^p is simply a dilation of Φ_m^1, by a factor of $2p$. Hence in both cases, dilations are chosen to represent time delays. The effect of dilations on time constants is easily seen by observing that if

$$\begin{aligned} |f(t)| &\leq Ce^{-kt}, \quad k > 0 \\ \text{then } |f(at)| &\leq Ce^{-kat}, \quad k, a > 0. \end{aligned}$$

Hence for small dilation factors a, as are required by both WS and Laguerre models for good representations of long delays, the time constant is large. Therefore convergence of the WS series will in general be slow in cases where the time constants are small and the delay is long.

It is clear from the above discussion that *a priori* information about a dominant time constant T may be incorporated in WS models by selecting dilation indices m, such that,

$$a_0^{-m} T_\Psi \approx T,$$

where T_Ψ, is the dominant time constant of the analyzing wavelet Ψ. This of course corresponds to placing the poles of the WS model on specific vertical lines in the left half-plane. Note that WS models allow us to incorporate several scattered time constants in this manner as well.

4.5.2 Dominant Frequencies

Prior knowledge of the frequencies associated with various time constants may also be utilized in WS models by appropriate selection of dilation indices n. Approximate

knowledge of time constants and associated frequencies corresponds to approximate knowledge of the pole locations. Using dilations and translations together, poles of a WS model may be placed close to the approximate poles of the system. In fact the poles of the WS model may be placed so that they cover a region in which the poles of the true system are thought to be.

4.5.3 Optimizing the Analyzing Wavelet

Thus far we have not really utilized the full flexibility of frame theory other than to construct decompositions in terms of rational analyzing wavelets. The underlying structure of a wavelet system decomposition consists of the analyzing wavelet Ψ, the dilation stepsize a_0, and the translation stepsize b_0. There exists a great deal of freedom in the choice of the triple (Ψ, a_0, b_0), within the restrictions of admissibility and rationality of Ψ and the sequence $\{\Psi_{m,n}\}$ forming a frame. Thus we can consider the problem of optimizing (Ψ, a_0, b_0), so as to suit the particular problem at hand. As mentioned earlier, this is essentially the idea in choosing the Laguerre shift parameter p, for the Laguerre basis.

For the sake of convenience and to clarify the discussion, we restrict discussion to the case where the analyzing wavelet Ψ is of McMillan degree $N = 2$, and has no zeros. Let $\{\gamma, \overline{\gamma}\}$ denote the poles of Ψ. Hence the poles of the WS transfer function $G^{m,n}$, are

$$\begin{array}{ll} a_0^{-m}(\gamma + inb_0) & a_0^{-m}(\overline{\gamma} + inb_0) \\ a_0^{-m}(\gamma - inb_0) & a_0^{-m}(\overline{\gamma} - inb_0) \end{array}$$

Assume that we have *a priori* knowledge of a pole ν of the system to be approximated. Then we can try to reflect this knowledge in a WS model by: (1) selecting dilation indices m such that,

$$a_0^{-m} \approx \frac{\Re e\ \nu}{\Re e\ \gamma}, \tag{4.5.17}$$

and (2) selecting translations corresponding translation indices n, such that

$$a_0^{-m} n b_0 \approx \mathcal{I}m\ \nu - a_0^{-m} \mathcal{I}m\ \gamma. \tag{4.5.18}$$

In general (4.5.17) and (4.5.18) will have only approximate solutions m and n. However we could also obtain exact solutions by modifying the frame $\Psi_{m,n}$ in the following manner. Assume a_0 is fixed.

(1) Select the pole γ, of the analyzing wavelet such that

$$\Re e\ \gamma = \Re e\ \nu. \tag{4.5.19}$$

Note that this involves simply dilating the analyzing wavelet Ψ, and therefore causes no problems with admissibility or forming frames.

(2) Select the translation stepsize b_0, such that (Ψ, a_0, b_0), generates an affine frame, and

$$n^* = b_0^{-1}\left(\mathcal{I}m\ \nu - Im\gamma\right), \tag{4.5.20}$$

for some integer n^*. Note that there always exists such solutions to (4.5.20) since by Theorem 2.6 there exists B_c, such that (Ψ, a_0, b_0), generates an affine frame for every $b_0 \in (0, B_c)$. Thus ,

$$b_0 = \frac{1}{n}\left(\mathcal{I}m\ \nu - Im\gamma\right) \in (0, B_c)$$

for $|n|$ large enough.

This procedure places a pole of G^{0,n^*} at ν.

Multiple time constants $(T_1, \ldots, T_k)$, may be handled by looking for solutions $(m_1, \ldots, m_k)$, to

$$\frac{1}{\log a_0}\log\left(-\Re e\ \gamma/T_j\right) = m_j, \quad j = 1, \ldots, k. \tag{4.5.21}$$

In general the above equations may have no exact solution and will therefore have to be solved in an approximate (e.g. least squares) sense. Another approach would be to match the longest time constant exactly according to the method described above for a single time constant, and then solve (4.5.21) approximately to represent the remaining time constants. Multiple frequencies associated with the time constants may be handled analogously.

A further level of optimization would be to tailor the form of the actual analyzing wavelet to suit the problem. Here again the flexibility of frame theory can be utilized. We will not discuss this approach here, but give reference to [CW90] for a discussion of these types of ideas.

4.6 WS versus Laguerre Decompositions

There exist many similarities and as well as differences between wavelet system models and Laguerre models. In this section we highlight some of these similarities and differences. A key similarity between wavelet system decompositions and Laguerre decompositions of $H^2_{\mathbb{R}}(\Pi^+)$, is that they both provide representations of $H^2_{\mathbb{R}}(\Pi^+)$ in terms of rational functions. Hence truncations of either of these representations give rational (H^2) approximations to transfer functions in $H^2_{\mathbb{R}}(\Pi^+)$. We restrict the following discussion to the class $H^2_{\mathbb{R}}(\Pi^+)$, as for all practical purposes this is the class of interest when dealing with real physical systems with transfer functions in $H^2(\Pi^+)$.

4.6.1 Parallel versus Series Decompositions

There exists an essential structural difference between wavelet system decompositions and Laguerre decompositions of $H^2_{\mathbb{R}}(\Pi^+)$. Wavelet system decompositions, as noted in Chapter 3, are inherently parallel decompositions in terms of finite-dimensional systems in the sense that every term in the series is a rational function of degree less than or equal to $2N$ where N is the McMillan degree of the analyzing wavelet $\Psi \in RH^2(\Pi^+)$. Figure 4.5 graphically illustrates this parallel decomposition. Laguerre decompositions (4.3.10), when viewed as parallel decompositions, consist of terms with unbounded MacMillan degree (see Figure 4.6). It is perhaps more natural to think of Laguerre decompositions as series decompositions via rational functions of fixed degree, in particular degree 1 (see Figure 4.7). This structural difference is important both from the point of view of identification and approximation. In the case of system identification, we give the following argument in favor of the parallel decomposition

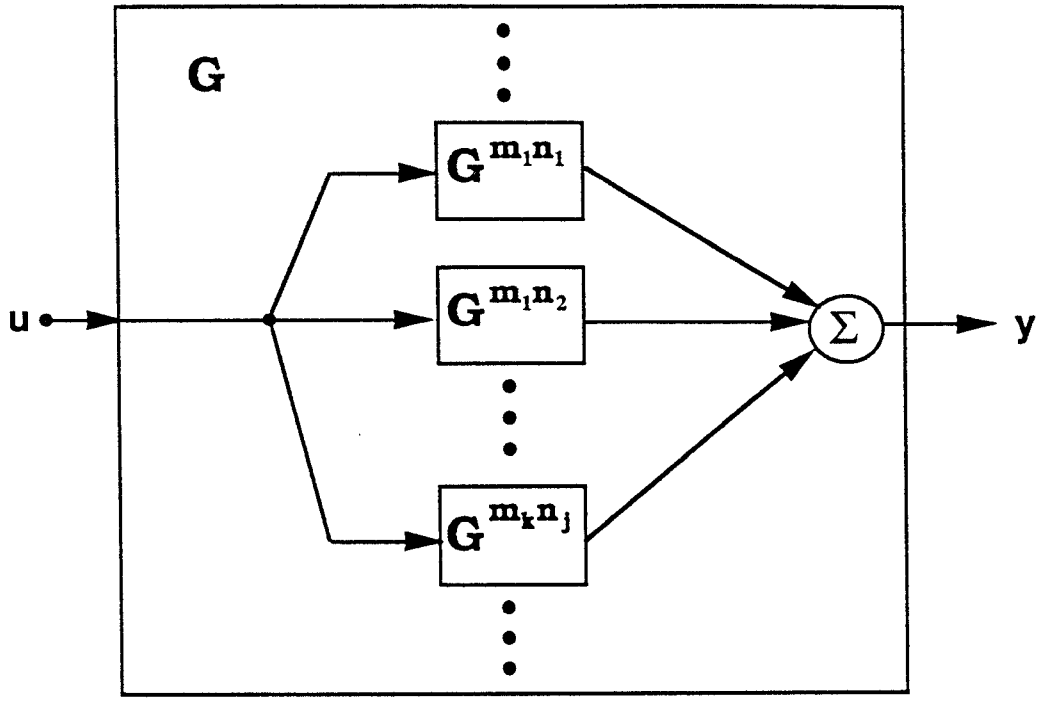

Figure 4.5: Parallel decomposition via WS representations.

structure of wavelet system representations. Let,

$$G_{WS}(s;\alpha^*) = \sum_{(m,n)\in\mathcal{J}} G^{m,n}(s,\alpha^*_{m,n}), \tag{4.6.22}$$

be the 'identified' wavelet system model of a unknown system G, i.e. α^* is the parameter vector obtained via a chosen identification method. Similarly let,

$$G_L(s;c^*) = \sum_{m=0}^{n-1} c^*_m \Phi^p_m(s) = \sum_{m=0}^{n-1} c^*_m \frac{\sqrt{2p}}{s+p}\left(\frac{s-p}{s+p}\right)^m, \tag{4.6.23}$$

be the identified Laguerre model of the same system. Let $\mathcal{D}_{WS}(\alpha^*)$ denote the set of indices of zero (or negligible) components of the parameter vector α^*, i.e.

$$\mathcal{D}_{WS}(\alpha^*) = \left\{(m,n) \;:\; \left|\alpha^*_{m,n}\right| < \epsilon;\ (m,n)\in\mathcal{J}\right\},\quad \epsilon \geq 0.$$

Similarly for the Laguerre model let,

$$\mathcal{D}_L(c^*) = \{m \;:\; |c^*_m| < \epsilon;\ m \in \{0,1,\ldots,n-1\}\},\quad \epsilon \geq 0.$$

Now we can ask the the question; is it possible to further reduce the order of the model given knowledge of the zero (negligible) coefficients ($\mathcal{D}_{WS}(\alpha^*)$ and $\mathcal{D}_L(c^*)$), without

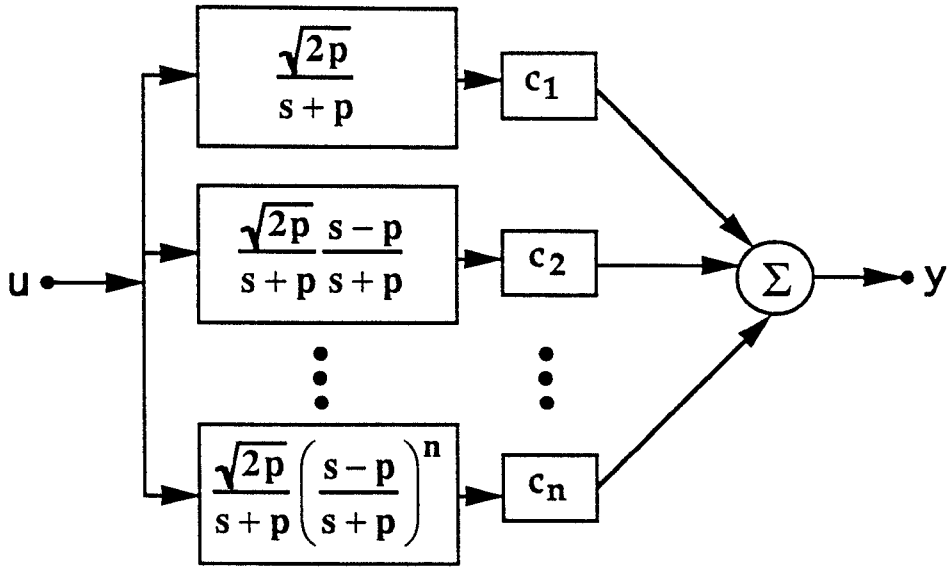

Figure 4.6: Laguerre representations in parallel form

adversely affecting the quality of the model? Clearly, in the case of the series structure of the Laguerre model, this is directly possible if and only if $n-1 \in \mathcal{D}_L(c^*)$. In that case the Laguerre model order is reduced at least from n to $n-1$. However, in the case of the WS model, the decoupled nature of the parallel structure allows us to reduce the model order by simply removing any terms $G^{m,n}$ with indices $(m,n) \in \mathcal{D}_{WS}(\alpha^*)$.

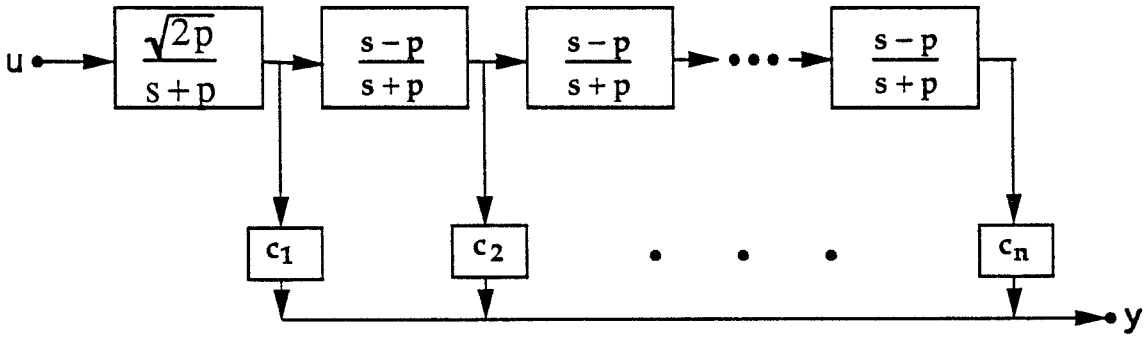

Figure 4.7: Series form of Laguerre representation

The resulting decrease in model order is

$$N \times |\{(m,n) \in \mathcal{D}_{WS}(\alpha^*) \ : \ n = 0\}| + 2N \times |\{(m,n) \in \mathcal{D}_{WS}(\alpha^*) \ : \ n \neq 0\}|,$$

where N is the McMillan degree of the analyzing wavelet. (Assuming the minimality conditions of 3.4.5 are satisfied.)

Hence in the case of WS models, it is possible to start with high-order models, and then reduce the model order after parameters have been estimated by simply removing terms corresponding to negligible parameter values.

4.6.2 A Priori Knowledge in WS Models versus Laguerre Models

A crucial basis for comparison of WS models and Laguerre models, is the manner in which each of these two techniques facilitate the incorporation of *a priori* information. A priori knowledge in these models was discussed in in Sections 4.2.1 and 4.5, in the WS case and in Section 4.4 for Laguerre models. The following is a qualitative list comparing *a priori* knowledge in WS models with *a priori* knowledge in Laguerre models.

(1) Both models facilitate the use of time constant and delay information. Furthermore both models suffer from a tradeoff between representing long delays and representing short time constants.

(2) There exists no mechanism for incorporating frequency information such as imaginary parts of poles in Laguerre models. Such information may be used in WS models in the selection of translations.

(3) WS models can incorporate knowledge of multiple time constants while Laguerre models may accurately represent only one.

(4) The only parameter of a Laguerre model is the Laguerre shift parameter p. This is the primary cause of any shortfalls of the Laguerre models. WS models, on the other hand, are extremely flexible. In selecting a WS model, one has the

freedom to choose: (1) dilation and translation indices, (2) frame parameters a_0, and b_0, (3)pole locations of the analyzing wavelet, and (3) the form of the analyzing wavelet. This flexibility can be utilized to adapt the model to a given problem.

4.6.3 Frames versus Orthonormal Laguerre Bases in $H^2(\Pi^+)$

Of some interest in this comparison of WS models and Laguerre models, are the consequences of using frames rather than orthonormal bases. The two formulations can be discussed in terms of ease of computation and 'robustness' of representation.

Given a particular (known) transfer function in $H^2_{\mathbb{R}}(\Pi^+)$, in general it is easier to compute the decomposition with respect to an orthonormal basis, than the decomposition with respect to a frame. In the specific case of Laguerre bases, the computation is even further simplified by the well known recursion formula for Laguerre polynomials, i.e.

$$L_k(t) = \frac{2k-1-t}{k} L_{k-1} - \frac{1-k}{k} L_{k-2}, \quad k \geq 2,$$

with $L_0(t) = 1$ and $L_1(t) = 1 - t$. For frames in general it is necessary to compute the decomposition via the inverse frame operator, except for in the case of tight frames where the computation is equivalent to that for a general orthonormal basis. However, for identification purposes, there is little or no computational advantage in using orthonormal systems since the parameters need to estimated via an identification method and not computed directly from knowledge of the transfer function. A possible exception to this is in the case where the model is is fit to a nonparametric model by explicitly computing the expansion coefficients as in [CW92].

From the discussion in Section 2.3.1, redundant frame representations are more robust with respect to perturbations in the coefficients than are orthonormal basis representations. From the point of view of identification, this is an important property since parameter estimates are subject to inaccuracies including the effects of numerical computation.

4.6.4 Convergence In Other Norms

One of the important properties of Laguerre bases is the property of being *uniformly bounded bases* (4.3.7). Uniform boundedness of the Laguerre bases is important in establishing conditions for convergence of the partial sums of the Laguerre series in norms other than $H^2(\Pi^+)$. Of particular significance for the purpose of robust control synthesis is convergence in the $H^\infty(\Pi^+)$norm. Convergence results in $H^\infty(\Pi^+)$, and $L^1(0,\infty)$, with emphasis on the rate of convergence are discussed in [Mak90a, Mak90b, GLP91b, Mak91], for Laguerre series representations. As yet we have no analogous results for WS representations, although there is reason to believe that suitable smoothness and decay hypotheses should lead to similar results.

4.7 Examples: WS vs Laguerre Decomposition

To illustrate some features of the comparison between Laguerre and WS models, we consider the following two examples. In these examples, we use the $H^2(\Pi^+)$ analyzing wavelet of Section 3.3.1, Example 1, with $\gamma = 5.0, \xi = 1.0$, and frame parameters $a_0 = 2.0, b_0 = 8.3$. The corresponding frame bounds are approximately $A = 4.6, B = 6.6$, which gives $B/A = 1.4$. The examples discussed below are based on approximating frequency responses using both the Laguerre and WS models. The method used to construct WS approximations in these examples is as follows. First a WS approximation is first computed using a high-order model. The lower-order approximations are then computed by sequentially selecting terms with the largest coefficients in the high-order approximation, and then refitting the corresponding rational functions to the data using singular value decomposition to solve the appropriate normal equations (c.f. remarks at the end of Section 2.4).

4.7.1 Rational Modeling of Cochlear Filters

Within the mammalian inner ear lies a key component of auditory system known as the cochlea. The cochlea performs much of the initial processing of acoustic signals.

The basilar membrane is a structure contained within the cochlea which roughly speaking performs a frequency analysis of the signals. The basilar membrane is often modeled as a bank of linear, constant-Q, bandpass filters. As a result of physiological experiments, nonparametric models have been constructed to describe the frequency response of these cochlear filters (see [YWS92]). For convenience in working with these filters, parametric models are used to approximate the frequency response. These models may be nonrational. However, it is also of considerable interest to construct integrated circuit implementations of these filters (c.f. [Mea89, LKTS92]). For circuit implementations of the cochlear filters, rational models are required. Figure 4.8, shows the frequency response of one of these filters.

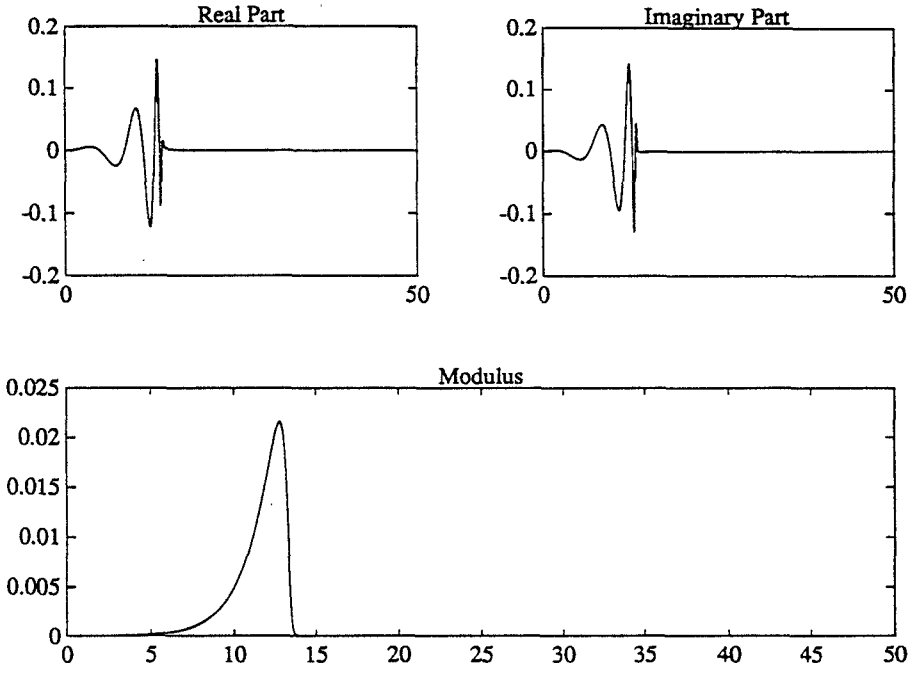

Figure 4.8: Frequency response of a cochlear filter.

In this Section we apply both WS models and Laguerre models to approximating the frequency response of the cochlear filters, and compare the results. For this example, 1000 samples of the frequency response from $\omega = 0$, to $\omega = 50$, were used in the approximation.

WS Approximation of Cochlear Filters

The nonparametric model shown in Figure 4.8, provides precisely the forms of frequency and time domain *a priori* information required to choose the initial dilation and translation indices to be used in a WS model. Having selected the appropriate dilation and translation indices, the resulting WS model (which may be of fairly high order) can then be fit to the data. Figures 4.9–4.10 show the results of this process. Figure 4.9 are three-dimensional and density plots of the magnitude of the coefficients of the resulting rational approximation to the cochlear filter. The approximation together with the original function and impulse response are shown in Figure 4.10. It is clear that the number of 'significant' coefficients is small. Thus to reduce the model order, we can systematicly select truncations of this high-order model by eliminating terms with small coefficients. In doing so, we generate a sequence of rational approximations to the transfer function of the cochlear filter. Figures 4.11 – 4.13 show the results of this process for different model orders N. The normalized (L^2) approximation error is plotted as a function of model order in Figure 4.17. It is clear that we can select a reasonably low-order rational approximation to the cochlear filter based on the approximation error. However, we can also ask the question; what are the key properties of the cochlear filters which should be captured by the model in order to call it a 'good' approximation. It has been suggested, (c.f. [Sha85a, Sha85b]) that three important properties of the the cochlear filters are: (i) location of the peak magnitude of the frequency response, (ii) the sharp cutoff for high frequencies, and (iii) rapid decay in the time domain. Due to the sharp cutoff for high frequencies, the decay in the time domain is governed by how the frequency response behaves as ω goes to zero. From Figures 4.11 – 4.13, we see that all of these three properties can be captured by rational WS approximations of fairly low order.

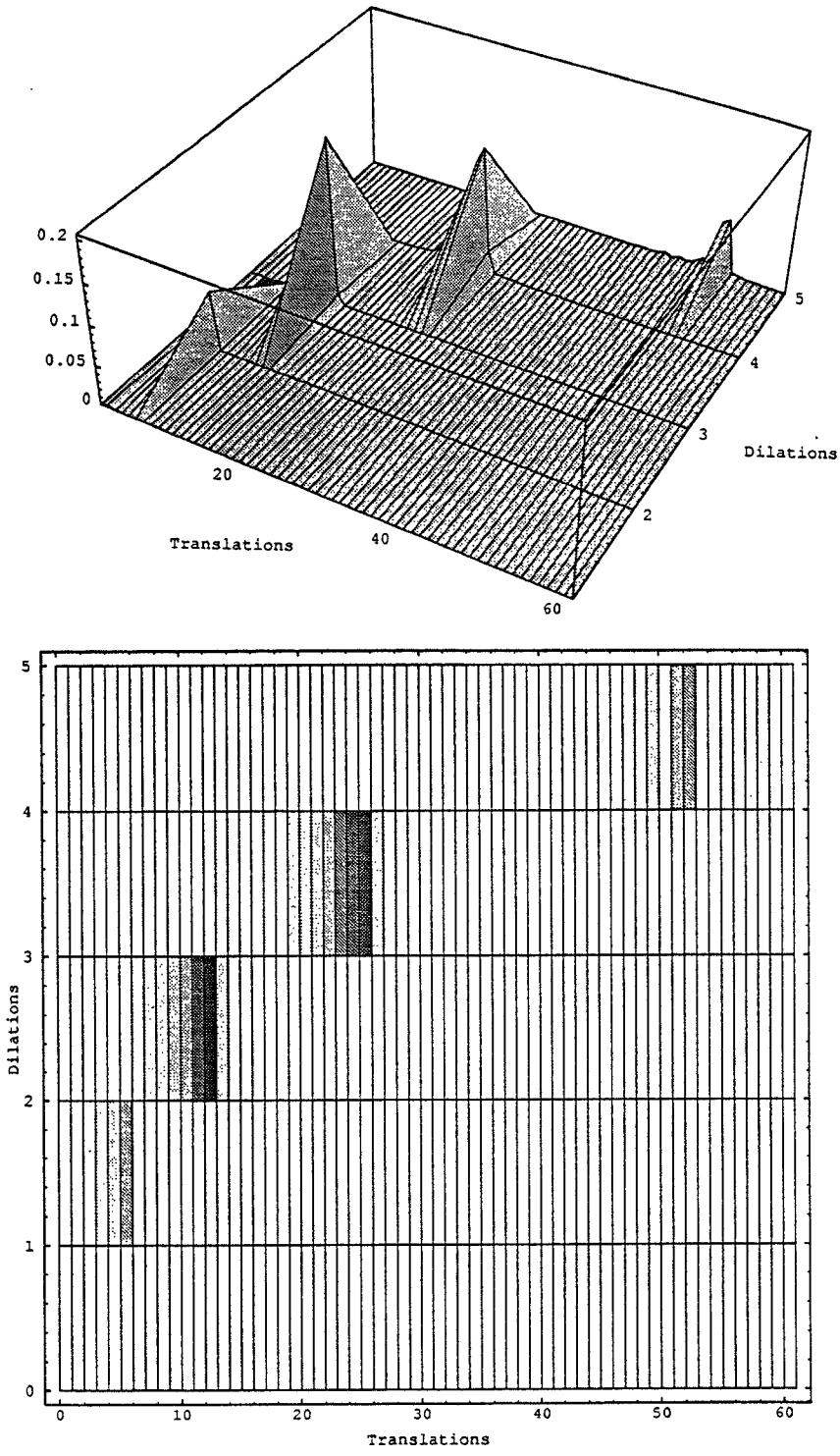

Figure 4.9: Magnitude of coefficients in WS approximation to cochlear filter. Three-dimensional plot (top) and density plot (bottom)

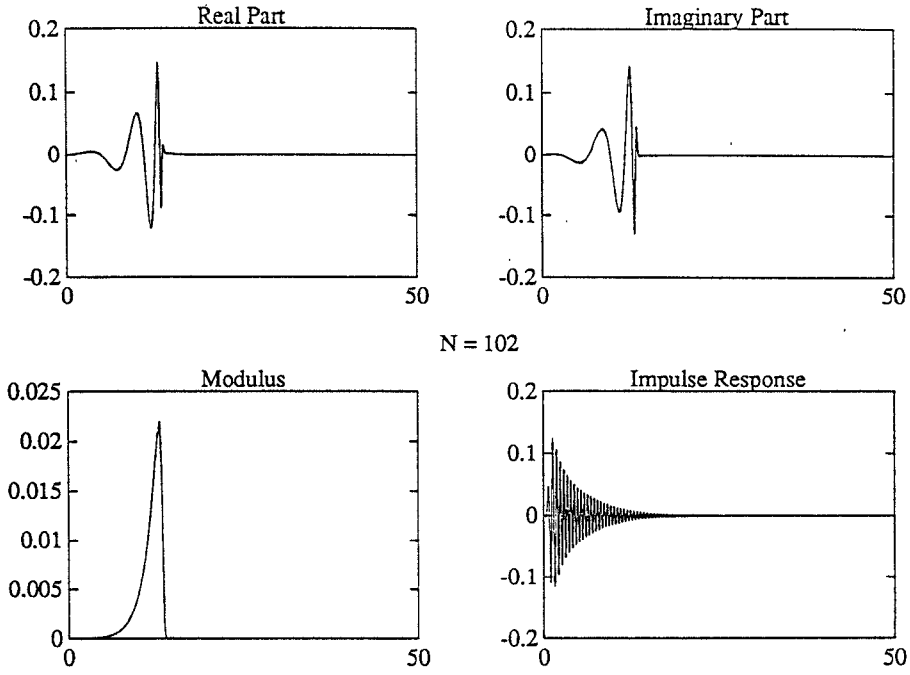

Figure 4.10: High order WS approximation to cochlear filter frequency response.

Laguerre Approximation of Cochlear Filters

Laguerre models may also be used for rational approximation of the cochlear filter frequency response. The Laguerre shift parameter p, was selected via a manual optimization for a Laguerre model of order $N = 10$. Figures 4.14 – 4.16, show the resulting Laguerre approximations for different models orders. As should be expected, the Laguerre model demonstrates slow convergence in this case due to the resonant components of the system. Moreover, it is evident that a very high order Laguerre model is required to capture the three important properties of the system mentioned above.

Discussion

Figure 4.17 is a plot of normalized approximation error versus model order for both the Laguerre and WS model approximations to the cochlear filter frequency response. It is clear from this plot that the WS models provide higher quality approximants at low model orders. The error of the Laguerre approximant decreases exponentially

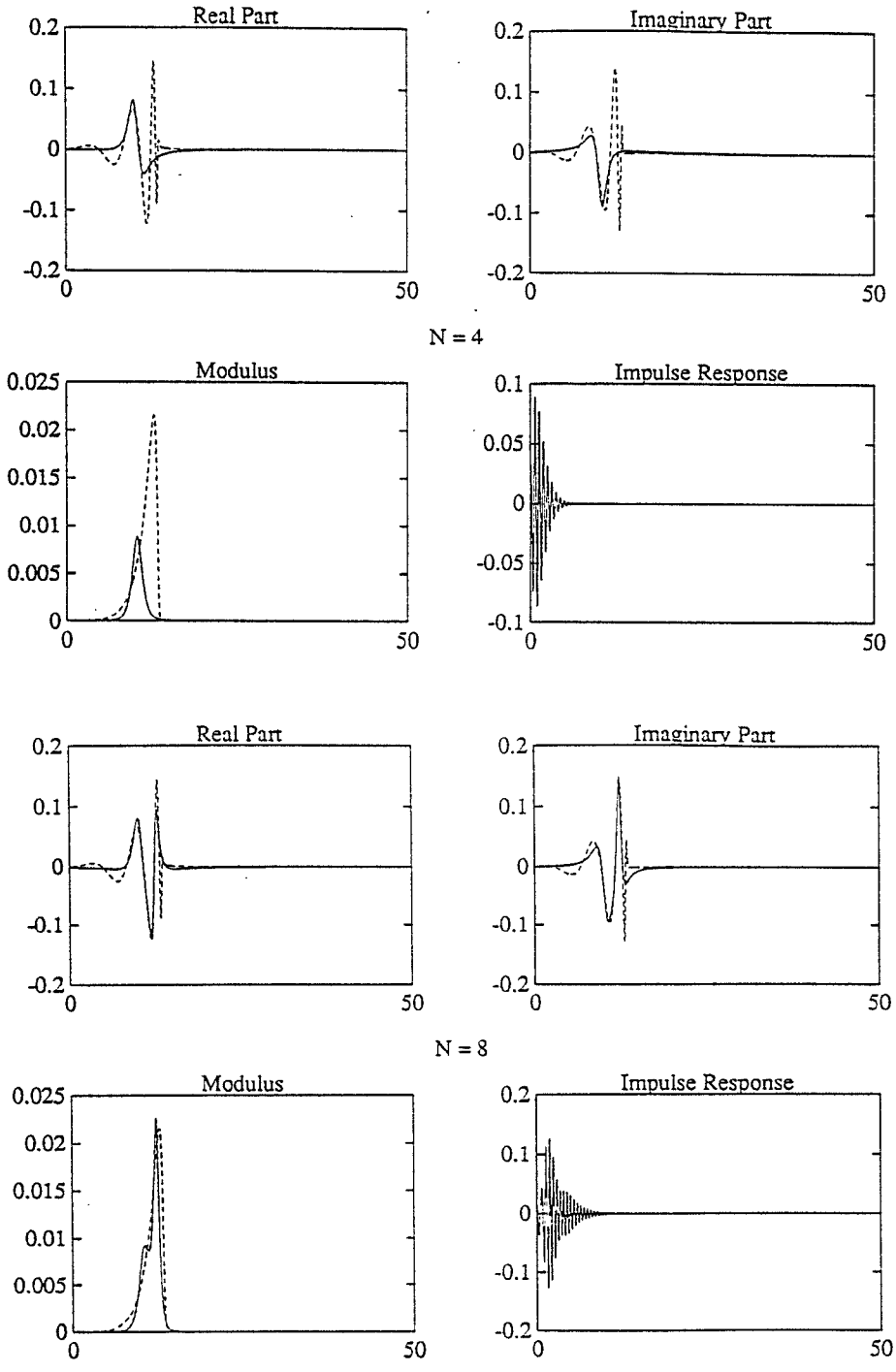

Figure 4.11: WS approximation of cochlear filter for $N = 4$ (top), and $N = 8$ (bottom). Solid curve: approximation; Dashed curve: nonparametric model

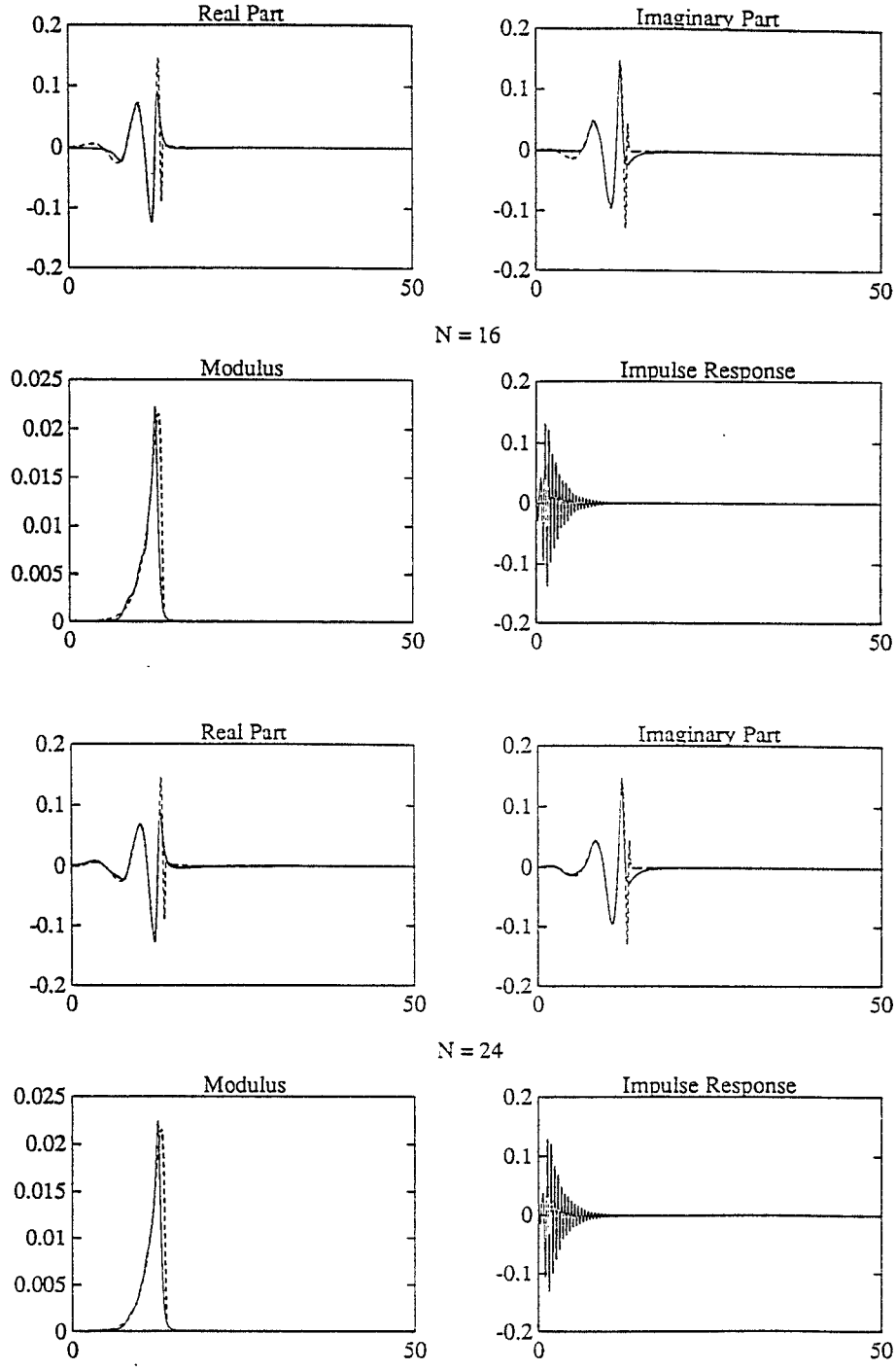

Figure 4.12: WS approximation of cochlear filter for $N = 16$ (top), and $N = 24$ (bottom). Solid curve: approximation; Dashed curve: nonparametric model

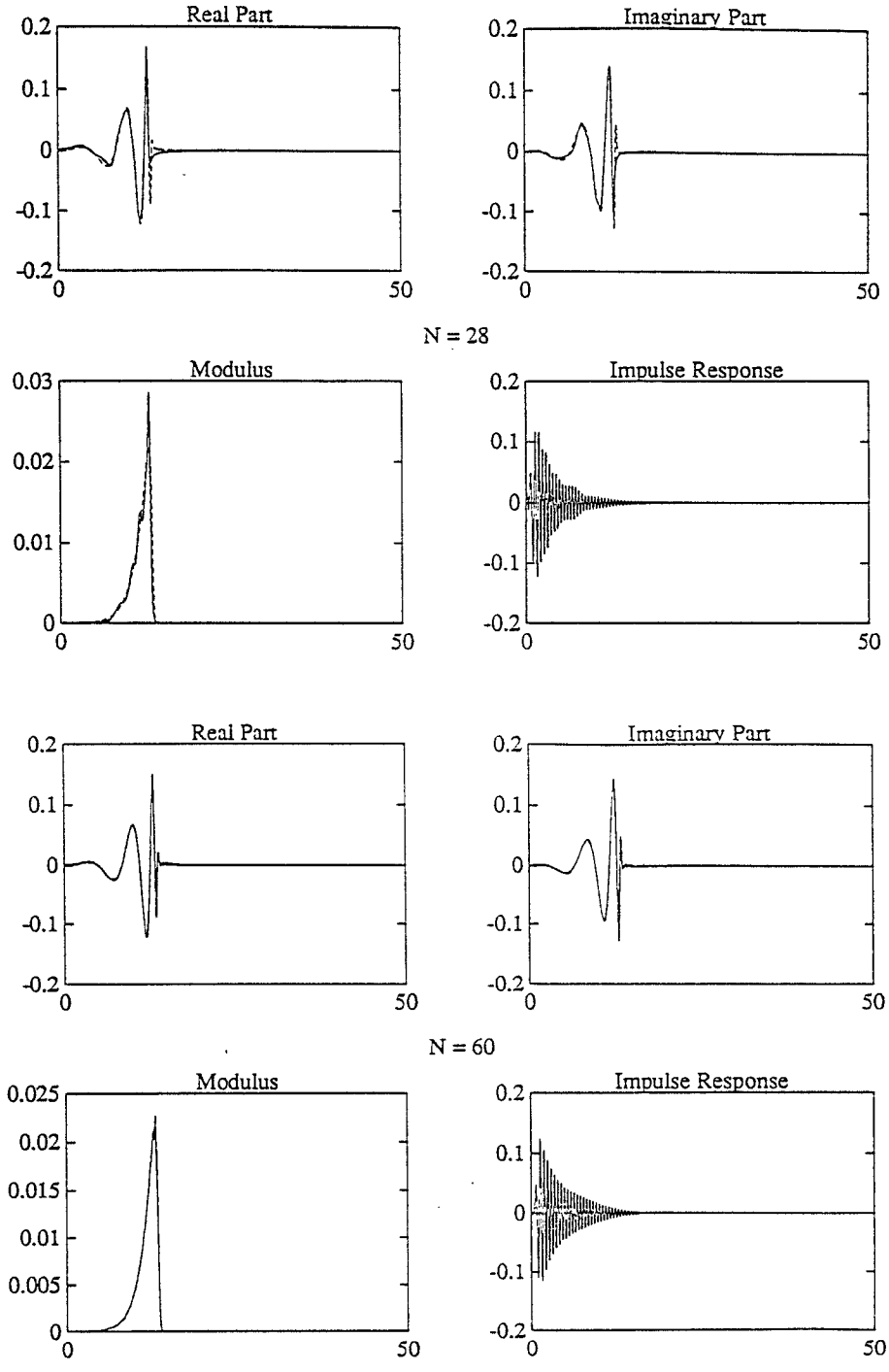

Figure 4.13: WS approximation of cochlear filter for $N = 28$ (top), and $N = 60$ (bottom). Solid curve: approximation; Dashed curve: nonparametric model

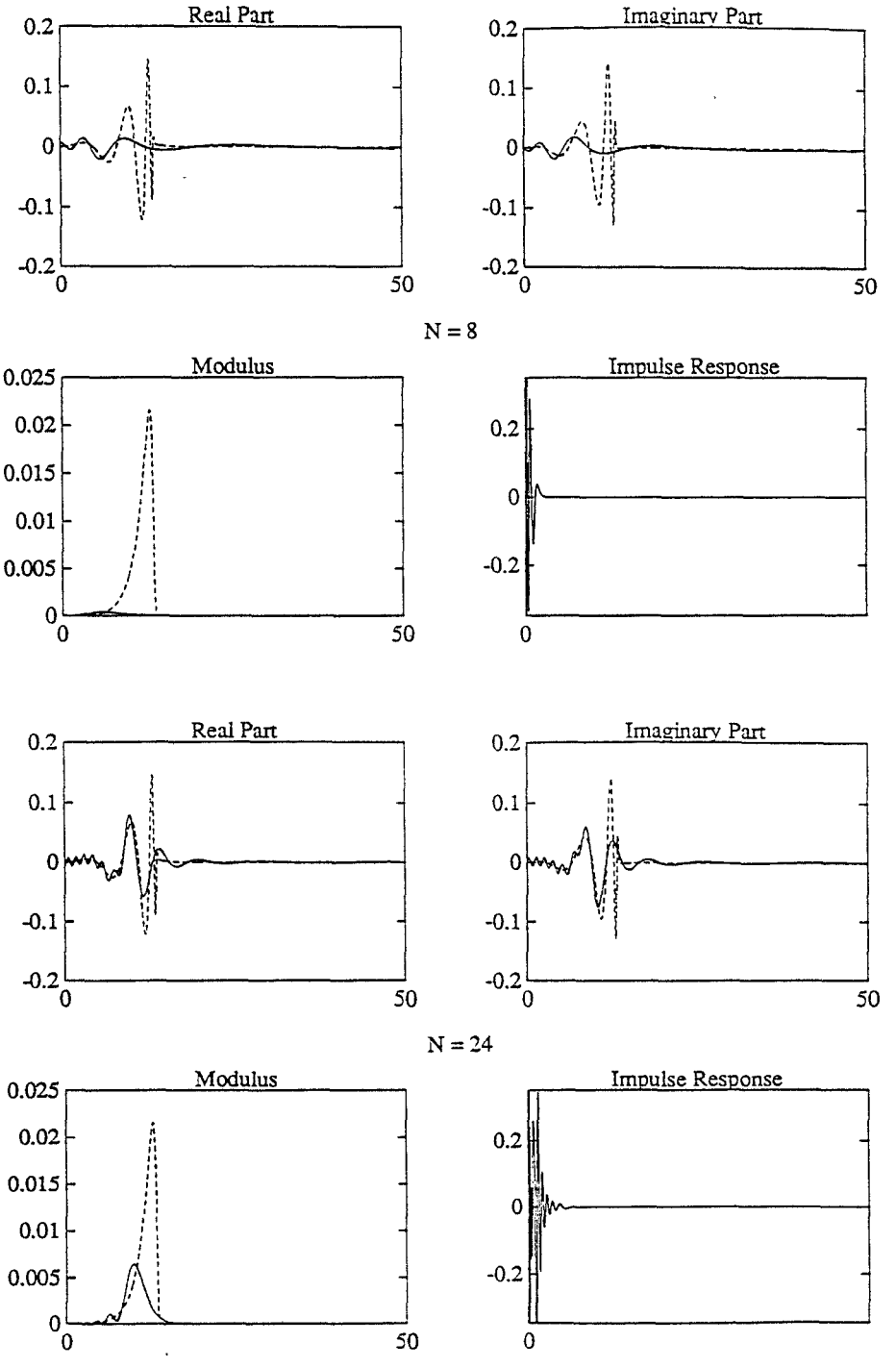

Figure 4.14: Laguerre approximation ($p = 8.4$) of cochlear filter for $N = 8$ (top), and $N = 24$ (bottom). Solid curve: approximation; Dashed curve: nonparametric model

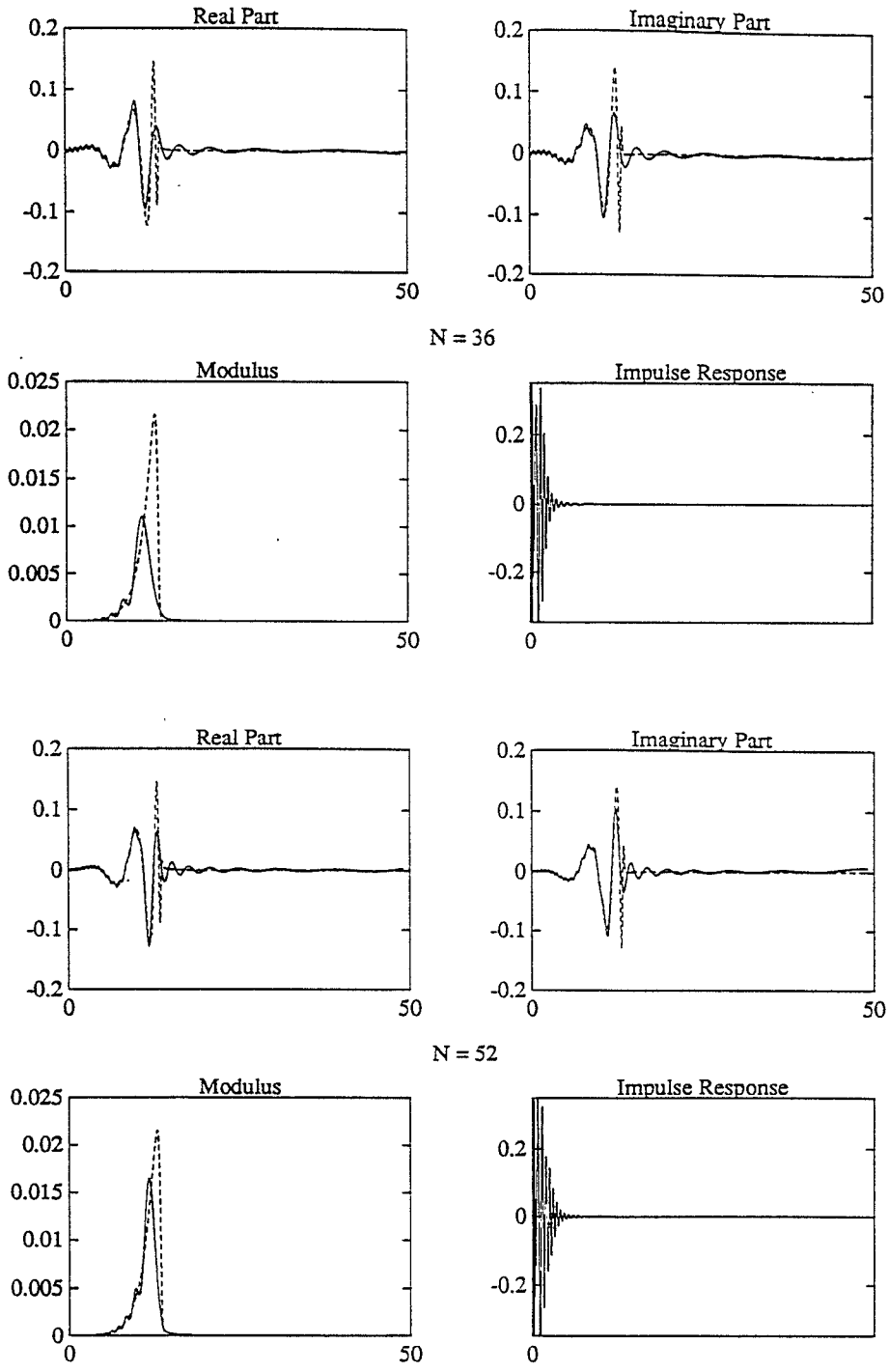

Figure 4.15: Laguerre approximation ($p = 8.4$) of cochlear filter for $N = 36$ (top), and $N = 52$ (bottom). Solid curve: approximation; Dashed curve: nonparametric model

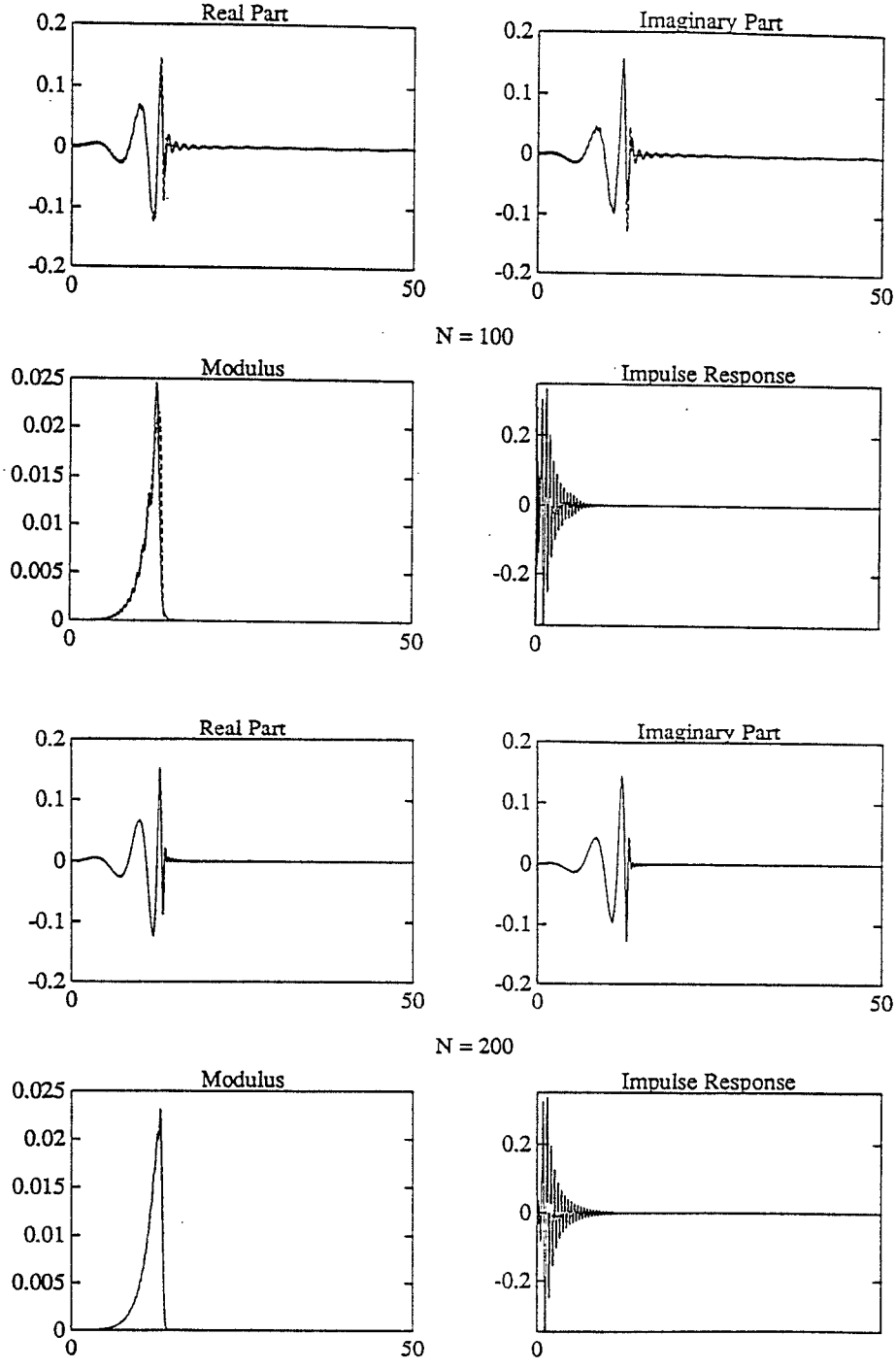

Figure 4.16: Laguerre approximation ($p = 8.4$) of cochlear filter for $N = 100$ (top), and $N = 200$ (bottom). Solid curve: approximation; Dashed curve: nonparametric model

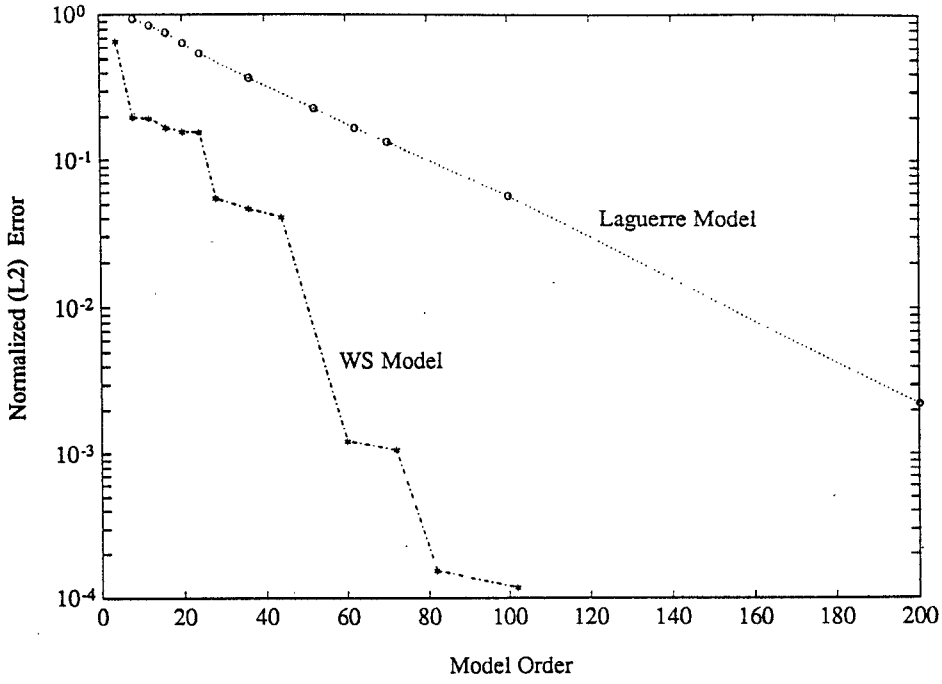

Figure 4.17: Normalized approximation error versus model order for approximation of cochlear filter frequency response using WS and Laguerre models

with model order, but the constant factor in the exponential is small (as is indicated by the slope of the curve on a logarithmic scale). Although the error decreases quite rapidly for the WS approximations, there is no clearly defined exponential rate of convergence. This highlights a difficulty with the WS models, which is that convergence rate estimates are difficult to obtain because of manner in which truncations are selected. However, in any application, it is more important to have good convergence than to have good theoretical estimates of the convergence rate. Note that the the cochlear filter clearly defines a system which lends itself to compact time-frequency localized representation. In some applications, keeping the number of parameters that need to be estimated small may be more important than the model order, e.g. for on-line estimation of parameters. A Nth-order Laguerre model requires N parameters, whereas, for the example analyzing wavelet used here the number of parameters in a Nth order model is $N/2$, ($N/4$ complex parameters). Figure 4.18 is equivalent to Figure 4.17, where now the abscissa represents the number of parameters in the

model.

4.7.2 Approximation of a Delay System

Consider now the simple delay system with transfer function,

$$G(s) = \frac{e^{-s\tau}}{s^2 + q_1 s + q_2}. \tag{4.7.24}$$

Once more, we apply both WS and Laguerre techniques to approximating this system. To make this example somewhat more interesting, we select τ, q_1, and q_2, such that the representation of the delay and the time constant of the system cause poor convergence of both the Laguerre and WS approximations. We wil use $\tau = 2.0, q_1 = 1.25, q_2 = 0.40625$. For this example, 700 samples of the frequency response from $\omega = 0$, to $\omega = 20$, were used.

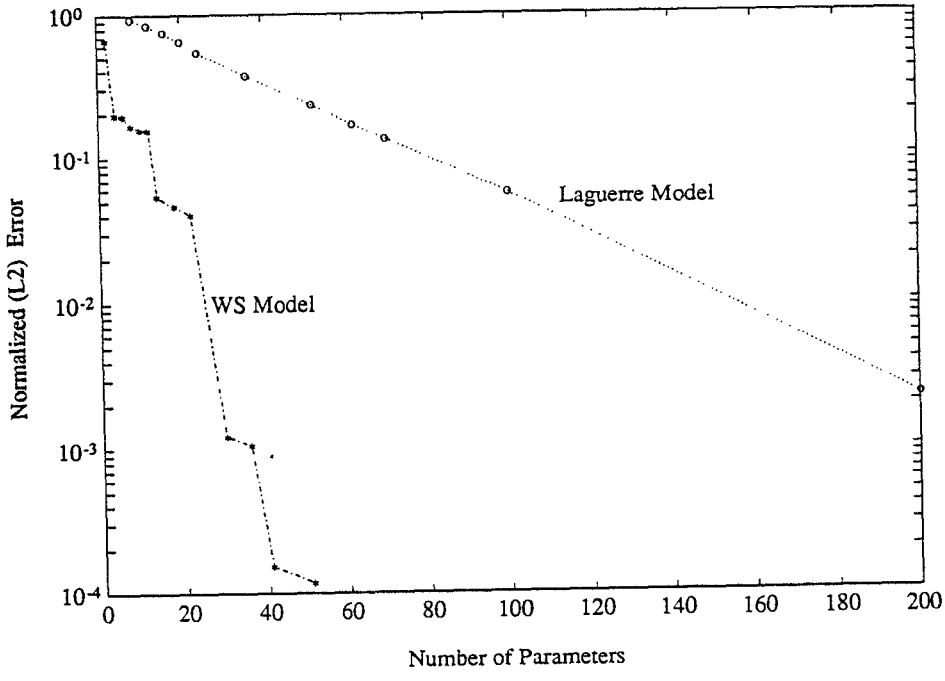

Figure 4.18: Normalized approximation error versus number of parameters for approximation of cochlear filter frequency response using WS and Laguerre models

WS Approximation of Delay System

It is more revealing in this example to consider the quality of the various approximations in the time domain. In Figure 4.19 the coefficient magnitudes for a high order WS approximation of the delay system (4.7.24) are plotted. Note that the coefficients are well-localized. An interesting feature of the decomposition shown in Figure 4.19 is that if we equate the dilation axis to the time axis and the translation axis to the frequency axis, we see that the delay in the system is visually evident in the coefficients. Figures 4.20–4.21 show the WS approximations of the impulse response of the system 4.7.24 for various model orders N.

Laguerre Approximation of Delay System

Laguerre approximation of the delay system 4.7.24 requires a careful selection of the Laguerre shift parameter p. In many cases optimal selection of p, may be quite difficult as we shall show shortly. To illustrate just how significant the choice of p can be, consider Figure 4.22 in which two curves are plotted for the time-domain approximation error for Laguerre approximants of the system (4.7.24). For the first curve p, was held constant at $p = 1.56$, as the model order was varied. This value of p was chosen by manual optimization for a eighth order model. Note that the convergence of the Laguerre approximants in this case is too slow to be of any practical utility. The second curve, which demonstrates much better convergence, was obtained by manual optimization of p, every time the model order was changed. The problem with the time domain convergence of the Laguerre approximants with p fixed can partly be attributed to the finite length of the data in the frequency domain and the fact that the Laguerre functions decay only as s^{-1}, at infinity. The point to be made however is that the choice of p, can be crucial especially for low order approximants as noted in [CW92]. The problem of choosing optimal values of p, may in fact prove to be quite difficult due to the complicated dependence of the error on p . This is perhaps best illustrated by Figure 4.23, which is taken from Cluett and Wang [CW92]. The

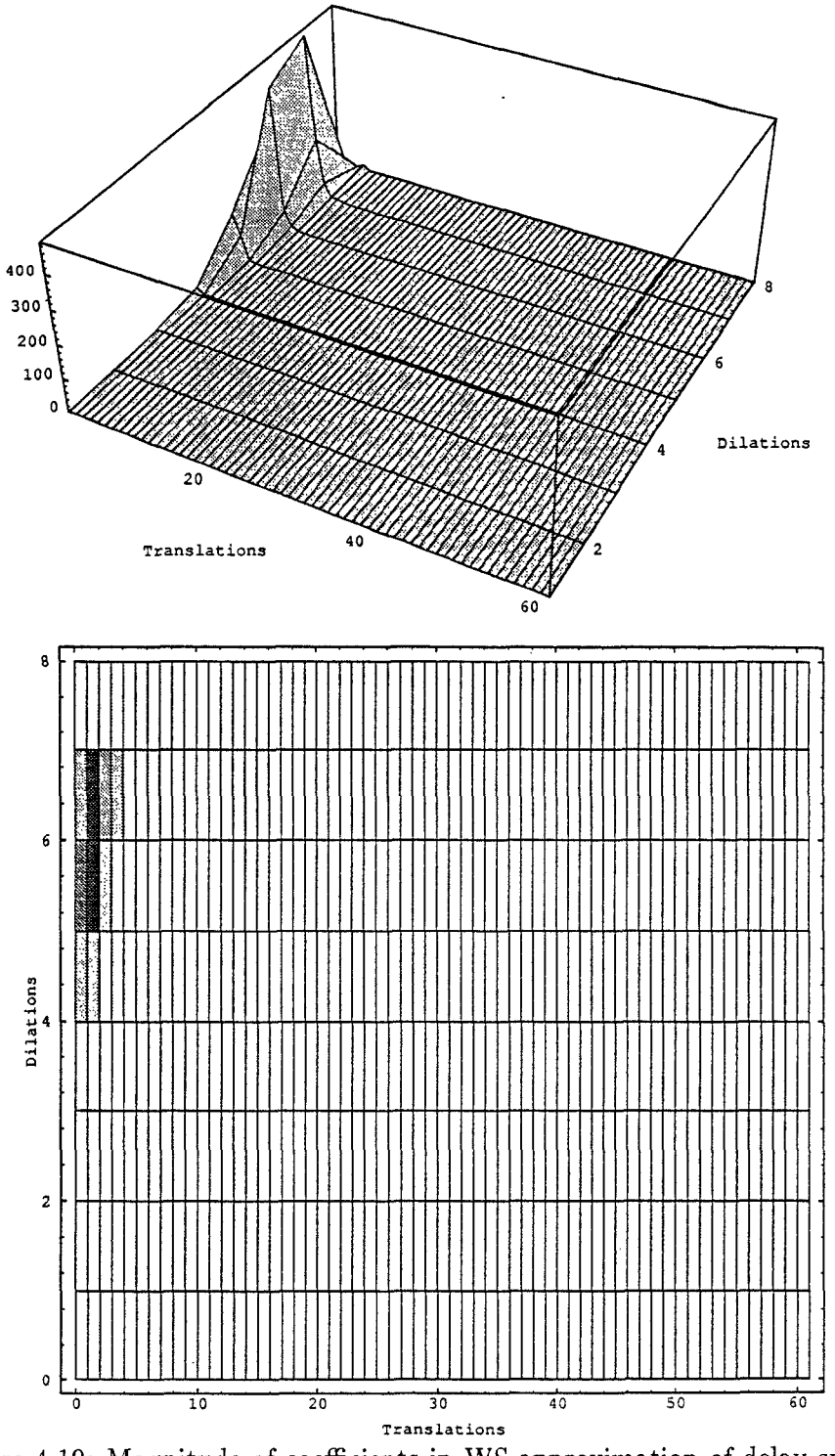

Figure 4.19: Magnitude of coefficients in WS approximation of delay system. Three-dimensional plot (top) and density plot (bottom)

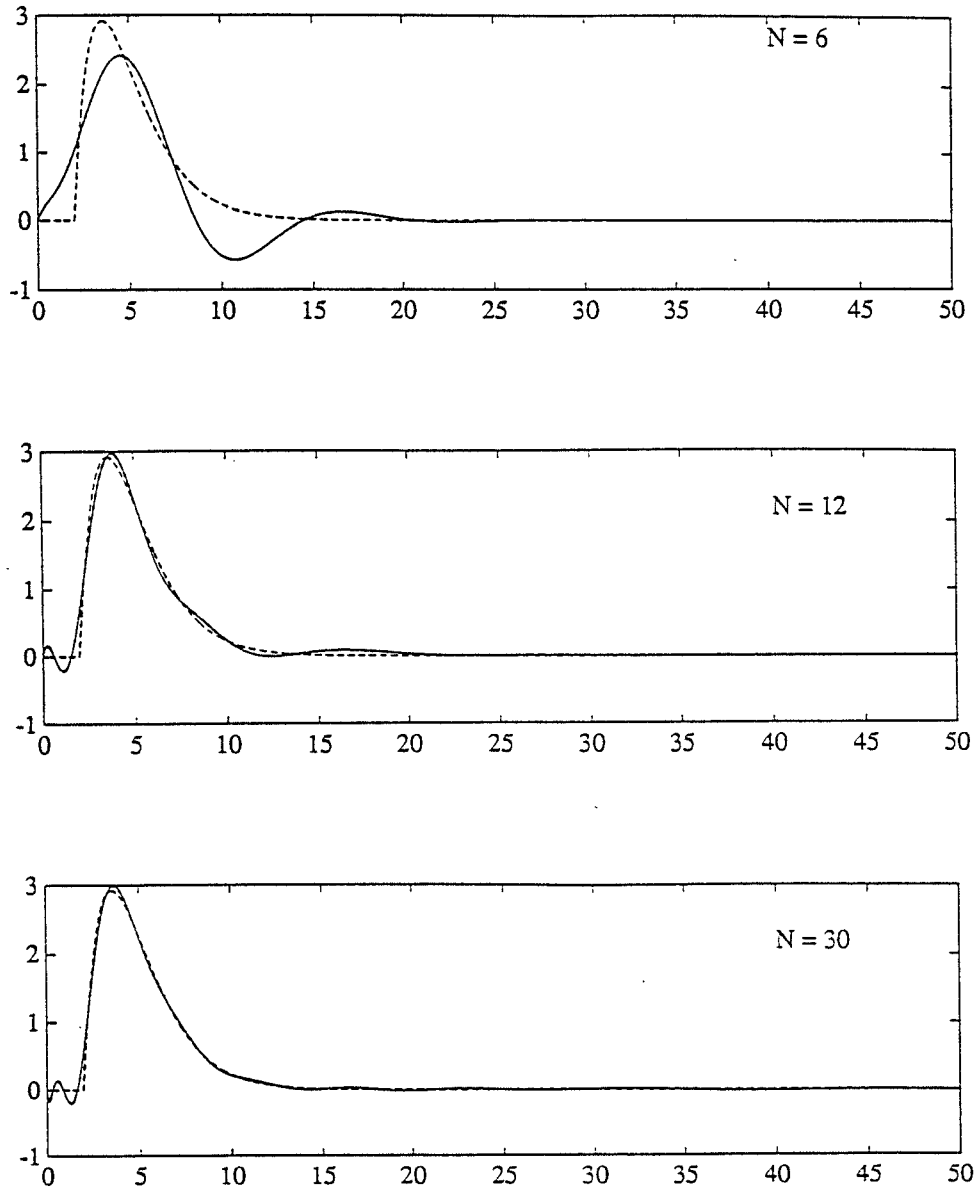

Figure 4.20: WS approximation of delay system for $N = 6, 12, 30$. Solid curve: approximation of impulse response; Dashed curve: actual impulse response

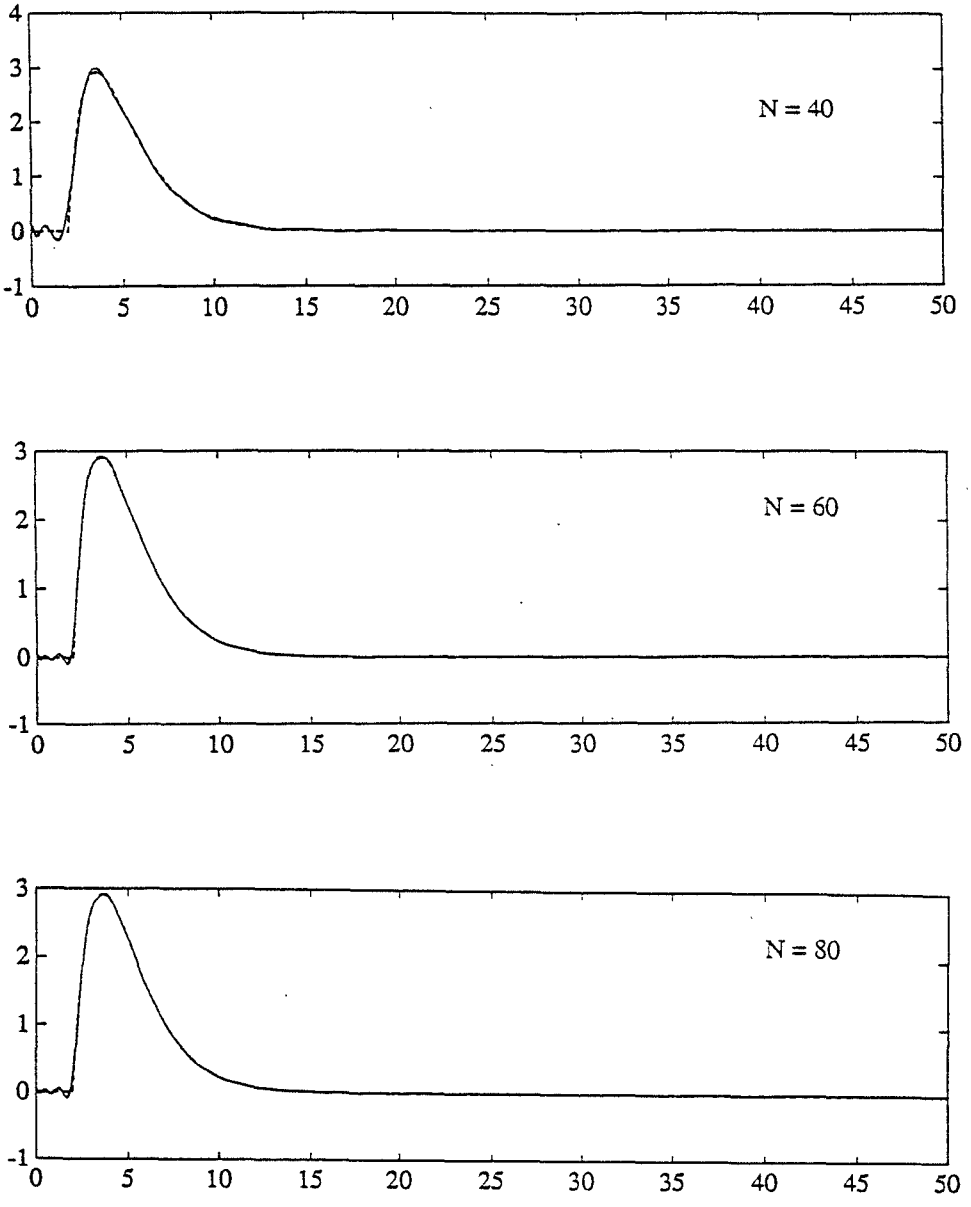

Figure 4.21: WS approximation of delay system for $N = 40, 60, 80$. Solid curve: approximation of impulse response; Dashed curve: actual impulse response

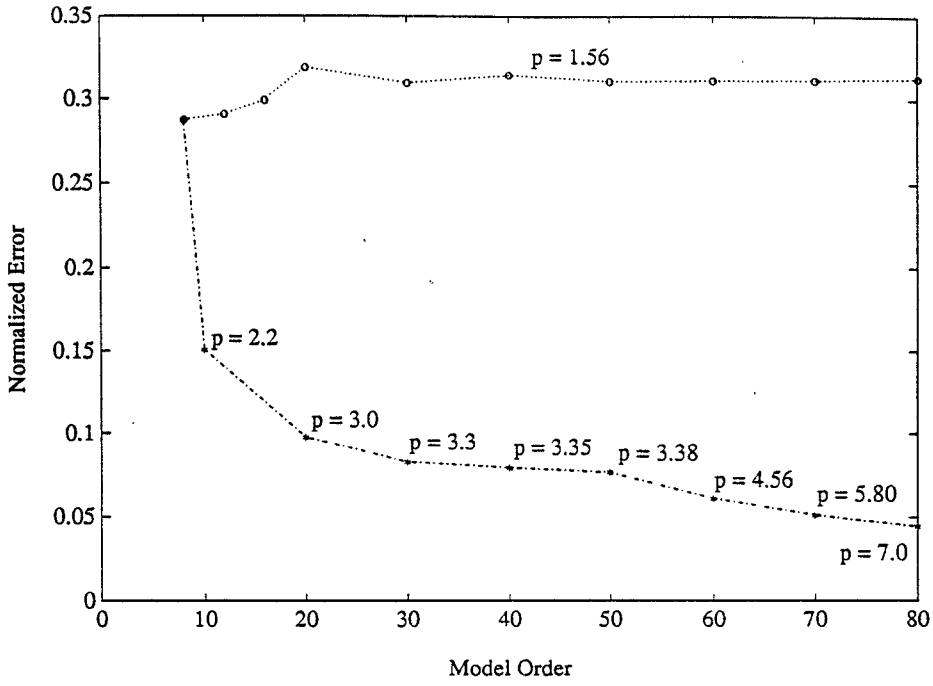

Figure 4.22: Normalized (time-domain) error in Laguerre approximation of the example delay system

surface shown in Figure 4.23 is the ℓ^2 norm of the first N, Laguerre coefficients, where N is model order, in the Laguerre approximation to a frequency response estimate for a laboratory scale process trainer (see [Lju87]; data available in MATLAB (DRYER2)). For good approximations, it is desirable to choose p so as to maximize the value of the function plotted in Figure 4.23. It should be noted that the surface in Figure 4.23, is for approximation of a particular system and in general the dependence of the error on p, and model order may be far more complicated.

Figures 4.24–4.25 show the Laguerre approximation of the impulse response of the system (4.7.24), using the manually determined values of p, shown in Figure 4.22. The (time-domain) approximation error is plotted against the model order in Figure 4.26 for both the Laguerre and WS models.

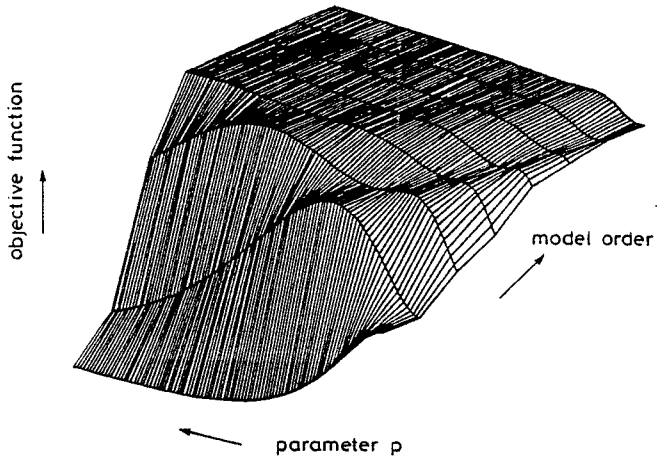

Figure 4.23: Surface representing norm of Laguerre approximant to a frequency response estimate for a laboratory scale process trainer. Taken from Cluett and Wang (1992)

4.8 Summary

In this chapter we examined some aspects of the use of truncated WS representations as parametric 'black box' models for system identification. The manner in which WS representations are used here is closest in spirit to the use of Laguerre function representations in the approximation and identification of linear systems. Some properties of WS models which make them amenable to use in problems of system identification and rational approximation are:

(1) WS models are linear-in-parameters.

(2) Both time and frequency domain *a priori* information may be incorporated in WS models.

(3) The parallel nature of the models allow for a second stage of model reduction following parameter estimation.

(4) The underlying building blocks of WS models are based on frames and thus there exists a great deal of flexibility in the choice of these building blocks.

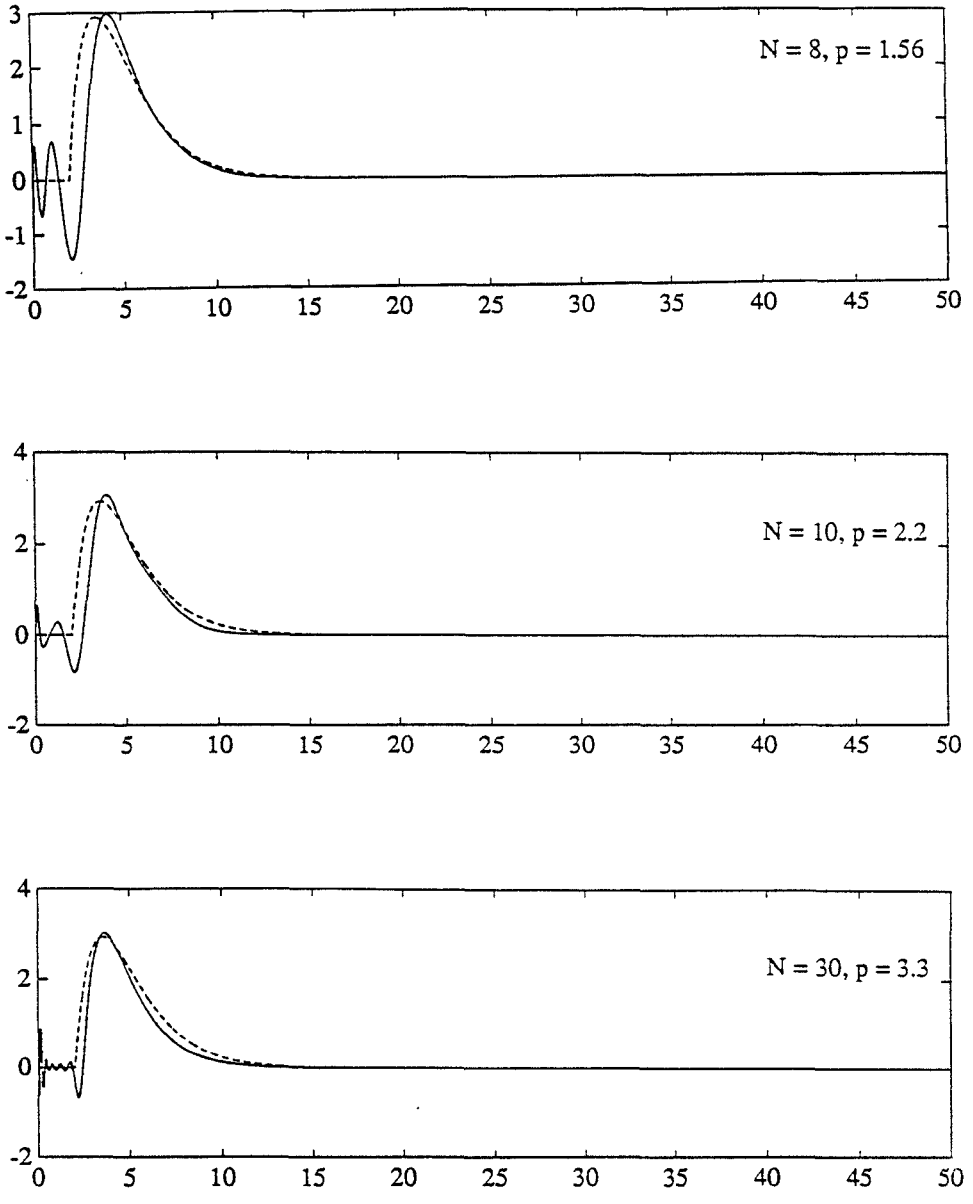

Figure 4.24: Laguerre approximation of delay system for $N = 8, 10, 30$. Laguerre shift parameter p is indicated on the plots. Solid curve: approximation of impulse response; Dashed curve: actual impulse response

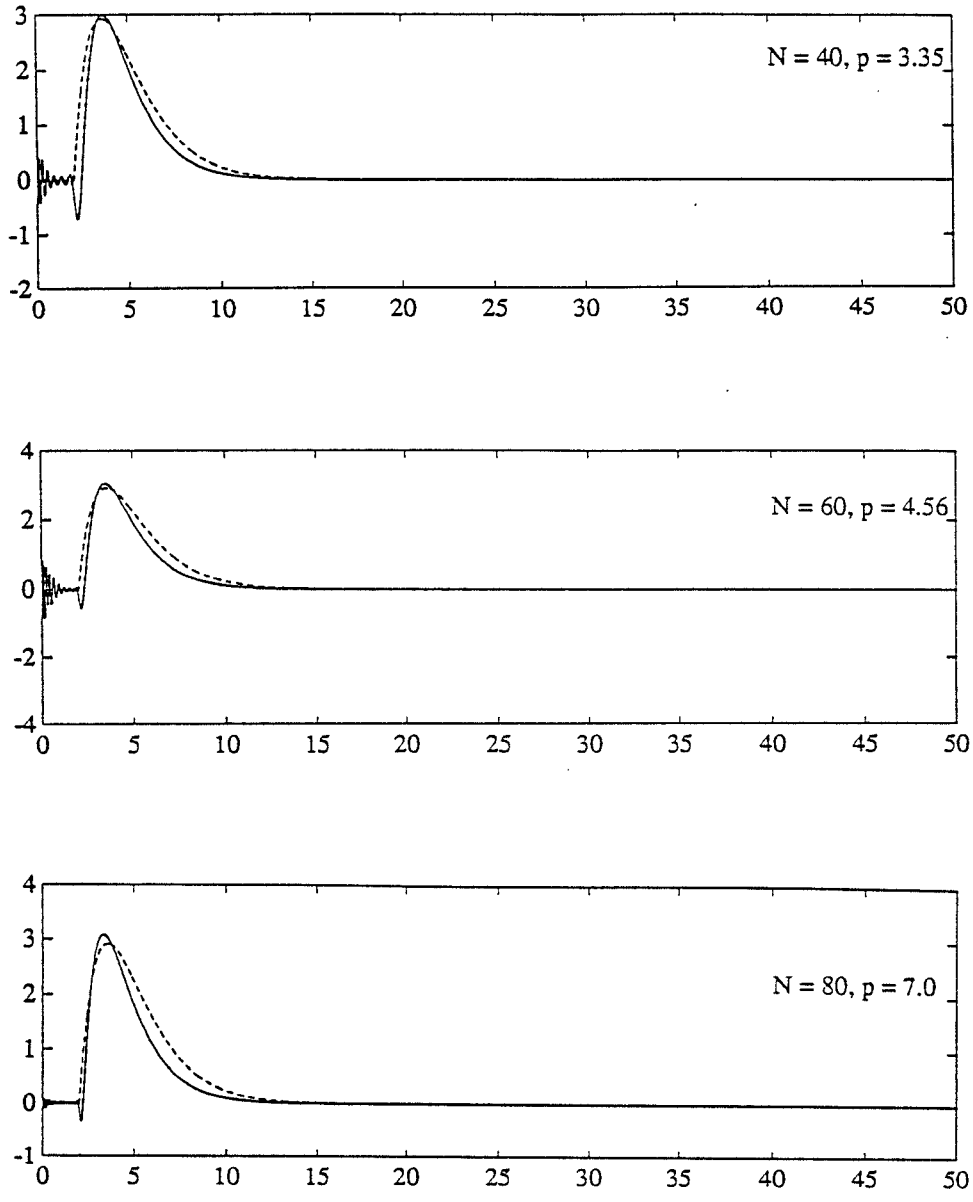

Figure 4.25: Laguerre approximation of delay system for $N = 40, 60, 80$. Laguerre shift parameter p is indicated on the plots. Solid curve: approximation of impulse response; Dashed curve: actual impulse response

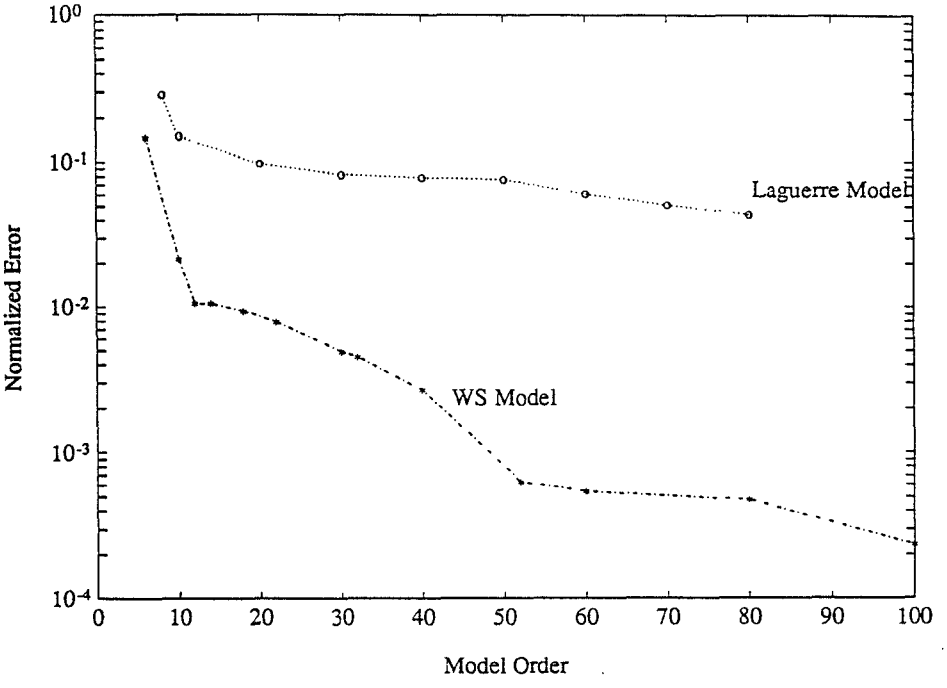

Figure 4.26: Approximation error versus model order for approximation of the example delay system by Laguerre models and WS models. The Laguerre shift parameter p, was 'manually optimized' each time the model order was increased.

It was shown that WS models may perform considerably better than Laguerre models for certain classes of problems. Much of the difficulty with the Laguerre model can be associated with the fact that there is only one parameter, namely the Laguerre shift parameter p, which can be used to control the performance of the Laguerre model far any given problem. Table 4.1 briefly summarizes some aspects for comparison of WS models and Laguerre models. A column is included for the extended Laguerre models (c.f. Section 4.4) which possess some characteristics of both WS models and the classical Laguerre models.

Some, as yet unanswered, questions which we regard as topics for further research are

(1) What are the theoretical rates of convergence for WS approximation of various classes of transfer functions, and how do these compare with other known rational approximation techniques such as Laguerre approximation.

(2) What can be said about the selection of truncations of WS representations so as to ensure optimal' convergence.

(3) Under what conditions can convergence of WS approximations in other norms, in particular the $H^{\infty}(\Pi^{+})$ norm, be established.

The answer to the first question above may in general be quite complicated since it depends on the particular scheme employed for the selection of truncations.

We also showed that the *ad hoc* procedure (c.f. (4.4.15)) suggested by Wahlberg [Wah91], for improving the performance of Laguerre models on systems with multiple dispersed time constants, leads to a class of extended Laguerre series representations when viewed from the viewpoint of frame theory. This observation creates a framework for analyzing the convergence properties of such models.

	WS	Laguerre	Extended Laguerre
Model type	black-box, linear-in-parameters	black-box, linear-in-parameters	black-box, linear-in-parameters
Approximation space	$H^2(\Pi^+)$	$H^2(\Pi^+)$	$H^2(\Pi^+)$
Decomposition structure	parallel	series	parallel-series
A priori knowledge	multiple time constants, delays, frequency ranges	time constant, delay	multiple time constants, delays
Representation	frames	orthonormal bases	frames
Adaptability of model	m, n, (a_0, b_0, Ψ)	p, model order	$\{p_j\}_{j=1}^{K}$, K, model order
Sensitivity to parameter perturbations	robust for redundant frames	sensitive	robust due to redundancy
Convergence in other norms	Undetermined	$H^\infty(\Pi^+)$, $L^\infty(\mathbb{R}^+)$, for certain classes	—

Table 4.1: WS vs Laguerre models

Chapter 5

Wavelet Analysis and Synthesis of Feedforward Neural Networks

In this chapter, we investigate the use of affine wavelet frames in analyzing and synthesizing feedforward neural networks. Feedforward neural networks are 'biologically inspired' computational architectures which have found application in problems of approximating static mappings based on discrete data. As noted in Chapter 1, problems of this nature arise in a wide variety of fields. Clearly feedforward networks are not the only means of solving such problems. Approximation theory is a very well-developed area of mathematics, and there exist numerous 'conventional' approaches to these problems (e.g. orthogonal basis approximations). The main attraction of the neural network approach has been the empirically demonstrated success in problems involving mappings with high-dimensional domains and/or ranges. For such problems, where the domain is high dimensional, the more structured techniques of classical approximation theory often lead to computationally intractable formulations. The use of neural networks may be thought of as a somewhat naive approach in the sense that to date there does not exist much structure in the approach. It has been known for some time that feedforward networks with particular classes of 'activation functions' are capable of generating 'good' approximations to certain classes of mappings.

These results (c.f. [Cyb89, Cyb88, HSW89, HSW90]) have for the most part been based on arguments of density of the class of mappings implementable in feedforward networks, in various function spaces. These results may be regarded as justification for the use of such networks in approximation problems. However, the nature of these arguments do not reveal precisely the feedforward network implementation of a given mapping. In this sense, they are nonconstructive results. It is thus natural to ask whether there is an alternative formulation which allows one to describe the approximation properties of feedforward networks and at the same time gain some insight into the exact feedforward network implementation of a given mapping. In this chapter it is shown that affine wavelet theory can provide precisely this type of formulation. Our approach to this problem was initially motivated by the observation that feedforward neural network architectures inherently posses a translation and dilation structure. Furthermore, since the theory of frames permits a great deal of flexibility in the choice of analyzing wavelets, it was natural to try to combine these two observations to formulate a wavelet description of feedforward networks.

For the sake of completeness, we briefly review some of the salient features of the feedforward network approach to approximation in Section 5.1. The remainder of this chapter is organized as follows.

In Section 5.2 it is shown that the inherent translation and dilation structure of feedforward networks may be utilized to implement affine wavelet decompositions within the standard architecture of feedforward neural networks. For simplicity we restrict discussion primarily to single-input-single-output networks. However, the theoretical results of this chapter apply to the higher-dimensional settings as well, as is briefly discussed in Sections 5.2.3 and 5.4.

Among topics which have received some research attention in the are of neural networks, is the choice of 'activation functions'. One of the most commonly used activation functions is the so-called sigmoidal function. Section 5.2.1 is concerned with constructing affine (wavelet) frames using combinations of sigmoids. It is important to point out that there is no a priori need to restrict oneself to sigmoidal activation

functions. However, by doing so the power and flexibility of frame theory is clearly demonstrated.

The main analysis result of this chapter is Theorem 5.1 which states that wavelet decompositions of $L^2(\mathbb{R})$ may be implemented within the standard architecture of feedforward networks with sigmoidal activation functions. Thus for a given mapping in $L^2(\mathbb{R})$, the feedforward network implementation can be readily computed. Theorem 5.1 is easily extended to higher dimensions ($L^2(\mathbb{R}^n)$), and we briefly describe this extension in Section 5.2.3.

In Section 5.3 we outline two schemes in which spatio-spectral localization properties of wavelets are used to formulate synthesis procedures for feedforward neural networks. It is shown that such synthesis procedures can result in systematic definition of network topology and simplified network 'training' problems. Most of the weights in the network are determined via the synthesis process and the remaining weights may be obtained as a solution to a *convex* optimization problem. Since the resulting optimization problem is one of least squares approximation, the remaining weights can also be determined by solving the associated 'normal equations'. The synthesis schemes may be theoretically extended to higher dimensions. However,

A few simple numerical simulations of the methods of this chapter are provided in Section 5.3.4.

5.1 Background on Feedforward Neural Networks

In this section we provide a brief introduction to the use of feedforward neural networks to functional approximation problems.

Let Θ be a set containing pairs of sampled inputs and the corresponding outputs generated by an unknown map, $f : \mathbb{R}^m \rightarrow \mathbb{R}^n$, $m, n < \infty$, i.e. $\Theta = \{(x^i, y^i) : y^i = f(x^i);\ x^i \in \mathbb{R}^m,\ y^i \in \mathbb{R}^n, i = 1, \ldots, K,\ K < \infty\}$. We call Θ the *training set.* Note that the samples in Θ need not be uniformly distributed. The problem at hand is to use the data provided in Θ to 'learn' (approximate) the map f. Many existing schemes

to perform this task are based on parametrically fitting a particular functional form to the given data. Simple examples of such schemes are those which attempt to fit linear models or polynomials of fixed degree to the data in Θ. More recently, nonlinear feedforward neural networks have been applied to the task of 'learning' the map f.

5.1.1 Feedforward Neural Networks

The basic component in a feedforward neural network is the single 'neuron' model depicted in Figure 5.1(a). Where $u_1, \ldots, u_n$ are the inputs to the neuron, $k_1, \ldots, k_n$

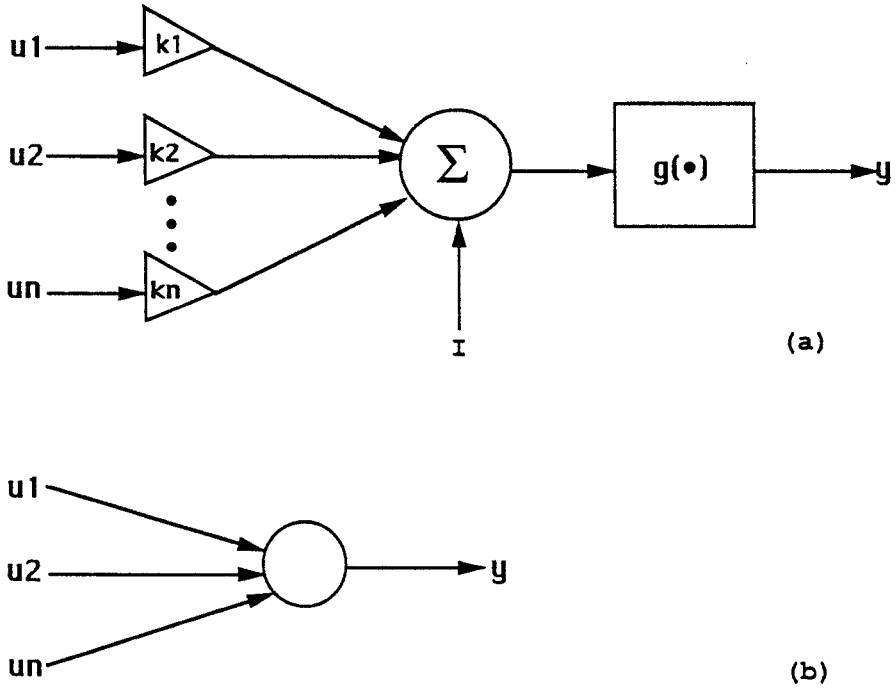

Figure 5.1: (a)Single neuron model. (b) Simplified schematic of single neuron

are multiplicative weights applied to the inputs, I is a biasing input, $g : \mathbb{R} \rightarrow \mathbb{R}$, and y is the output of the neuron. Thus $y = g(\sum_{i=1}^{n} k_i u_i + I)$. The 'neuron' of Figure 5.1(a) is often depicted as shown in Figure 5.1(b) where the input weights, bias, summation, and function g are implicit. Traditionally, the *activation* function

g has been chosen to be the sigmoidal nonlinearity shown in Figure 5.2. This choice

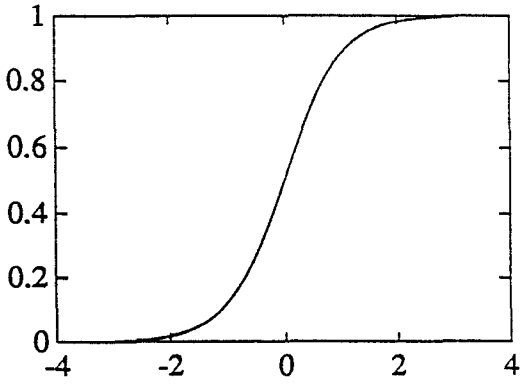

Figure 5.2: Sigmoidal activation function.

of g was initially based upon the observed firing rate response of biological neurons. A feedforward neural network is constructed by interconnecting a number of neurons (such as the one shown in Figure 5.1) so as to form a network in which all connections are made in the forward direction (from input to output without feedback loops) as in Figure 5.3. Neural networks of this type usually consist of an input layer, a number of hidden layers, and an output layer. The input layer consists of neurons which accept external inputs to the network. Inputs and outputs of the hidden layers are internal to the network, and hence the term 'hidden'. Outputs of neurons in the output layer are the external outputs of the network. Once the structure of a feedforward network has been decided, i.e the number of hidden layers and the number of nodes in each hidden layer has been set, a mapping is 'learned' by varying the connection weights, w_{ij}'s and the biases, I_j's so as to obtain the desired input-output response for the network[1].

One method often used to vary the weights and biases is known as the backpropagation algorithm in which the weights and biases are modified so as to minimize a

[1]We will use w_{ij} to denote the weight applied to the output O_j of the j^{th} neuron when connecting it to the input of the i^{th} neuron. I_j is the bias input to the j^{th} neuron.

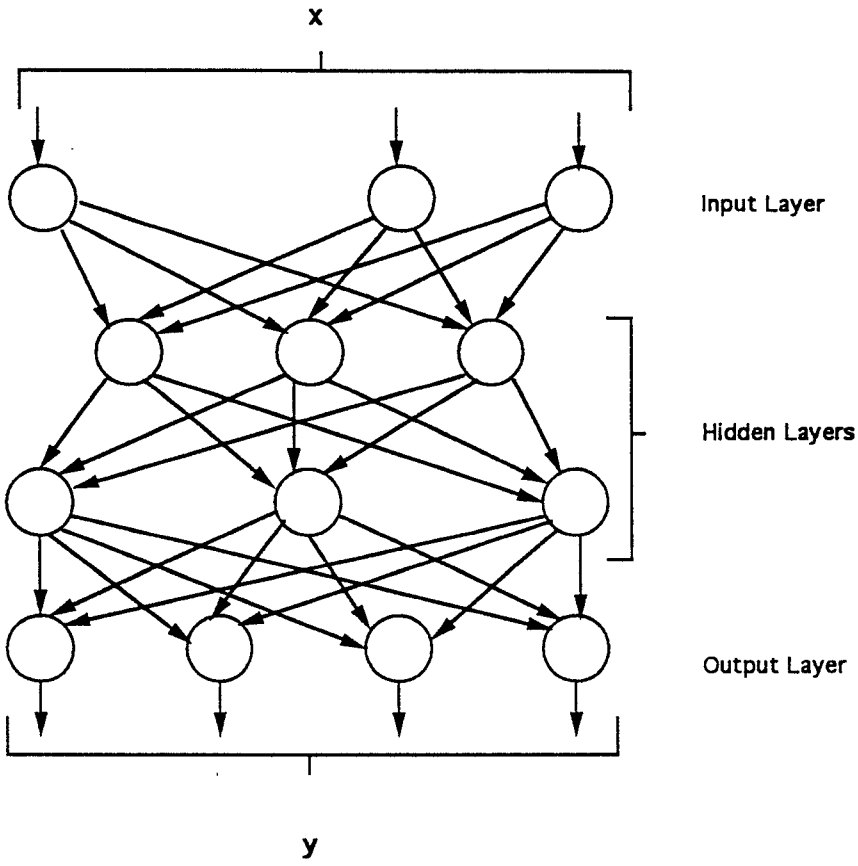

Figure 5.3: Multilayered feedforward neural network.

cost functional of the form,

$$E = \sum_{(x^i,y^i)\in\Theta} \|O^i - y^i\|^2_{\mathbb{R}^n}, \tag{5.1.1}$$

where O^i is the output vector (at the output layer) of the network when x^i is applied at the input. Backpropagation employs gradient descent to minimize E. That is, the weights and biases are varied in accordance with the rules,

$$\Delta w_{ij} = -\epsilon \frac{\partial E}{\partial w_{ij}} \quad \text{and} \quad \Delta I_j = -\epsilon \frac{\partial E}{\partial I_j}.$$

Remarks: Although feedforward neural networks have empirically demonstrated an ability to approximate complicated maps very well using the technique just described, to date there does not really exist a satisfactory theoretical foundation for such an

approach. To clarify the meaning of a *satisfactory* theoretical foundation, let us list some of the problems that one should be able to address within a good theoretical setting.

(1) Development of a well-founded systematic approach to choosing the number of hidden layers and the number of nodes in each hidden layer required to achieve a given level of performance in a given application.

(2) Learning algorithms often ignore much of the information contained in the training data, and thereby overlook potential simplification of the weight setting problem. As we will show later, preprocessing of training data can simplify the training problem.

(3) An inability to adequately explain empirically observed phenomena. For example, the cost functional E may possess many local minima due to the nonlinearities in the network. A gradient descent scheme such as backpropagation is bound to settle to such local minima. However, in many cases, it has been observed that settling to a local minimum of E does not adversely affect overall performance of the network. Observations such as this demand a suitable explanatory theoretical framework.

The methods of this chapter offer a framework within which it is possible to address at least the first two issues above.

5.2 Dilations and Translations in SISO Neural Networks

In this section we shall demonstrate how affine wavelet decompositions of $L^2(\mathbb{R})$ can be implemented within the architecture of single-input-single-output (SISO) feedforward neural networks with sigmoidal activation functions. Consider the SISO feedforward neural network shown in Figure 5.4. Input and output layers of this network each consist of a single node, whose activation function is linear with unity gain. In

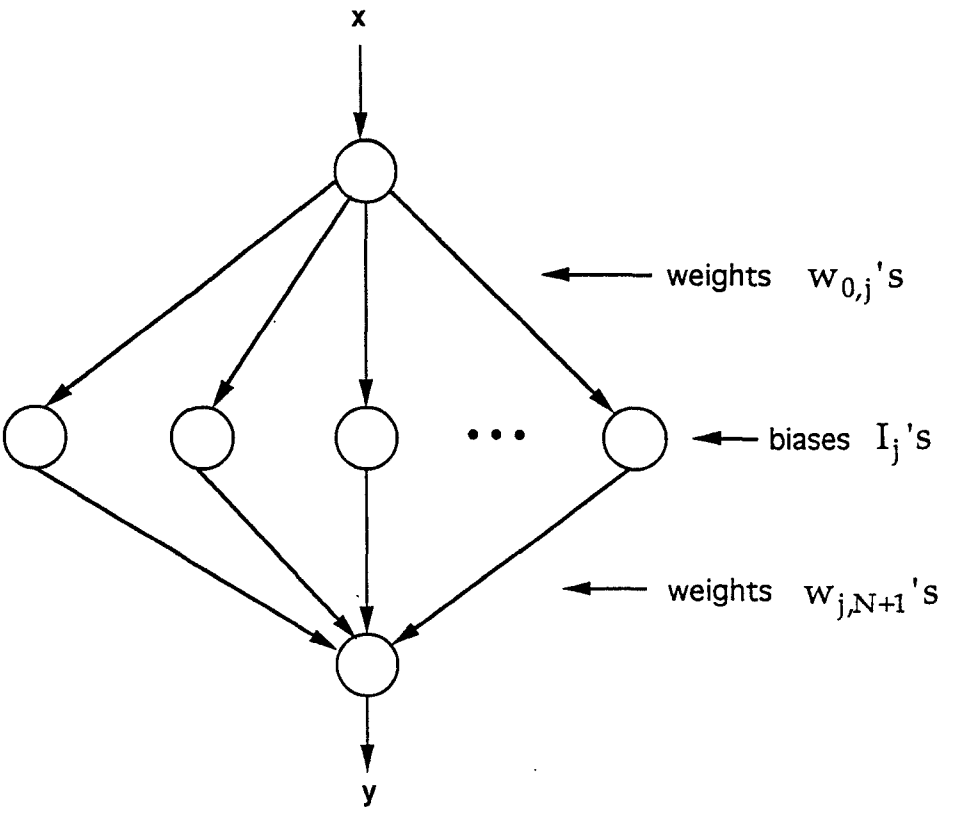

Figure 5.4: SISO feedforward neural network

addition, the network has a single hidden layer with N nodes, each with activation function $g(\cdot)$. Hence the output of this network is given by

$$y = f(x) = \sum_{j=1}^{N} w_{j,N+1} g(w_{0,j}x - I_j), \tag{5.2.2}$$

where we have labeled the input node 0 and the output node $N + 1$.

The key observation here is that the mapping f (5.2.2) implemented by the SISO feedforward network, is a linear combination of dilates and translates of a single function (the activation function g). Thus the mapping implemented in a SISO feedforward neural network is precisely of the form of an affine wavelet decomposition (2.2.25). The key differences are: (i) The summation in (5.2.2) is finite, and (ii) Even if we permit infinitely many hidden layer nodes, and let $g_j = g(w_{0,j}x - I_j)$, the infinite sequence $\{g_n\}$ will not necessarily be a frame for $\mathrm{L}^2(\mathbb{R})$.

To formulate a wavelet description of the feedforward network of Figure 5.4, it is thus necessary to investigate frames generated by translations and dilations of the

activation function g. In the next section we discuss how sigmoidal activation functions may be combined to construct admissible analyzing wavelets and thereby affine frames.

5.2.1 Affine Frames From Sigmoids

As mentioned earlier, sigmoidal functions are among the most commonly used activation functions in feedforward networks. Although it is not necessary to restrict attention to sigmoidal activation functions, we do so here to illustrate the power and flexibility offered by frame theory in the construction of analyzing wavelets. Recall from Chapter 2 that essentially the only restriction on the analyzing wavelet is the admissibility condition (2.2.8).

Consider the sigmoidal function, $s(x) = (1 + e^{-x})^{-1}$ shown in Figure 5.2. Since $s \notin \mathrm{L}^2(\mathbb{R})$, it is impossible to construct a frame for $\mathrm{L}^2(\mathbb{R})$ using individual translated and dilated sigmoids as frame elements. Note however, that the difference of two translated sigmoids is in $\mathrm{L}^2(\mathbb{R})$ for finite translations and that in general if we let

$$\varphi(x) = \sum_{n=1}^{M} s_{a_n b_n}(x) - \sum_{n=1}^{M} s_{c_n d_n}(x) \tag{5.2.3}$$

where $M < \infty$ and $s_{ab}(x) = s(ax - b)$, $a, b < \infty$ then $\varphi \in \mathrm{L}^2(\mathbb{R})$. Furthermore, note that the combinations (5.2.3) are precisely of the form which can be implemented in the architecture of a feedforward network. With these observation, it is easily shown that affine frames for $\mathrm{L}^2(\mathbb{R})$ may be constructed using analyzing wavelets generated as combinations of sigmoids of the form (5.2.3).

Let $s(x) = (1 + e^{-qx})^{-1}$, where $q > 0$ is a constant which controls the 'slope' of the sigmoid . To obtain a function in $\mathrm{L}^2(\mathbb{R})$, we combine two sigmoids as in (5.2.3). Let

$$\varphi(x) = s(x + d) - s(x - d),\ 0 < d < \infty. \tag{5.2.4}$$

So, $\varphi(\cdot)$ is an even function which decays exponentially away from the origin. Now, let

$$\psi(x) = \varphi(x + p) - \varphi(x - p). \tag{5.2.5}$$

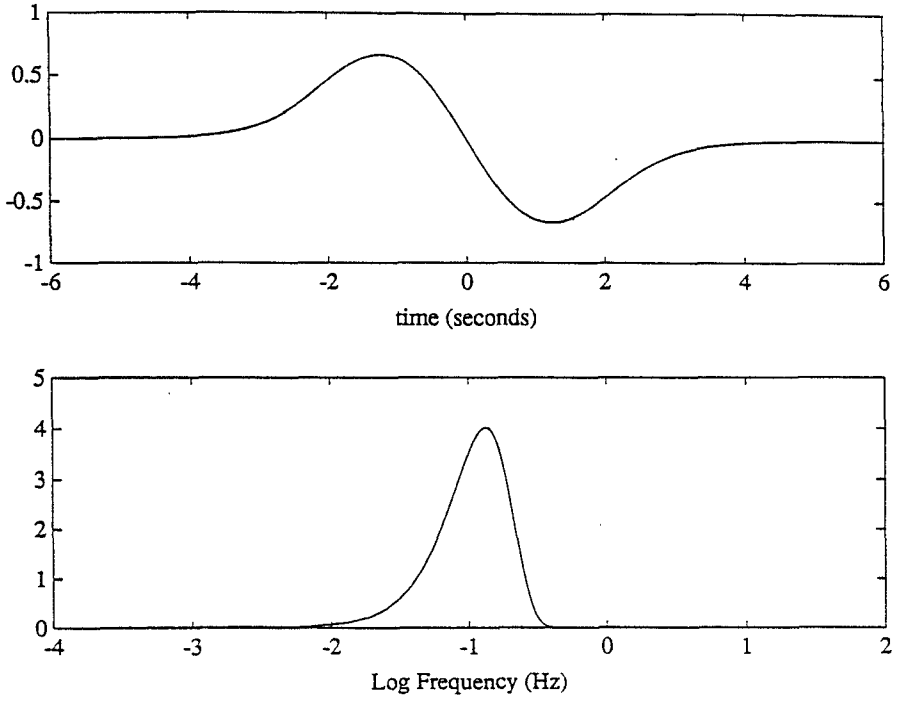

Figure 5.5: (Top) Analyzing wavelet candidate constructed from three sigmoids ($\psi(x) = s(x+2) - 2s(x) + s(x-2)$). (Bottom) Square magnitude of the Fourier transform of ψ, ($|\widehat{\psi}|^2$).

Thus $\psi(\cdot)$ (see Figure 5.5) is an odd function, with $\int \psi(x)dx = 0$, which is dominated by a decaying exponential. It is easily shown that ψ satisfies the admissibility condition (2.2.8). The Fourier transform of φ is given by

$$\widehat{\varphi}(\omega) = \int_{\mathbb{R}} \varphi(x) e^{-j\omega x} dx = \frac{2\pi}{q} \frac{\sin(\omega d)}{\sinh(\frac{\pi\omega}{q})} . \tag{5.2.6}$$

Therefore the Fourier transform of ψ is,

$$\widehat{\psi}(\omega) = e^{-jp\omega}\widehat{\varphi}(\omega) - e^{jp\omega}\widehat{\varphi}(\omega) = -j\frac{4\pi}{q} \frac{\sin(p\omega)\sin(d\omega)}{\sinh(\frac{\pi\omega}{q})}. \tag{5.2.7}$$

The function ψ and the square magnitude of its Fourier transform ($|\widehat{\psi}|^2$) are shown in Figure 5.5 for $p = d = 1$ and $q = 2$. Note that the function ψ is reasonably

well-localized in both the time and frequency domains. Table 5.1 lists some relevant parameters describing the (numerically determined) localization properties of ψ. For this choice of (p, d, q) (and in general whenever $p = d$) ψ is a linear combination of three sigmoids,

$$\psi(x) = s(x+2) - 2s(x) + s(x-2).$$

Figure 5.6 shows the implementation of ψ in a feedforward network.

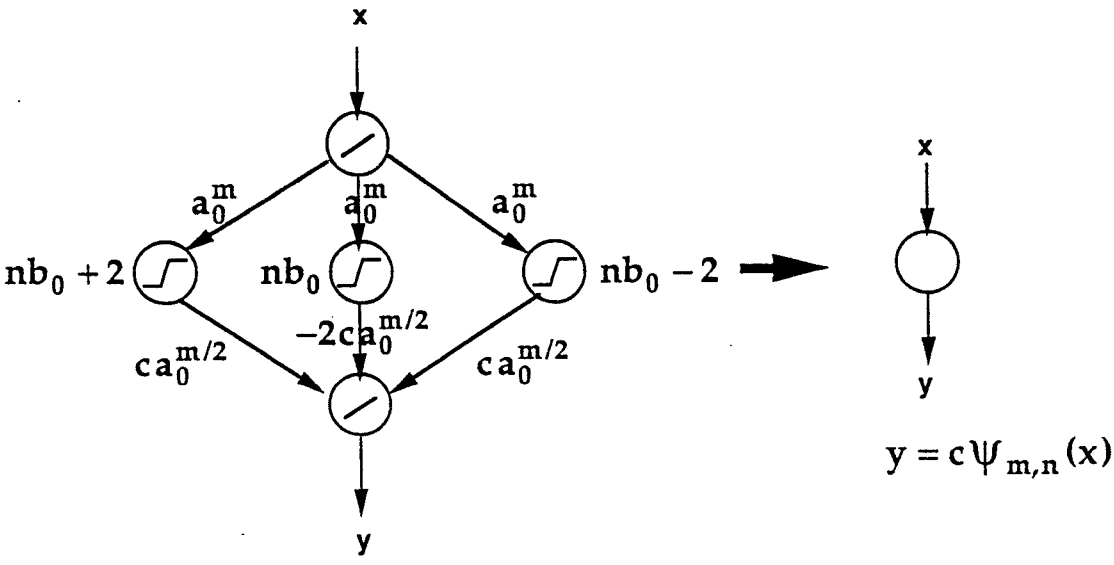

Figure 5.6: Feedforward network implementation of ψ

ϵ	$\widehat{\epsilon}$	$x_c(\psi)$	$\omega_c(\lvert\widehat{\psi}\rvert^2)$	ϵ-supp(ψ, ϵ)	ϵ-supp$(\lvert\widehat{\psi}\rvert^2, \widehat{\epsilon})$
0.1	0.1	0.0	0.9420	$[-2.15, 2.15]$	[0.2920, 1.5920]

Table 5.1: Time-frequency localization properties of ψ for $(p, d, q) = (1, 1, 2)$

Dilation and Translation Stepsizes for the Wavelet Constructed From Sigmoids

As in Chapter 3, Theorem 2.6 may be applied to numerically determine translation and dilation stepsizes a_0 and b_0, for which the family of functions $\{\psi_{m,n}\}$, forms an affine frame for $L^2(\mathbb{R})$, where the analyzing wavelet ψ is as in (5.2.5). Numerical results of applying Theorem 2.6 and Corollary 2.1, with dilation stepsize $a = 2.0$, to the construction of an affine frame using the analyzing wavelet ψ (5.2.5) with $(p, d, q) = (1, 1, 2)$ are shown in Figures 5.7–5.8. Figure 5.7 shows the estimates of the upper and lower frame bounds, A and B, for various values of the translation stepsize b. Figure 5.8 is a plot of the ratio B/A versus the translation stepsize. From these results we see that for $a = 2_0$ and $0 < b \leq 3.5$, (ψ, a, b) generates an affine frame for $L^2(\mathbb{R})$.

Remarks

The conditions in Theorem 2.6 and subsequently those in Corollary 2.1, in general may be very conservative since the theorem relies on the *Cauchy-Schwarz inequality* to establish bounds.

In some applications, it may be desirable to use a 'sparsely distributed' frame to 'cover' a given time interval and frequency band using a small number of frame elements. As can be seen from Figure 5.8, sparsity can be achieved to some extent at the cost of 'tightness' of the frame.

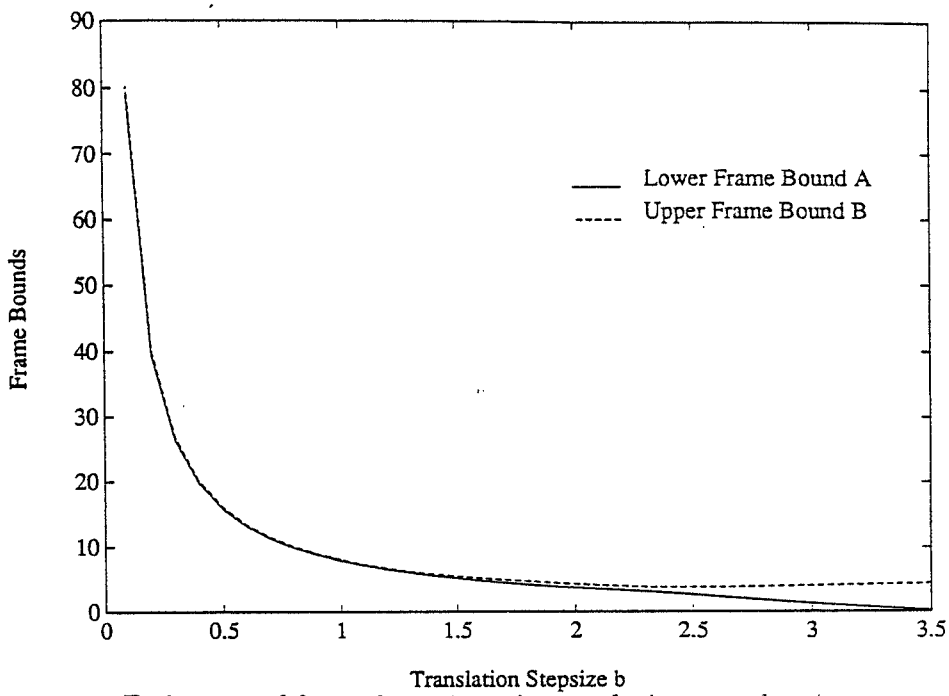

Figure 5.7: Estimates of frame bounds, using analyzing wavelet ψ constructed from sigmoids, with $a_0 = 2$, as translation stepsize b_0 is varied. Solid curve: lower frame bound A; Dashed curve: upper frame bound B.

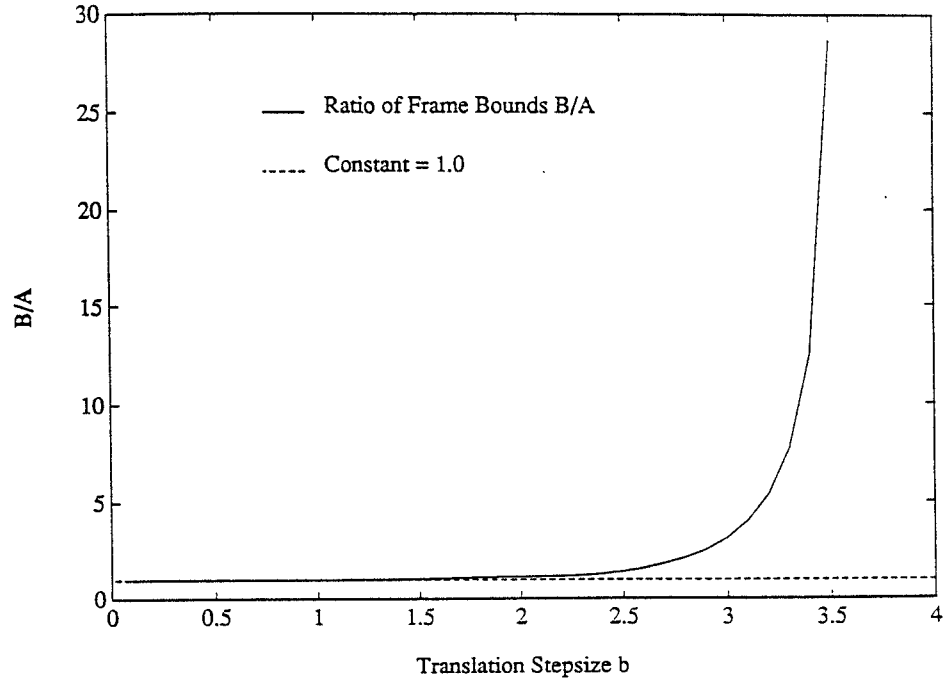

Figure 5.8: Ratio (B/A) of estimated frame bounds using analyzing wavelet ψ constructed from sigmoids, with $a_0 = 2$, as translation stepsize b_0 is varied. Solid curve: B/A Dashed line: constant=1.0

5.2.2 Feedforward Network Analysis Theorem

It now follows that we have constructively proved the following analysis result for SISO feedforward networks with sigmoidal activation functions.

Theorem 5.1 *Feedforward neural networks with sigmoidal activation functions and a single hidden layer can represent any function* $f \in L^2(\mathbb{R})$. *Moreover, given* $f \in L^2(\mathbb{R})$, *all weights in the network are determined by the wavelet frame expansion of* f,

$$f(x) = \sum_{m,n} \left\langle f, S^{-1}\psi_{mn} \right\rangle \psi_{mn}(x).$$

Remarks:

(a) In this section we have concentrated on wavelets constructed from sigmoids. We would however like to point out that the methods of this section are applicable to a wide variety of choices of the activation function. For some examples of other activation functions we refer the reader to [SW89].

(b) Among other activation functions used in neural networks, is the discontinuous sigmoid (step) function. Note that using such a step function together with the methods of this section results in a analyzing wavelet ψ which is the Haar wavelet. Dilates and translates of the Haar function generate an orthonormal basis for $L^2(\mathbb{R})$. The Haar transform is the earliest known example of an affine wavelet transform.

5.2.3 Wavelets For $L^2(\mathbb{R}^n)$ Constructed From Sigmoids

Although we shall primarily restrict attention to the one-dimensional setting ($L^2(\mathbb{R})$), wavelets for higher dimensional domains ($L^2(\mathbb{R}^n)$) may also be constructed within the standard feedforward network setting with sigmoidal activation functions. In applications such as image processing it is desirable to use wavelets which exhibit orientation selectivity as well as spatio-spectral selectivity. In the setting of Multiresolution

Analysis [Mal89c] for example, wavelet bases for $L^2(\mathbb{R}^2)$ are constructed using tensor products of wavelets for $L^2(\mathbb{R})$ and the corresponding 'smoothing' functions. This method results in three analyzing wavelets for $L^2(\mathbb{R}^2)$ each with a particular orientation selectivity. However neural network applications do not necessarily require such orientation selective wavelets. In this case, it is possible to use translates and dilates of a single 'isotropic' function to generate wavelet bases or frames for $L^2(\mathbb{R}^n)$ (c.f. [Mal89b]). Figures 5.9–5.10 show both an isotropic mother wavelet and an orientation selective mother wavelet for $L^2(\mathbb{R}^2)$ which are implemented in a standard feedforward neural network architecture with sigmoidal activation functions. The wavelets of Figures 5.9–5.10 are implemented by taking differences of 'bump' functions which are generated using a construction given by Cybenko in [Cyb88]. As before, if we let $s(\cdot)$ denote the sigmoidal activation function, Cybenko's construction gives the following formula for a N-dimensional bump function,

$$\varphi(x) = s\left(q\sum_{i=1}^{N} s(x_i + d) - s(x_i - d)\right),$$

where $x \in \mathbb{R}^N$, and x_i denotes the i^{th} component of x. This is the N-dimensional equivalent of the 'bump' function φ (see (5.2.4)), of the one-dimensional case. The difference is that *two hidden layers* are required in the general N-dimensional case. Figure 5.11 shows the feedforward network implementation of a two-dimensional bump function. Admissible analyzing wavelets for $L^2(\mathbb{R}^N)$ may be constructed by taking appropriate differences of such bump functions. Thus the analysis result of Theorem 5.1 is easily extended to higher dimensions in this manner (with the appropriate modification for two hidden layers).

Remark: It is important to note however, that as the dimension N grows, the size of the network grows quite dramatically. This is primarily due to the number of sigmoidal nodes required to implement a single wavelet. Thus, although there are no theoretical problems with this formulation, practical considerations may weigh quite heavily in it's use. This already suggests that if the wavelet formulation is to find

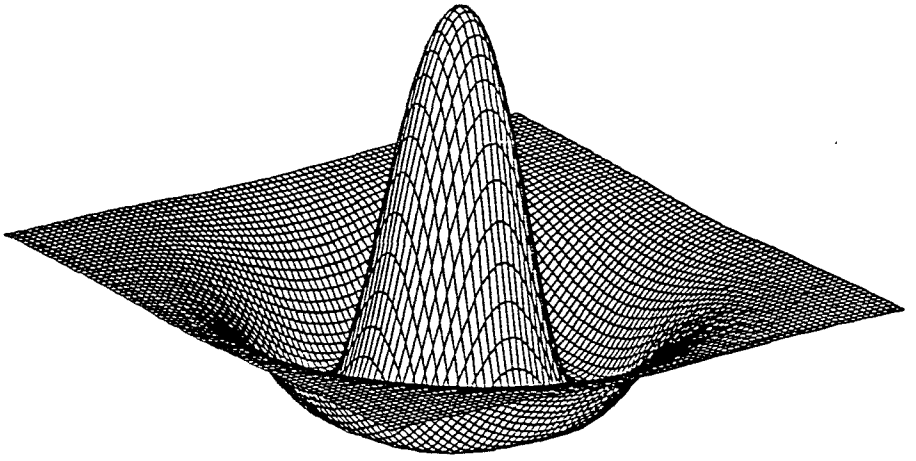

Figure 5.9: Two-Dimensional isotropic wavelet constructed from sigmoids in feedforward network architecture

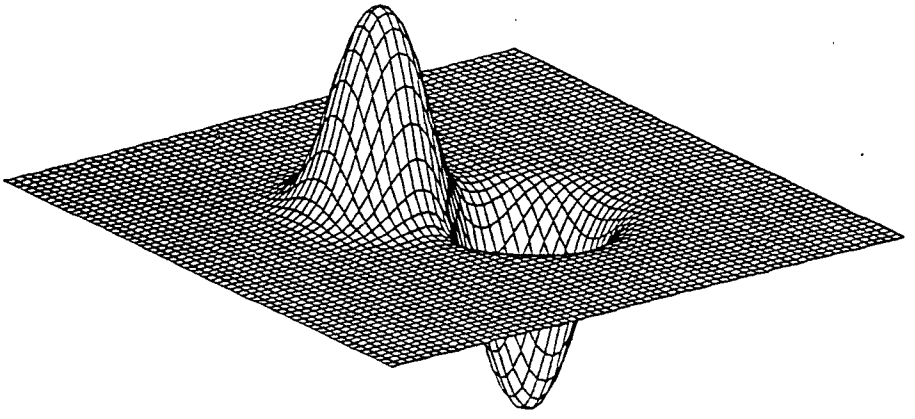

Figure 5.10: Two-Dimensional orientation selective wavelet constructed from sigmoids in feedforward network architecture

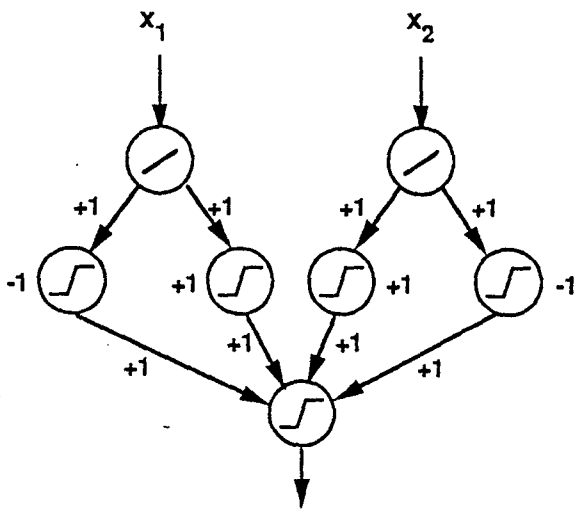

Figure 5.11: Feedforward network implementation of two-dimensional 'bump' function using sigmoidal activation functions.

practical use in feedforward neural networks, it is perhaps necessary to consider other activation functions which more naturally give rise to N-dimensional wavelets.

5.3 Synthesis of Feedforward Neural Networks Using Wavelets

In Section 5.2.1, it was shown that affine frames for $L^2(\mathbb{R})$ can be constructed based on analyzing wavelets ψ which are constructed as combinations of sigmoidal functions. From this was derived the analysis result Theorem 5.1 which states that any function in $L^2(\mathbb{R})$ may be approximated by a feedforward network with one hidden layer and sigmoidal activation functions. This result is analogous to the existence results mentioned in the beginning of this chapter. There is however an additional statement in Theorem 5.1. Namely, given a particular function in $L^2(\mathbb{R})$, its exact feedforward network implementation is given by its wavelet decomposition. In this

section, we shall examine some implications of the wavelet formalism for functional approximation based on sigmoids, in the synthesis of feedforward neural networks. As was described in Section 5.1.1, sigmoidal functions have served as the basis for functional approximation by feedforward neural networks. However, in the absence of an adequate theoretical framework, topological definitions of feedforward neural networks have for the most part been trial-and-error constructions. We will demonstrate, by means of the simple network discussed in Section 5.2, how, it is possible to incorporate the joint time and frequency domain characteristics of any given approximation problem into the initial network configuration.

Let $f \in L^2(\mathbb{R})$ be the function which we are trying to approximate. In other words, we are provided a set Θ of sample input-output pairs under the mapping f,

$$\Theta = \{(x^i, y^i) : y^i = f(x^i);\ x^i, y^i \in \mathbb{R}\},$$

and we would like to obtain a good approximation of f. To perform the approximation using a neural network, the first step is to decide on a network configuration. For this problem, it is clear that the input and output layers must each consist of a single node. The remaining questions are how many hidden layers should we use and how many nodes should there be in each hidden layer. These questions can be addressed using the wavelet formulation of the last section. We consider a network of the form in Figure 5.4, i.e. with a single hidden layer. At this point, a traditional approach would entail fixing the number of nodes N, in the hidden layer and then applying a learning algorithm such as backpropagation (described in Section 5.1.1) to adjust the three sets of weights, input weights $\{w_{0,j}\}_{j=1}^{N}$, output weights $\{w_{j,N+1}\}_{j=1}^{N}$, and the biases $\{I_j\}$. We would like to use information contained in the training set Θ to, (1) decide on the number of nodes in the hidden layer, and (2)simplify the training algorithm.

Here we describe two possible schemes for use of the wavelet transform formulation in the synthesis of feedforward networks. The first scheme captures the essence of how time-frequency localization can be utilized in the synthesis procedure. However, this

scheme is difficult to implement when considering high dimensional mappings and in most cases will result in a network that is far larger than necessary. We also outline a second method which further utilizes the time-frequency localization offered by wavelets to reduce the size of the network. This second method is conceivably a more viable option in the case of higher dimensional mappings.

5.3.1 Network Synthesis: Method I

Let $f \in \mathrm{L}^2(\mathbb{R})$ be the function we are trying to approximate, and as before, let

$$\Omega(f) = [\omega_{\min}, \omega_{\max}],$$

denote the frequency concentration [2] of f. Also assume that there exists a finite interval

$$R(f) = [x_{\min}, x_{\max}],$$

in which we wish to approximate f. Our network synthesis procedure is described in algorithmic form below.

Synthesis Algorithm:

Step I Our first step is to perform a frequency analysis of the training data. In this step we wish to obtain an estimate $\widetilde{\Omega}(f)$, of the frequency concentration $\Omega(f)$, of f based on the data contained in Θ. A number of techniques can be considered for performing this estimate. We will not elaborate on such techniques here. Let $\widetilde{\omega}_{\min}$ be our estimate of $\omega_{\min}$, and $\widetilde{\omega}_{\max}$ be our estimate of $\omega_{\max}$.

Step II We now use the knowledge of $\widetilde{\Omega}(f)$ and $R(f)$, to choose the particular frame elements to be used in the approximation. The main idea in this step is to choose only those elements of the frame $\{\psi_{mn}\}$ which 'cover' the region $\widetilde{\mathcal{Q}}_f$ of the time-frequency plane defined by

$$\widetilde{\mathcal{Q}}_f = R(f) \times \widetilde{\Omega}(f),$$

[2] Assuming f is real-valued, we need only consider positive frequencies.

which represents the concentration of f in time and frequency as determined from the data Θ. Recall that, the time frequency concentration of the wavelets $\psi_{m,n}$ is denoted by,

$$\mathcal{Q}_{m,n}(\psi) = R_{m,n}(\psi) \times \Omega_{m,n}(\psi).$$

Figure 5.12 shows the location of $\mathcal{Q}_f$, and the $\mathcal{Q}_{m,n}$'s together with the time-frequency concentration centers $(x_c(\psi_{m,n}), \omega_c(|\widehat{\psi}_{m,n}|^2)$ of the frame elements. Therefore to 'cover' $\mathcal{Q}_f(\epsilon, \hat{\epsilon})$ we need to determine the index set $\mathcal{I}$ of pairs (m,n) of integer translation and dilation indices such that,

$$\mathcal{Q}_{m,n} \cap \mathcal{Q}_f \neq \emptyset, \text{ for } (m,n) \in \mathcal{I}.$$

Step III Given $\mathcal{I}$, it is now possible to configure the network. From the manner in which $\mathcal{I}$ is defined, we expect to be able to obtain an approximation to f of the form

$$f(x) \approx \sum_{(m,n)\in\mathcal{I}} c_{m,n}\psi_{m,n}(x) \;=\; \widetilde{f}(x). \tag{5.3.8}$$

for $x \in [x_{\min}, x_{\max}]$. The approximation error in (5.3.8) can be made arbitrarily small by allowing ϵ and $\hat{\epsilon}$ to go to zero in the computation of the various concentration regions used to define the sets $\mathcal{Q}_f$ and $\mathcal{Q}_{mn}$. This is because we know that $\{\psi_{m,n}\}$ is a frame and therefore it is possible to write f as

$$f(x) = \sum_{m,n\in\mathbb{Z}} c_{m,n}(f)\psi_{m,n} \tag{5.3.9}$$

for some coefficients $\{c_{m,n}(f)\}$. Returning to the single-hidden layer feedforward network shown in Figure 5.4, choose the number of nodes in the hidden layer to be equal to the number of elements in $\mathcal{I}$, i.e. $N = \#(\mathcal{I})$ where the activation function of each node is taken to be ψ (as in 5.2.5). Now if we set the weights from the input node to the hidden layer and the biases on each hidden layer node to the dilation and translation coefficients indexed by $(m,n) \in \mathcal{I}$, then the output of the network can be written as

$$y = \sum_{(m,n)\in\mathcal{I}} c_{m,n}\psi_{m,n}(x) \tag{5.3.10}$$

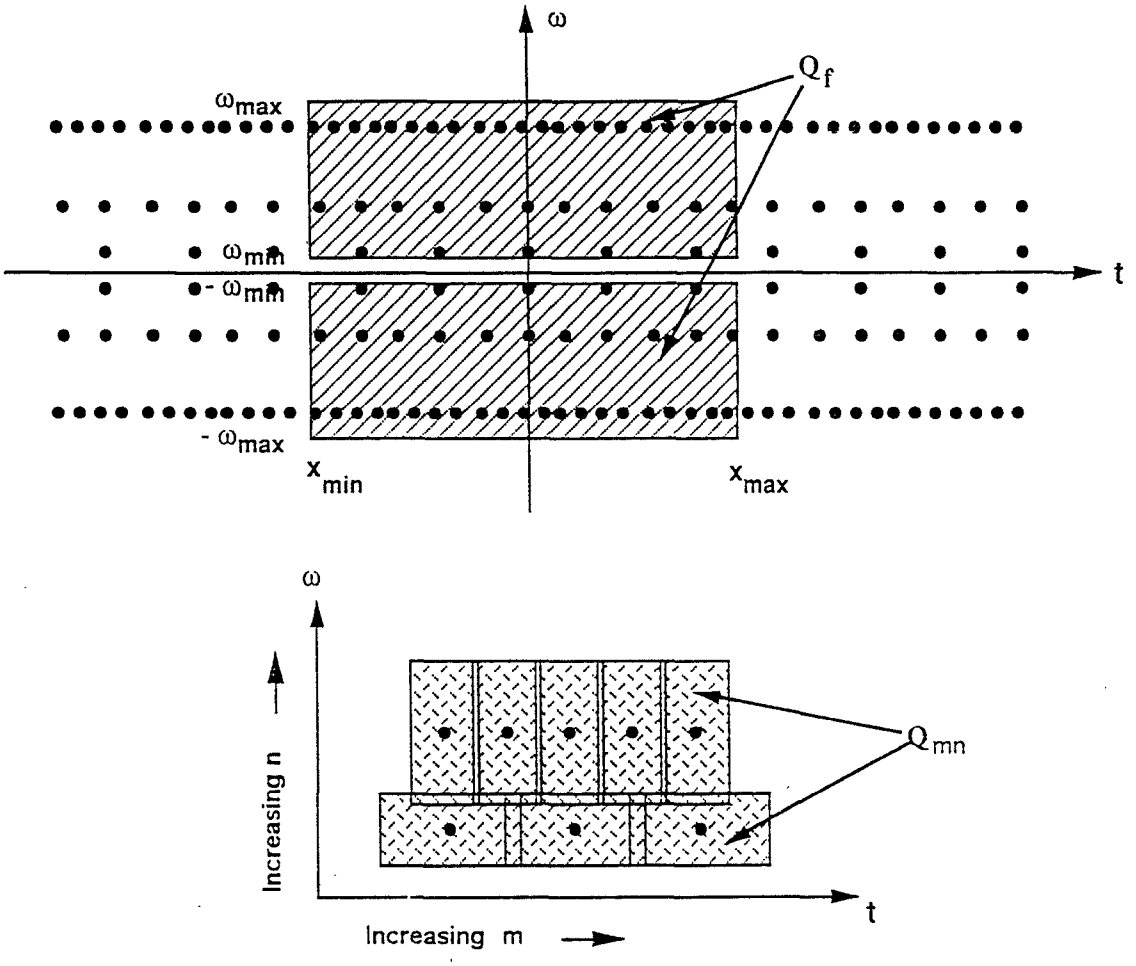

Figure 5.12: (Top) Time-frequency concentration $\mathcal{Q}_f$ and concentration centers $(x_c(\psi_{mn}), \omega_c(|\widehat{\psi}_{m,n}|^2)$ of the frame elements.(Bottom) Time-frequency concentrations $\mathcal{Q}_{mn}$'s, of wavelets.

where x is the input of the network and $c_{m,n}$'s are the weights from the hidden layer to the output node. We have therefore obtained a network configuration which defines an output function (5.3.10) that is exactly of the form required to approximate the function f (Equation (5.3.8)).

It remains to determine the coefficients $c_{m,n}$'s in (5.3.10) that will result in the desired approximation.

5.3.2 Network Synthesis: Method II

The synthesis algorithm described above in Section 5.3.1 uses identification of an 'important' region $\mathcal{Q}_f$ of the time-frequency plane. Critical to identification of this region is the 'bandwidth' estimate made in Step I. There are two significant drawbacks of making such a bandwidth estimate:

(1) Estimation of spectral concentration of signals in high dimensions is computationally expensive.

(2) Any estimate of spectral concentration which relies on Fourier techniques is going to generate a generalized rectangle in joint time-frequency space. For many functions such a rectangular concentration in time-frequency is simply an artifact of the spatial nonlocality of the Fourier basis. For example, an estimate of the frequency concentration of the signal in Figure 2.1 will generate a rectangle in time-frequency as the concentration of the signal. If we then use this rectangle to choose which elements of a wavelet basis to use to approximate the signal, the time-frequency rectangle will dictate that large dilations (corresponding to high frequencies) of the wavelets be used over the entire time interval. However, since each wavelet is also localized in time, and high frequency components of the signal are localized as well, this is clearly an excessive number of wavelets. Large dilations can be used locally where needed.

Spatio-spectral localization properties of wavelets can be further exploited to reduce the number of network nodes (wavelets) used in the approximation. The basic idea

is that since wavelets are well-suited to identify spatially local regions of fine scale (high frequency) features in a signal, locations and values local maxima of the wavelet approximation coefficients at one scale (dilation) indicate whether or not it is necessary to locally refine the approximation by the use of wavelets at finer scales (c.f. [MH]). A network synthesis algorithm using this idea would be an adaptive procedure of the following form.

(1) Construct and train a network to approximate the mapping at some scale a_0^m over the entire spatial region of interest.

(2) Identify local maxima of the wavelet coefficients and locally refine the approximation by adding new dilations (nodes) to the network where needed.

(3) Repeat (2) until some stopping criterion has been satisfied.

Using a scheme such as this would result in approximations being performed over regions of time-frequency of the form shown in Figure 5.13. Some aspects of this

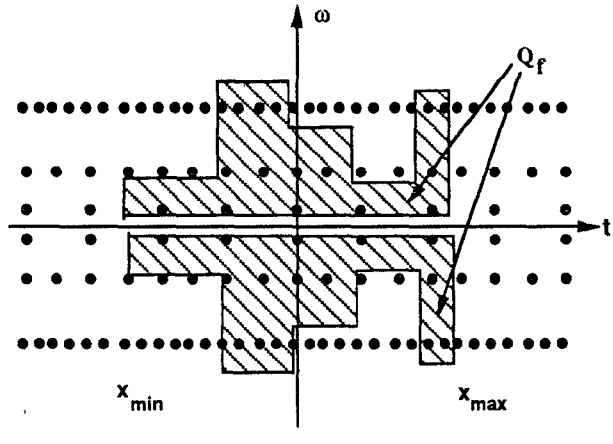

Figure 5.13: Form of time-frequency coverage from approximation scheme of Section 5.2.

scheme are discussed in [Pat91].

5.3.3 Computation of Coefficients (Training)

Variational computation of wavelet coefficients based on training data

Although the problem of determining the wavelet coefficients in a finite approximation can be well formulated, we know of no analytic solution to the problem of explicitly computing the coefficients, given only (possibly irregularly spaced) samples of the function. We can however formulate the coefficient computation problem as a variational principle in a fashion analogous to learning algorithms such as backpropagation. We define our cost functional to be

$$E = \sum_{(x^i,y^i)\in\Theta} \|O^i - y^i\|^2 = \sum_{(x^i,y^i)\in\Theta} | \sum_{(m,n)\in\mathcal{I}} c_{m,n}\psi_{m,n}(x^i) - y^i|^2, \qquad (5.3.11)$$

where O^i is the output of the network when x^i is the input as in Section 5.1.1. We choose the wavelet coefficients as those which minimize E. As a result of the wavelet formulation, the weights to be determined appear linearly in the output equation of the network. Thus E is a *convex* function of the coefficients $\{c_{m,n}\}$ and therefore any minimizer $c^* = \{c^*_{m,n}\}_{(m,n)\in\mathcal{I}}$ of E is a *global minimizer*. Simple iterative optimization algorithms such as gradient descent can be used to minimize E.

Remark: Since the cost functional (5.3.11) defines a linear least squares problem, the training problem may also be solved via the normal equations as discussed in Chapter 2.

5.3.4 Simulations

As a test of the neural network synthesis procedure described above, we simulated a few simple examples. As a first test we chose the bandlimited function comprised of two sinusoids at different frequencies, specifically $f(x) = sin(2\pi 5x) + sin(2\pi 10x)$ which is shown in Figure 5.14. Taking $x_{\min} = 0.0$ and $x_{\max} = 0.3$, 50 randomly spaced samples of the function were included in the training set Θ. A single dilation of the mother wavelet was chosen ($m = 6$) which covered the frequency range adequately

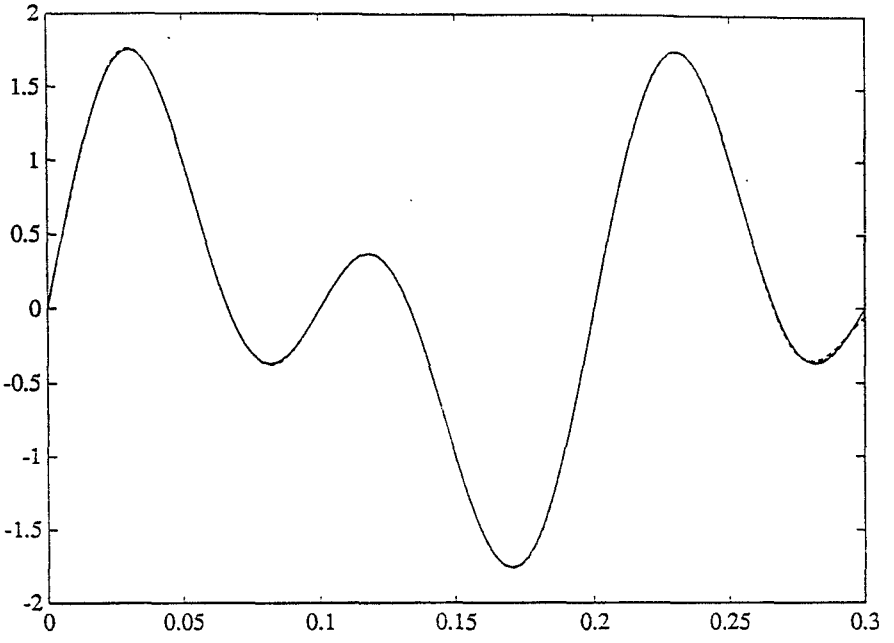

Figure 5.14: Original bandlimited function $f(x) = \sin(2\pi 5x) + \sin(2\pi 10x)$, (solid curve), and finite wavelet approximation (dashed curve).

(see Figure 5.15). Translations[3] of this dilation of ψ which contributed significantly in the interval $[x_{\min}, x_{\max}]$ were used, resulting in 40 hidden units. Applying a simple gradient descent scheme to minimize E, an approximation to f was obtained. The resulting approximation is shown in Figure 5.14 along with the original function.

A second, slightly more complicated, example was simulated by first generating a random spectrum (Figure 5.16) which is concentrated in frequency and then sampling the corresponding function in the time domain. The result of this simulation using again just one dilation of the mother wavelet is shown in Figure 5.17.

[3]These translations were integer multiples of the translation stepsize b.

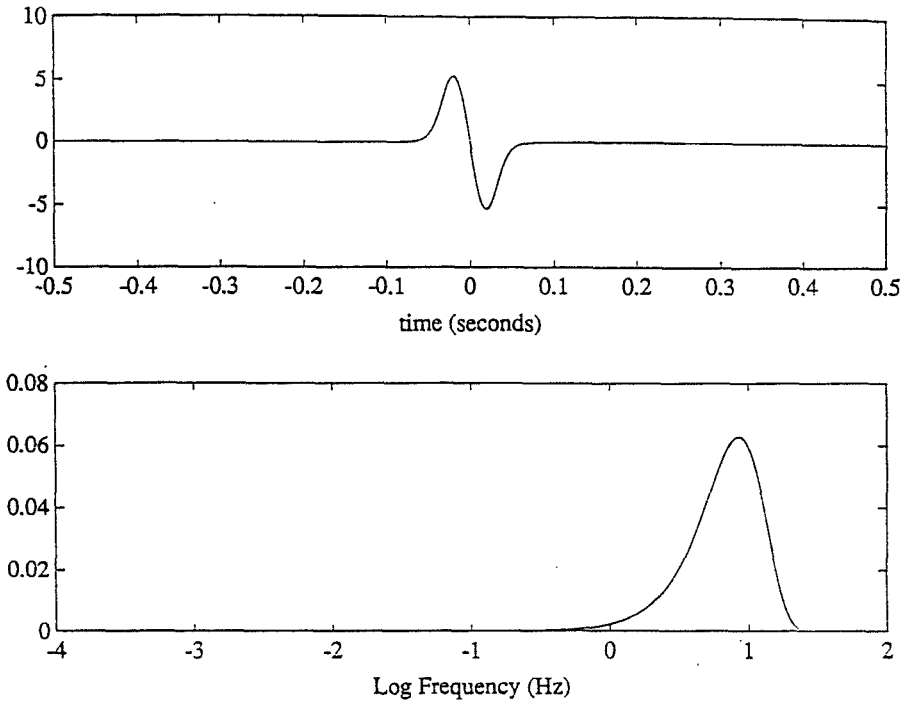

Figure 5.15: (Top) Wavelet $\psi_{m,n}$ for $n = 0, m = 6$, (Bottom) Square magnitude of Fourier transform of ψ_{mn} $(n = 0, m = 6)$.

5.4 Summary

We have demonstrated that it is possible to construct a theoretical description of feedforward neural networks in terms of wavelet decompositions. This description follows naturally from the inherent translation and dilation structure of such networks. The wavelet description of feedforward networks easily characterizes the class of mappings which can be implemented in such architectures. Although such characterizations have been previously provided in a number of different forms [Cyb89, Cyb88, HSW89], to our knowledge, no previous characterization using sigmoidal activation functions is capable of defining the exact network implementation of a given function. What is distinctly different about the wavelet viewpoint is that it provides an extremely flexi-

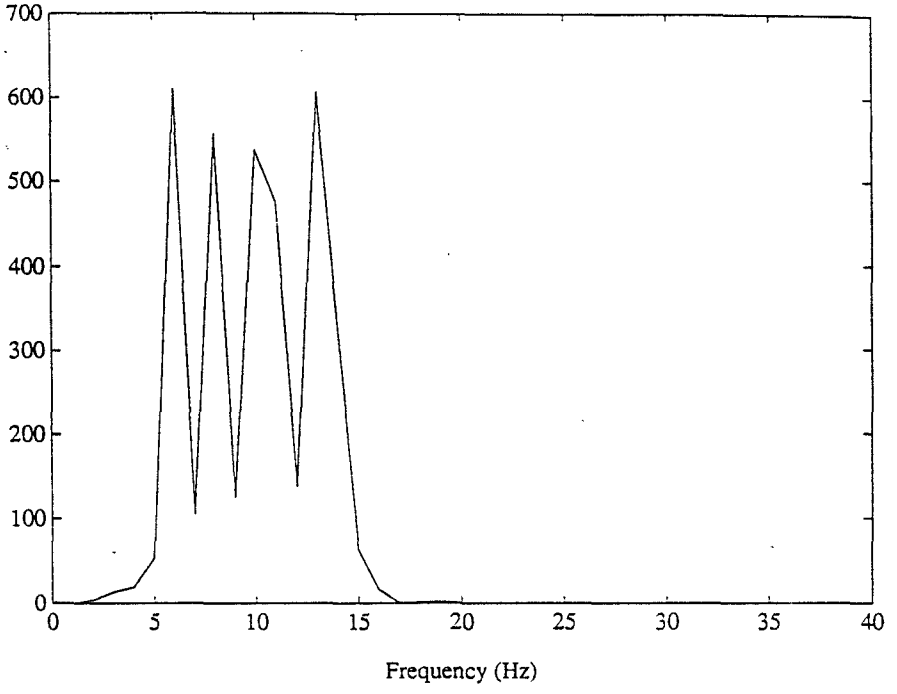

Figure 5.16: Frequency-concentrated 'random' spectrum.

ble (not necessarily orthogonal) transform formalism. This flexibility has been utilized in this chapter to construct a transform based upon combinations of sigmoids. Once again, we would like to point out that in general there is nothing special about sigmoidal functions and that a variety of different activation functions, including e.g. orthogonal wavelets can be of significant interest. Sigmoidal functions however hold one attraction; such functions can be easily implemented in analog integrated circuitry (see e.g.[Mea89]). Aside from this, we have chosen to work with sigmoidal functions only to demonstrate the general methodology that can be applied in the context of feedforward neural networks.

In addition to providing a theoretical framework within which to perform analysis of feedforward networks, the wavelet formalism supplies a tool which can be used to incorporate spatio-spectral information contained in the training data in structuring of

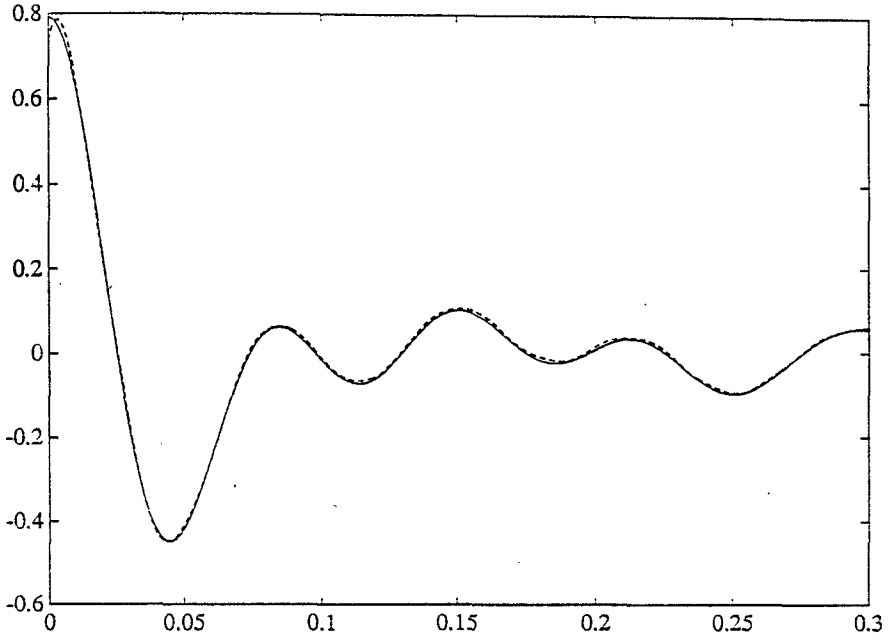

Figure 5.17: Frequency-concentrated signal corresponding to random spectrum in Figure 14 (solid curve), and finite wavelet approximation (dashed curve).

the network. Two possible schemes to perform this task were described in Section 5.3. Minimality in terms of the number of nodes in the network cannot be guaranteed using these methods[4]. However, it is possible to estimate the approximation error ([Dau90]) in terms of the signal energy lying outside the chosen spatio-spectral region.

Here, attention has been primarily restricted to approximating functions in $L^2(\mathbb{R})$. Most applications where neural networks are particularly useful involve mappings in higher dimensional domains (e.g. in vision, robot motion control, etc). Although extensions of the methods of this chapter to higher dimensions are possible (as described in Section 5.2.3), such extensions have the potential to be computation-

[4]This problem of large networks is particularly limiting when considering mappings in higher dimensions

ally expensive. We are currently studying the formulation of more computationally viable synthesis techniques for approximation of higher dimensional mappings using feedforward neural networks.

Using the wavelet formalism to synthesize networks results in a greatly simplified training problem. Unlike the situation in traditional feedforward neural network constructions, the cost functional is convex and thereby admits *global* minimizing solutions only. Convexity of the cost functional is a result of fixing the weights in the arguments of the nonlinearities so as to provide the required dilations and translations. Simple iterative solutions to this problem such as gradient descent are thus justifiable and are not in danger of being trapped in local minima.

Chapter 6

Conclusions and Discussion

In this dissertation we have examined two problems, both of which may be considered under the heading of approximation theory. Specifically we considered the problems of (i) rational approximation and identification of stable linear systems, and (ii) developing a theoretical framework for analysis and synthesis of feedforward neural networks. These problems were both addressed within the nonclassical setting of frames and time-frequency localized representations. The key argument to be made in support of the use of frames rather than orthonormal systems is the tremendous flexibility offered by frame theory in the selection of 'basis' functions. In many applications such as those considered in this dissertation, the choice of 'bases' with suitable properties is more important than orthogonality or even linear independence. The role played by time-frequency localization in these applications is one of providing a systematic procedure for approximation.

In Chapter 3 it was shown that frames for the Hardy space $H^2(\Pi^+)$, may be constructed via dilations and translations of a single rational analyzing wavelet. Furthermore, a characterization of all rational $H^2(\Pi^+)$ analyzing wavelets was given in Theorem 3.4. One of the main results of Chapter 3 is Theorem 3.3, which states that transfer functions in $H^2_{\mathbb{R}}(\Pi^+)$, may be represented as infinite sums of time-frequency localized real-rational functions of bounded McMillan degree. The representation of Theorem 3.3 arises via a regrouping of terms in wavelet series representations, where

the analyzing wavelet is chosen to be real-rational. The series obtained via this regrouping is called a *wavelet system (WS) decomposition.* Wavelet system decompositions are a means of representing causal LTI systems with square-integrable weighting patterns as parallel combinations of time-frequency localized finite-dimensional systems. The key property of such decompositions, which makes them useful in problems of rational approximation is the property of time-frequency localization. There are of course systems for which time-frequency localization may offer no significant advantage in the construction of low-order approximants, e.g. systems with very large 'bandwidths', and slowly decaying impulse responses. However, for an important class of physical systems, time-frequency localization can lead to compact representations. For such systems, we showed that rational approximants of fairly low order may be obtained by suitable truncations of the WS series. Furthermore we showed that minimal state space realizations for the approximating systems may be generated under easily verified hypotheses on the poles of the analyzing wavelet. A coarse bound on the approximation error was derived based on the ℓ^2 norm of the expansion coefficients. The methods of Chapter 3 were illustrated by the example of a nonrational transfer function arising from the heat equation with Dirichlet boundary control.

In Chapter 4 we considered the use of truncated WS series as black-box rational parametric models in problems of system identification. In this case as well, the key property of of WS representations was shown to be time-frequency localization. It was shown that time-frequency localization provides a convenient means of incorporating *a priori* information about the unknown system into the formal properties of the parametric model. Moreover, time and frequency domain *a priori* knowledge may be treated simultaneously via WS models. We made both qualitative and numerical comparisons of WS models and the classical Laguerre filter models. It was shown by examples that the performance of WS models can be significantly better than Laguerre models for some commonly encountered classes of systems. The main difficulty with the Laguerre models is due to the fact that too much emphasis is placed on a single parameter, namely the Laguerre shift parameter p. This difficulty has been noted on

a number of occasions in the past. We showed that the improvement on the Laguerre model suggested by Wahlberg [Wah91] which involved the use of a finite number of Laguerre shift parameters p_j, may be formally interpreted in the context of frames.

In Chapter 5 we demonstrated that it is possible to construct a mathematical description of feedforward neural networks via affine wavelet theory. In this description the inherent translation and dilation structure of such networks is utilized. The wavelet description of feedforward networks identifies L^2 as a class of mappings which can be implemented in such architectures. The flexibility of frame theory was utilized in constructing wavelet transforms based on sigmoidal functions. It was pointed out that we use sigmoidal functions here mainly to demonstrate the general methodology, and to show that this methodology is applicable to the most commonly used activation function. A key difference between the wavelet formulation and previous characterizations of the approximating properties of feedforward networks with sigmoidal activation functions, is the (nonorthogonal) transform formalism which gives the exact feedforward network implementation of a given mapping.

We also discussed the use of spatio-spectral localization properties of of affine wavelets as a tool for the synthesis of feedforward networks, and showed that such synthesis schemes lead to convex training problems.

Appendix A

Proof of Daubechies' Theorem

Since this dissertation makes extensive use of Theorem 2.6 and its Corollary, we include the proof for the sake of completeness. The proof also illustrates the applicability of this theorem in the case of the Hardy space H^2. Proof of Theorem 2.6 relies on the Poisson summation formula which we state below.

Lemma A.1 (Poisson Summation Formula) *Let $\widehat{f}$ denote the Fourier transform of f. Then*

$$\sum_{n\in\mathbb{Z}} f(t+nT) = \frac{1}{T}\sum_{n\in\mathbb{Z}} e^{in2\frac{2\pi}{T}t}\widehat{f}(n\frac{2\pi}{T})$$

A commonly used form of the Poisson summation formula is,

$$\sum_{n\in\mathbb{Z}} e^{inat} = \frac{2\pi}{a}\sum_{n\in\mathbb{Z}} \delta(t-\frac{2\pi n}{a}). \tag{1.0.1}$$

Proof of Theorem 2.6

$$\begin{aligned}
&\sum_{m,n} |\langle f, h_{m,n}\rangle|^2 \\
&= \sum_{m,n} \left|\frac{1}{2\pi}\left\langle \widehat{f}, \widehat{h}_{m,n}\right\rangle\right|^2 \\
&= \frac{1}{4\pi^2}\sum_{m,n} a_0^{-m}\int_{\mathbb{R}}\int_{\mathbb{R}} e^{inb_0a_0^{-m}(\omega-\omega_1)}\overline{\widehat{h}(a_0^{-m}\omega)}\widehat{h}(a_0^{-m}\omega_1)\widehat{f}(\omega)\overline{\widehat{f}(\omega_1)}d\omega d\omega_1
\end{aligned}$$

Applying the Poisson summation formula to the sum over n,

$$\begin{aligned}
&\sum_{m,n} |\langle f, h_{m,n}\rangle|^2 \\
&= \frac{1}{2\pi b_0} \sum_{m,k} \int_{\mathbb{R}} \int_{\mathbb{R}} \delta(w - w_1 - \frac{2\pi a_0^m k}{b_0}) \overline{\widehat{h}(a_0^{-m}\omega)} \widehat{h}(a_0^{-m}\omega_1) \widehat{f}(\omega) \overline{\widehat{f}(\omega_1)} d\omega d\omega_1 \\
&= \frac{1}{2\pi b_0} \sum_{m,k} \int_{\mathbb{R}} \overline{\widehat{h}(a_0^{-m}\omega)} \widehat{h}(a_0^{-m}\omega - \frac{2\pi}{b_0}k) \widehat{f}(\omega) \overline{\widehat{f}(\omega - \frac{2\pi}{b_0}k)} d\omega.
\end{aligned}$$

Separating out the $k = 0$ term,

$$\begin{aligned}
&\sum_{m,n} |\langle f, h_{m,n}\rangle|^2 \\
&= \frac{1}{2\pi b_0} \sum_{m} \left|\widehat{h}(a_0^{-m}\omega)\right|^2 \left|\widehat{f}(\omega)\right|^2 d\omega \\
&+ \frac{1}{2\pi b_0} \sum_{m} \sum_{k\neq 0} \int_{\mathbb{R}} \overline{\widehat{h}(a_0^{-m}\omega)} \widehat{h}(a_0^{-m}\omega - \frac{2\pi}{b_0}k) \widehat{f}(\omega) \overline{\widehat{f}(\omega - \frac{2\pi}{b_0}k)} d\omega \\
&\geq \frac{1}{b_0} m(h;a) \|f\|^2 + \frac{1}{2\pi b_0} \sum_{m} \sum_{k\neq 0} \int_{\mathbb{R}} \overline{\widehat{h}(a_0^{-m}\omega)} \widehat{h}(a_0^{-m}\omega - \frac{2\pi}{b_0}k) \widehat{f}(\omega) \overline{\widehat{f}(\omega - \frac{2\pi}{b_0}k)} d\omega
\end{aligned}$$

By first applying the Cauchy-Shwarz inequality to the integral on the right, and then to the sum over m, we get

$$\begin{aligned}
&\sum_{m,n} |\langle f, h_{m,n}\rangle|^2 \\
&\geq \frac{1}{b_0} m(h;a) \|f\|^2 \\
&- \frac{1}{2\pi b_0} \sum_{k\neq 0} \left[\sum_{m} \int_{\mathbb{R}} \left|\widehat{h}(a_0^{-m}\omega)\right| \left|\widehat{h}(a_0^{-m}\omega - \frac{2\pi}{b_0}k)\right| \left|\widehat{f}(\omega)\right|^2 d\omega \right]^{1/2} \\
&\cdot \left[\sum_{m} \int_{\mathbb{R}} \left|\widehat{h}(a_0^{-m}\omega + \frac{2\pi}{b_0}k)\right| \left|\widehat{h}(a_0^{-m}\omega)\right| \left|\widehat{f}(\omega)\right|^2 d\omega \right]^{1/2} \\
&\geq \frac{1}{b_0} m(h;a) \|f\|^2 - \frac{1}{b_0} \sum_{k\neq 0} \left(\beta(-\frac{2\pi}{b_0}k) \beta(\frac{2\pi}{b_0}k) \right)^{1/2} \|f\|^2.
\end{aligned}$$

Hence by hypothesis (3) there exists $b_0 > 0$, such that

$$m(h;a) - \sum_{k\neq 0} \left(\beta(-\frac{2\pi}{b_0}k) \beta(\frac{2\pi}{b_0}k) \right)^{1/2} > 0,$$

which gives the lower frame bound $A > 0$. The upper frame bound follows in a similar fashion. ■.

Appendix B

Proofs from Chapter 3

Proof of Proposition 3.2

Without loss of generality we can consider the case $m = 0$. Therefore we need to check that for $b \in \mathbb{R}$,

$$\int_{\mathbb{R}} f(\omega)g(\omega+b)d\omega - \overline{\left(\int_{\mathbb{R}} f(\omega)g(\omega-b)d\omega\right)} = 0. \tag{2.0.1}$$

Consider the real and imaginary parts of the l.h.s. of Equation (2.0.1) separately.

Real part Taking the real part of Equation (2.0.1) ,

$$\begin{aligned}
& \Re e\left(\int_{\mathbb{R}} f(\omega)g(\omega+b)d\omega - \overline{\left(\int_{\mathbb{R}} f(\omega)g(\omega-b)d\omega\right)}\right) \\
= \; & \Re e\left(\int_{\mathbb{R}} f(\omega)g(\omega+b)d\omega - \int_{\mathbb{R}} f(\omega)g(\omega-b)d\omega\right) \\
= \; & \Re e\left(\int_{-\infty}^{0} f(\omega)\left(g(\omega+b)-g(\omega-b)\right)d\omega + \int_{0}^{\infty} f(\omega)\left(g(\omega+b)-g(\omega-b)\right)d\omega\right) \\
= \; & \Re e\left(-\int_{\infty}^{0} f(-\omega)\left(g(-\omega+b)-g(-\omega-b)\right)d\omega\right. \\
& \left. + \int_{0}^{\infty} f(\omega)\left(g(\omega+b)-g(\omega-b)\right)d\omega\right) \\
= \; & \Re e\left(\int_{0}^{\infty} f(-\omega)\left(g(-(\omega-b))-g(-(\omega+b))\right)d\omega\right. \\
& \left. + \int_{0}^{\infty} f(\omega)\left(g(\omega+b)-g(\omega-b)\right)d\omega\right) \\
= \; & \Re e\left(\int_{0}^{\infty} \underbrace{\overline{f}(\omega)\left(\overline{g}(\omega-b)-\overline{g}(\omega+b)\right)}_{H(\omega)}d\omega + \int_{0}^{\infty} \underbrace{f(\omega)\left(g(\omega+b)-g(\omega-b)\right)}_{-\overline{H}(\omega)}d\omega\right)
\end{aligned}$$

$$= \Re e \left(\int_0^\infty \left[H(\omega) - \overline{H}(\omega) \right] d\omega \right) = 0$$

Imaginary part

$$\begin{aligned}
& \mathcal{I}m \left(\int_{\mathbb{R}} f(\omega) g(\omega + b) d\omega - \overline{\left(\int_{\mathbb{R}} f(\omega) g(\omega - b) d\omega \right)} \right) \\
= \; & \mathcal{I}m \left(\int_{\mathbb{R}} f(\omega) g(\omega + b) d\omega + \int_{\mathbb{R}} f(\omega) g(\omega - b) d\omega \right) \\
= \; & \mathcal{I}m \left(\int_{-\infty}^{0} f(\omega) \left(g(\omega + b) + g(\omega - b) \right) d\omega + \int_0^\infty f(\omega) \left(g(\omega + b) + g(\omega - b) \right) d\omega \right) \\
= \; & \mathcal{I}m \left(- \int_{\infty}^{0} f(-\omega) \left(g(-\omega + b) + g(-\omega - b) \right) d\omega \right. \\
& \left. + \int_0^\infty f(\omega) \left(g(\omega + b) + g(\omega - b) \right) d\omega \right) \\
= \; & \mathcal{I}m \left(\int_0^\infty f(-\omega) \left(g(-(\omega - b)) + g(-(\omega + b)) \right) d\omega \right. \\
& \left. + \int_0^\infty f(\omega) \left(g(\omega + b) + g(\omega - b) \right) d\omega \right) \\
= \; & \mathcal{I}m \left(\int_0^\infty \underbrace{\overline{f}(\omega) \left(\overline{g}(\omega - b) + \overline{g}(\omega + b) \right)}_{H(\omega)} d\omega + \int_0^\infty \underbrace{f(\omega) \left(g(\omega + b) + g(\omega - b) \right)}_{\overline{H}(\omega)} d\omega \right) \\
= \; & \mathcal{I}m \left(\int_0^\infty \left[H(\omega) + \overline{H}(\omega) \right] d\omega \right) = 0
\end{aligned}$$

Which proves the proposition ■.

B.1

Proof of Theorem 3.5

We outline here the proof of Theorem 3.5.

Proof of part (a): Since (3.4.28–3.4.30) is a $2N$-dimensional realization of $G^{m,n}(s)$, we need only prove that the rational function $G^{m,n}(s)$ is of order $2N$ for all $n \in \mathbb{Z}$, $n \neq 0$ if and only if (3.4.36) holds.

The poles of $G^{m,n}(s)$ (see (3.4.18)) are,

$$\{\eta_k(m,n), \overline{\eta_k}(m,n), \nu_k(m,n), \overline{\nu_k}(m,n)\}$$

where $\eta_k(m,n)$ and $\nu_k(m,n)$ are defined by (3.4.17). Assuming (3.4.36) holds, $\eta_k(m,n)$ and $\nu_k(m,n)$ have nonzero imaginary parts for all $m,n \in \mathbb{Z}$. Therefore, at $s = \eta_k(m,n)$ for example, the term,

$$\prod_k (s - \overline{\eta_k}(m,n))(s - \overline{\nu_k}(m,n))$$

which appears in the numerator polynomial $N_{m,n}(s)$ of $G^{m,n}$ will be nonzero. Furthermore, the assumption that Ψ is of order N, implies that $p_j \neq z_k$ for all z,k. Therefore at $s = \eta_k(m,n)$ the remaining (nonzero) term in the numerator of $G^{m,n}$ will be,

$$N_{m,n}(\eta_k(m,n)) = \alpha \prod_j (s - \beta_j(m,n))(s - \gamma_j(m,n)) \prod_k (s - \overline{\eta_k}(m,n))(s - \overline{\nu_k}(m,n)),$$

which shows that $G^{m,n}$ has no zeros at $\eta_k(m,n)$. Exactly the same argument can be used to show that there is no cancellation with zeros for the remaining poles. Thus $G^{m,n}$ is of order $2N$.

The converse is readily proved using a similar pole-zero cancellation argument. ■

Proof of part (b): By hypothesis, $(A_{m,n}, B_{m,n}, C_{m,n})$ is a minimal realization of $G^{m,n}(s) = N_{m,n}(s)/D_{m,n}(s)$ for all $(m,n) \in \mathcal{J}$. Therefore $N_{m,n}$ and $D_{m,n}$ are coprime polynomials. Consider the parallel combination of two WS transfer functions.

$$G_{\mathcal{J}}(s) = G_{m_1,n_1}(s) + G_{m_2,n_2}(s), \tag{2.1.2}$$

where $\mathcal{J} = \{(m_1,n_1),(m_2,n_2)\}$. In this case $(N_{m_1,n_1}(s), D_{m_2,n_2}(s))$ and $(N_{m_2,n_2}(s)D_{m_1,n_1}(s))$, are relatively coprime pairs. Rewriting (2.1.2),

$$\begin{aligned} G_{\mathcal{J}}(s) &= \frac{N_{\mathcal{J}}(s)}{D_{\mathcal{J}}(s)} \\ &= \frac{N_{m_1,n_1}(s)D_{m_2,n_2}(s) + N_{m_2,n_2}(s)D_{m_1,n_1}(s)}{D_{m_1,n_1}(s)D_{m_2,n_2}(s)}. \end{aligned}$$

Therefore $N_{\mathcal{J}}$ and $D_{\mathcal{J}}(s)$ will be relatively coprime if and only if D_{m_1,n_1} and $D_{m_2,n_2}(s)$ are relatively coprime. The roots of D_{m_1,n_1} and $D_{m_2,n_2}(s)$ are given by (3.4.18). Thus D_{m_1,n_1} and $D_{m_2,n_2}(s)$ will have a common root if and only if,

$$a_0^{-m_1}(p_l + in_1b_0) = a_0^{-m_2}(p_j \pm in_2b_0),$$

for some l and j. Solving for n_1,

$$\begin{aligned} n_1 &= \frac{-i}{b_0}\left(a_0^{m_1-m_2}p_j - p_l\right) \pm a_0^{m_1-m_2}n_2 \\ &= \frac{-i}{b_0}\left(a_0^{m_1-m_2}(\Re e\ p_j + i\mathcal{I}m\ p_j) - (\Re e\ p_l + i\mathcal{I}m\ p_l)\right) \pm a_0^{m_1-m_2}n_2 \\ &= \left(\frac{1}{b_0}\left(a_0^{m_1-m_2}\mathcal{I}m\ p_j - \mathcal{I}m\ p_l\right) \pm a_0^{m_1-m_2}n_2\right) \\ &\quad -\frac{i}{b_0}\left(a_0^{m_1-m_2}\Re e\ p_j - \Re e\ p_l\right) \end{aligned} \tag{2.1.3}$$

However, by hypothesis (3.4.37) there can be no integer solution n_1 to (2.1.3) since the imaginary part of (2.1.3) will always be nonzero. The above argument for two WS transfer functions is easily extended to any finite number of WS transfer functions in parallel. ■

Appendix C

Some Intuition on Frames

This appendix is included to help develop intuition and clarify some of the properties of frames. A few new results are presented as well. Often the familiar finite-dimensional Euclidean spaces $\mathbb{R}^N$, serve as a good place to develop intuition. For this reason, most of the examples below are in the setting of $\mathbb{R}^N$.

C.1 Simple Examples of Frames

Let us begin with a few examples of frames in the plane $\mathbb{R}^2$.

Example 1: Exact Frame with $A \neq B$

As a first example, consider the vectors,

$$x_1 = (1,0)^T \text{ and } x_2 = (\sin\theta, \cos\theta).$$

Then, $\{x_1, x_2\}$, is a frame for $\mathbb{R}^2$ with frame bounds

$$\begin{aligned} A &= 1 - \cos\theta \\ B &= 1 + \cos\theta. \end{aligned}$$

The vectors in this frame are linearly independent, and hence form a Riesz basis for $\mathbb{R}^2$. Note that with $\theta = \pi/2$, we get the standard orthonormal basis for $\mathbb{R}^2$.

Example 2: Redundant Tight Frame

Often the notion of tightness of a frame is confused with the notion of linear independence. This next example illustrates the disjoint nature of these two concepts. Let,

$$\begin{aligned} x_1 &= (1,0)^T \\ x_2 &= (-1/2, \sqrt{3}/2) \\ x_3 &= (-1/2, -\sqrt{3}/2) \end{aligned}$$

(see Figure C.1). Clearly the above three vectors are not linearly independent, but

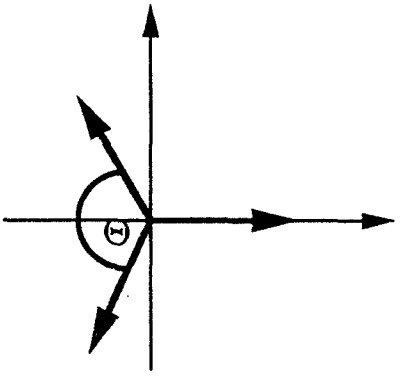

Figure C.1: A redundant tight frame for $\mathbb{R}^2$.

they do in fact form a tight frame for $\mathbb{R}^2$, with $A = B = 3/2$. Thus any vector $y \in \mathbb{R}^2$, may be written as

$$y = \sum_{k=1}^{3} \left\langle y, S^{-1}x_k \right\rangle x_k = \frac{2}{3} \sum_{k=1}^{3} \langle y, x_k \rangle x_k.$$

The interesting thing about this example is that any n unit-length vectors, where n is an odd, finite integer, will form a tight frame for $\mathbb{R}^2$ if they are distributed uniformly in the sense of the angles θ (see Figure C.1) between the vectors is $\theta = 2\pi/n$. By a leap of faith, it is convenient to think of tight frames as frames in which the frame elements are uniformly distributed. It is clear however that tightness does not imply

linear independence in any sense since by the above example, a tight frame may be made arbitrarily redundant. Moreover, linear independence does not imply tightness, as is clear from Example 1, and also the definition of Riesz bases.

C.2 Frame Expansion Coefficients

In this section we demonstrate some properties of frame expansions, in terms of the expansion coefficients. Let $\{h_n\}$ be a frame for a Hilbert space $\mathcal{H}$, and let $f \in \mathcal{H}$. Consider the frame representation,

$$f = \sum < f, S^{-1}h_n > h_n. \tag{3.2.1}$$

For a redundant frame, the frame representation (3.2.1) is not in general unique, and moreover, we know by Theorem 2.5 that if $\{a_n\}$ is another sequence such that $f = \sum_n a_n h_n$, then

$$\sum |a_n|^2 = \sum | < f, S^{-1}h_n > |^2 + \sum | < f, S^{-1}h_n > -a_n|^2. \tag{3.2.2}$$

The above equation defines a hyperplane in ℓ^2, and Theorem 2.5 may be interpreted as saying that $\{< f, S^{-1}h_n >\}$ is the unique sequence of expansion coefficients which is orthogonal to this hyperplane. Every sequence $\{a_n\}$ satisfying (3.2.2), does not however comprise a representation of f, as the following proposition states.

Proposition C.1 *Let $\{h_k\}$ be a frame for $\mathcal{H}$, and let $f \in \mathcal{H}$, and $\{a_n\} \in \ell^2$ such that (3.2.2) is satisfied. Then it does not follow that $f = \sum a_n h_n$.*

Proof: Let c_k denote $\langle f, S^{-1}h_k \rangle$, and assume $c_j \neq 0$ for some j. Now define a sequence $\{a_k\}$, by

$$a_k = \begin{cases} 0 & j \neq k \\ \frac{1}{c_j} \sum |c_k|^2 & j = k. \end{cases}$$

Then $\{a_k\}$ satisfies (3.2.2) since,

$$\begin{aligned} \sum |c_k - a_k|^2 &= \sum |a_k|^2 + \sum |c_k|^2 - 2\Re e \sum c_k \overline{a_k} \\ &= \sum |a_k|^2 + \sum |c_k|^2 - 2\Re e \; c_j \frac{1}{c_j} \sum |c_k|^2 \\ &= \sum |a_k|^2 - \sum |c_k|^2 \end{aligned}$$

However, it is clear that we in general cannot write,

$$f = \sum a_k h_k = a_j h_j,$$

unless f is a multiple of the frame element h_j. ■.

C.2.1 Distribution of Coefficients

An interesting property of the coefficients $c_n = \langle f, S^{-1}h_n \rangle$, is the manner in which they are 'distributed'. Roughly speaking, the among all possible coefficient sequences representing the function f, the sequence $\{c_n\}$ is the most 'uniformly distributed'. This uniform distribution of coefficients is directly related to the minimum norm property of $\{c_n\}$. To clarify this statement, consider the following example of a frame for $\mathbb{R}^2$.

$$h_1 = (1,0)^T \text{ and } h_2 = h_3 = (0,1)^T.$$

Thus $\{h_1, h_2, h_3\}$ is an inexact frame for $\mathbb{R}^2$ with A=1, and $B = 2$. Thus if we consider, the vector $y = (0,1)^T$ as a test vector, then all representations of y with respect to the frame $\{h_1, h_2, h_3\}$, i.e. all $\{a_1, a_2, a_3\}$ such that $y = \sum_{j=1}^{3} a_j h_j$, are given by,

$$a_1 = 0 \text{ and } a_2 + a_3 = 1.$$

Thus the minimum norm sequence is $\{c_1, c_2, c_3\} = \{0, 1/2, 1/2\}$. This minimum norm sequence clearly makes the most uniform use of the redundancy in the frame by distributing the contributions of h_2 and h_3 evenly. The most 'compact' representation of y in this case is $\{a_1, a_2, a_3\} = \{0, 1, 0\}$ (or $\{0, 0, 1\}$) , which makes no use of the redundancy.

In many applications, such as signal compression, it is desirable to work with the most compact representation. One criteria for measuring compactness of a representation is in terms of the entropy of the coefficients. For compactness, one would like to minimize the entropy. This idea has been employed by Coifman et. al. [CW90, CMQW90] for the selection of a 'best (wavelet) basis' for compression of

signals. By the above example, it is clear that although the most distributed representation is uniquely defined, the most compact representation is not in general unique for redundant frames. One drawback of selecting the most compact representation with respect to a redundant frame, is that the robustness properties of frame representations (see Section 2.3.1), are lost. This is because selection of the most compact representation, involves eliminating the effects of redundancy.

C.3 Addition of Frames

It is interesting to examine what happens when frames for two subspaces M and N of a Hilbert space $\mathcal{H}$, are combined and considered as a frame for the direct sum space $M \oplus N$. For the case in which the frames are actually orthonormal bases and the subspaces M and N are orthogonal to one another, it is well-known that the the union of the two frames forms an orthonormal basis for the *orthogonal* direct sum space $M \oplus N$. However, in the general setting of frames, and subspaces which are not orthogonal to one another, some fairly unexpected things can happen.

Here, we obtain results which rely on the subspaces M, and N being disjoint. We show in Section C.3.1 that given subspaces M and N of a Hilbert space, and frames associated with each of the subspaces, the union of the two frames is a frame for $M \oplus N$ whenever the minimum angle, θ_m between the two subspaces is bounded away from zero. We also show that the lower frame bound for the union of the two frames can be bounded below in terms of the quantity $(1 - \cos\theta_m)$, and bounded above by the minimum of the lower frame bounds associated with the frames for M and N individually. Results of this nature are useful when considering truncated frame approximations. Some simple examples in which the frame bounds can be explicitly computed are provided to demonstrate accuracy of the frame bound estimates.

C.3.1 Frames Generated by Subspace Addition

Definition C.1 *Given two subspaces M and N of a Hilbert space $\mathcal{H}$, the smallest*

angle θ_m between M and N is defined as,

$$\cos\theta_m = \sup_{\substack{x\in M \\ \|x\|=1}} \sup_{\substack{y\in N \\ \|y\|=1}} |< x, y >|,$$

where $\theta_m \in [0, \pi/2]$.

We shall make use of the following Theorem in proving the main result (Theorem C.2) of this section.

Theorem C.1 *Let M and N be subspaces of a Hilbert space $\mathcal{H}$ with $M \bigcap N = \{0\}$. And let P_M and P_N be orthogonal projectors on M and N respectively. Then*

$$\inf_{x\in M\oplus N,\ \|x\|\neq 0} \frac{\|(P_M - P_N)x\|}{\|x\|} = \sin\theta_m.$$

Proof: See [Ste73] ■

Theorem C.2 *Let M and N be nontrivial, closed subspaces of a Hilbert space $\mathcal{H}$. Let $\{x_j\}$ be a frame for M with frame bounds A_M and B_M, and $\{y_j\}$ be a frame for N with frame bounds A_N and B_N. Define $Q = \mathrm{Span}(\{x_j\} \bigcup \{y_j\})$.*

Let θ_m denote the minimum angle between the subspaces M and N.

Then if, $\theta_m > 0$ $\{x_j, y_j\}$ is a frame for Q with frame bounds

$$\begin{aligned} A_Q &\geq \widetilde{A}_Q = \min(A_M, A_N)(1 - \cos\theta_m) \\ B_Q &\leq \widetilde{B}_Q = \max(B_M, B_N)\min(2, \frac{1}{1-\cos\theta_m}) \end{aligned} \tag{3.3.3}$$

Proof:

Note that $M \bigcap N = 0$ by the hypothesis that $\theta_m > 0$. So $Q = M \oplus N$ and thus if $g \in Q$ there is a unique decomposition of g as $g = x + y$ where $x \in M$ and $y \in N$.

Lower Frame Bound:

Take $g \in Q$ and let P_M and P_N be orthogonal projection operators onto M and N respectively.

$$\begin{aligned} \sum_j |< g, x_j >|^2 + |< g, y_j >|^2 &= \sum_j |< P_M g, x_j >|^2 + |< P_N g, y_j >|^2 \\ &\geq A_M\|P_M g\|^2 + A_N\|P_N g\|^2 \\ &\geq \min(A_M, A_N)\left\{\|P_M g\|^2 + \|P_N g\|^2\right\} \end{aligned} \tag{3.3.4}$$

Now,

$$\begin{aligned}
\|P_M g\|^2 + \|P_N g\|^2 &= \|P_M g - P_N g\|^2 + 2\Re e\ \langle P_M g, P_N g\rangle \\
&\geq \left[\inf_g \frac{\|(P_M - P_N)g\|}{\|g\|}\right]^2 \|g\|^2 - 2\,|\langle P_M g, P_N g\rangle| \\
&= \sin^2\theta_m \|g\|^2 - 2\,|\langle P_M g, P_N g\rangle| \\
&\geq \sin^2\theta_m \|g\|^2 - 2\|P_M g\|\|P_N g\|\cos\theta_m \\
&\geq \sin^2\theta_m \|g\|^2 - \left(\|P_M g\|^2 + \|P_N g\|^2\right)\cos\theta_m
\end{aligned} \tag{3.3.5}$$

Therefore,

$$\left(\|P_M g\|^2 + \|P_N g\|^2\right)(1 + \cos\theta_m) \geq \sin^2\theta_m \|g\|^2. \tag{3.3.6}$$

Or equivalently,

$$\|P_M g\|^2 + \|P_N g\|^2 \geq \frac{\sin^2\theta_m}{1+\cos\theta_m}\|g\|^2 = \frac{1-\cos^2\theta_m}{1+\cos\theta_m}\|g\|^2 = (1-\cos\theta_m)\,\|g\|^2 \tag{3.3.7}$$

Thus from (3.3.4) and (3.3.7) we get

$$\sum_j |< g, x_j >|^2 + |< g, y_j >|^2 \geq \min(A_M, A_N)\,(1-\cos\theta_m)\,\|g\|^2$$

Upper Frame Bound:

$$\begin{aligned}
\sum_j |< g, x_j >|^2 + |< g, y_j >|^2 &\leq B_M\|P_M g\|^2 + B_N\|P_N g\|^2 \\
&\leq B_M\|g\|^2 + B_N\|g\|^2 \leq 2\max(B_M, B_N)\|g\|^2
\end{aligned} \tag{3.3.8}$$

Also,

$$\begin{aligned}
\|P_M g\|^2 + \|P_N g\|^2 &= \|P_M g - P_N g\|^2 + 2\Re e\ \langle P_M g, P_N g\rangle \\
&\leq \|g\|^2 + 2\Re e\ \langle P_M g, P_N g\rangle \\
&\leq \|g\|^2 + 2\|P_M g\|\|P_N g\|\cos\theta_m \\
&\leq \|g\|^2 + \left(\|P_M g\|^2 + \|P_N g\|^2\right)\cos\theta_m
\end{aligned} \tag{3.3.9}$$

Thus,

$$\left(\|P_M g\|^2 + \|P_N g\|^2\right) \leq \frac{1}{1-\cos\theta_m}\|g\|^2. \tag{3.3.10}$$

So we also have,

$$\sum_j |< g, x_j >|^2 + |< g, y_j >|^2 \leq \max(B_M, B_N)\frac{1}{1-\cos\theta_m}\|g\|^2 \tag{3.3.11}$$

Therefore (by (3.3.8) and (3.3.11)),

$$B_Q \leq \widetilde{B}_Q = \max(B_M, B_N)\min(2, \frac{1}{1-\cos\theta_m})$$

■

It should be noted that the conditions under which Theorem C.2 guarantees the union of two frames to be a frame for their combined span, are only sufficient conditions. In fact in all finite-dimensional cases, these conditions are not necessary. In these cases, estimates of the frame bounds can be made using knowledge of the correlations ($\langle x_i, x_j \rangle$) among the frame elements themselves. However as we show by example in the next section, in an infinite-dimensional setting, the union of two frames can fail to form a frame if $\theta_m = 0$.

As can be seen from Equation (3.3.3), the estimate $\widetilde{A}_Q$ of Theorem C.2 for the lower frame bound A_Q is always less than or equal to $\min(A_M, A_N)$. We now show that the actual lower frame bound A_Q must indeed be less than or equal to $\min(A_M, A_N)$. To show this we first prove the following lemma.

Lemma C.1 *Let M and N be nontrivial, closed subspaces of a Hilbert space $\mathcal{H}$, $M \bigcap N = \{0\}$. Define $Q = M \oplus N$. Then $\forall x^* \in M$, $\exists\ g^* \in Q$ such that*

$$P_M g^* = x^* \quad \text{and} \quad P_N g^* = 0. \tag{3.3.12}$$

In particular,

$$g^* = (I - P_N)(I - P_M P_N)^{-1} x^*,$$

satisfies (3.3.12).

Proof: First note that $\forall x \in Q$, $(I - P_N)x \in N^{\perp} \bigcap Q$ Secondly since $\|P_M P_N\| < 1$, $(I - P_M P_N)^{-1}$ exists and is given by

$$(I - P_M P_N)^{-1} x = \sum_{k=0}^{\infty} (P_M P_N)^k x. \tag{3.3.13}$$

For any $x \in M$, $(I - P_M P_N)^{-1} x \in M$ since every term of the series in the right hand side of Equation (3.3.13) is in M and M is closed. Now let $x = (I - P_M P_N)^{-1} x^*$ and let $g^* = (I - P_N)x$. Clearly $P_N g^* = 0$. Also,

$$\begin{aligned} P_M g^* &= P_M (I - P_N)(I - P_M P_N)^{-1} x^* \\ &= P_M (I - P_M P_N)^{-1} x^* - P_M P_N (I - P_M P_N)^{-1} x^* \\ &= (I - P_M P_N)^{-1} x^* - P_M P_N (I - P_M P_N)^{-1} x^* \\ &\qquad\qquad \text{(since } (I - P_M P_N)^{-1} x^* \in M) \\ &= (I - P_M P_N)(I - P_M P_N)^{-1} x^* = x^* \end{aligned} \tag{3.3.14}$$

■

Theorem C.3 *Let M and N be subspaces of a Hilbert space $\mathcal{H}$. Let $\{x_j\}$ be a frame for M with frame bounds A_M and B_M , and $\{y_j\}$ be a frame for N with frame bounds A_N and B_N. Let $\theta_m > 0$ denote the minimum angle between the subspaces M and N and define $Q = M \oplus N$. Then if A_Q is the lower frame bound for the frame $\{x_j\} \bigcup \{y_j\}$ of Q,*

$$A_Q \leq \min(A_M, A_N).$$

Proof:

Without loss of generality, assume $A_M \leq A_N$. Thus since A_M is the lower frame bound for the frame $\{x_j\}$ of M, for any $\epsilon > 0$, $\exists\ x^* \in M$ such that

$$\sum |\langle x^*, x_j \rangle|^2 \leq (A_M + \epsilon)\|x^*\|^2.$$

By Lemma C.1 $\exists\ g^* \in Q$ such that $P_M g^* = x^*$ and $P_N g^* = 0$.

Therefore,

$$\begin{aligned}
&\sum |\langle g^*, x_j\rangle|^2 + \sum |\langle g^*, y_j\rangle|^2 \\
&\qquad = \sum |\langle P_M g^*, x_j\rangle|^2 + \sum |\langle P_N g^*, y_j\rangle|^2 \\
&\qquad = \sum |\langle x^*, x_j\rangle|^2 + 0 \\
&\qquad \leq (A_M + \epsilon)\|x^*\|^2 \leq (A_M + \epsilon)\|g^*\|^2
\end{aligned}$$

Thus $A_Q \leq A_M + \epsilon$ and since $\epsilon > 0$ is arbitrary we have that $A_Q \leq A_M = \min(A_M, A_N)$. ∎

C.3.2 Examples

In this section we consider a few finite-dimensional examples in which the frame bounds can be explicitly computed. The general methodology in these examples is as follows.

Let $T : \mathcal{H} \to \ell^2$ be defined such that $T : f \to \{< f, x_j >\}$ where $\{x_j\}$ is a frame for $\mathcal{H}$. Therefore the frame operator $S = T^*T$. If we let $\{e_j\}$ be an orthonormal basis for $\mathcal{H}$ then the matrix representation of T with respect to this basis is given by

$$W = [w_{ij}] = [\langle x_i, e_j\rangle].$$

Hence the upper and lower frame bounds are given by the upper and lower spectral limits of W^*W. In the finite dimensional case, the frame bounds can be computed as the maximum and minimum eigenvalues of W^*W or equivalently, the squares of the maximum and minimum singular values of T.

Example I: A frame for $\mathbb{R}^2$ from frames for 1-D subspaces

Let, $x = (1, 0)^T$ and $y = (\sin\theta, \cos\theta)^T$. Define $M = \text{Span}\{x\}$, $N = \text{Span}\{y\}$; so x is a frame for M with frame bounds $A_M = B_M = 1$ and y is a frame for N with frame bounds $A_N = B_N = 1$. In this case $\theta_m = \theta$. Clearly for any angle $\theta > 0$,

Span$\{x, y\}$=$\mathbb{R}^2$ = Q. Using the standard orthonormal basis for $\mathbb{R}^2$, we get

$$W = \begin{bmatrix} 1 & 0 \\ \sin\theta & \cos\theta \end{bmatrix}$$

Hence

$$\begin{aligned} A_Q &= \lambda_{\min}(W^*W) &= 1 - \cos\theta \\ B_Q &= \lambda_{\max}(W^*W) &= 1 + \cos\theta \end{aligned}$$

Since here the lower frame bound is equal to the lower frame bound estimate of Theorem C.2, in this case Theorem C.2 provides both necessary and sufficient conditions. Figure C.2 shows the actual upper and lower frame bounds for this example.

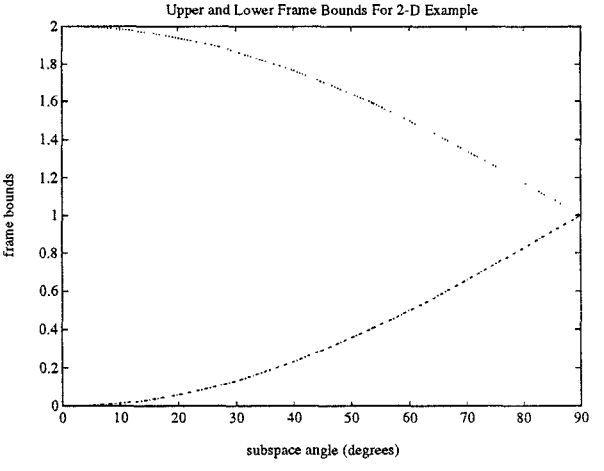

Figure C.2: Actual upper and lower frame bounds for two-dimensional example

Example II: A Frame for $\mathbb{R}^3$ from frames for $\mathbb{R}^2$ and $\mathbb{R}$

Let $x_1 = (1,0,0)^T$, $x_2 = (0,1,0)^T$ and $y = (\cos\omega\cos\theta, \sin\omega\cos\theta, \sin\theta)^T$. Let M = Span$\{x_1, x_2\}$ and N = Span$\{y\}$. Here $\theta_m = \theta$. So for any $\theta > 0$ $M \oplus N = \mathbb{R}^3$. For this example,

$$W = \begin{bmatrix} 1 & 0 & 0 \\ 0 & 1 & 0 \\ \cos\omega\cos\theta & \sin\omega\cos\theta & \sin\theta \end{bmatrix}$$

In this example as well, we have,

$$\begin{aligned} A_Q &= \lambda_{\min}(W^*W) = 1 - \cos\theta \\ B_Q &= \lambda_{\max}(W^*W) = 1 + \cos\theta \end{aligned}$$

Example III: Other Frames for $\mathbb{R}^3$ from frames for $\mathbb{R}^2$ nd $\mathbb{R}$.

Let $x_1 = (1,0,0)^T$, $x_2 = (\cos\gamma, \sin\gamma, 0)^T$ and $y = (\cos\omega\cos\theta, \sin\omega\cos\theta, \sin\theta)^T$. Let $M = \text{Span}\{x_1, x_2\}$ and $N = \text{Span}\{y\}$. Here $A_N = 1$, $A_M = 1 - \cos\gamma$ and $\theta_m = \theta$. So for any $\theta > 0$ $M \oplus N = \mathbb{R}^3$. So,

$$W = \begin{bmatrix} 1 & 0 & 0 \\ \cos\gamma & \sin\gamma & 0 \\ \cos\omega\cos\theta & \sin\omega\cos\theta & \sin\theta \end{bmatrix}$$

In this case, analytical expressions for the eigenvalues of W^*W are quite complicated. Therefore we shall demonstrate the lower frame bounds numerically for a few values of γ and ω. Figures C.3–C.7 each show for a particular value of γ, the actual lower frame bounds and the estimate provided by Theorem C.2 for different values of ω.

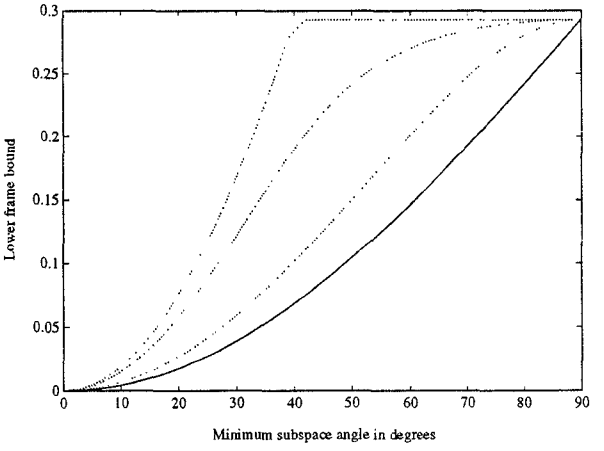

Figure C.3: Example III with $\gamma = \pi/4$. Solid Line: Lower frame bound estimate; Dashed lines: Actual lower frame bound for different values of ω

It can be seen that the lower frame bound estimate becomes increasingly accurate as γ approaches $\pi/2$. For small γ the estimate is quite conservative for certain values of ω,

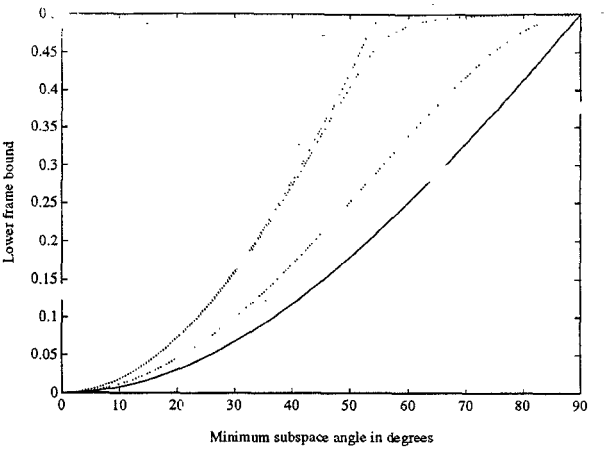

Figure C.4: Example III with $\gamma = \pi/3$. Solid Line: Lower frame bound estimate; Dashed lines: Actual lower frame bound for different values of ω

however in these cases, there also exist values of ω for which the lower frame bound is close to the estimate of Theorem C.2. In this loose sense, the estimate of Theorem C.2 is as good an estimate as can be derived using knowledge of the minimum subspace angle alone.

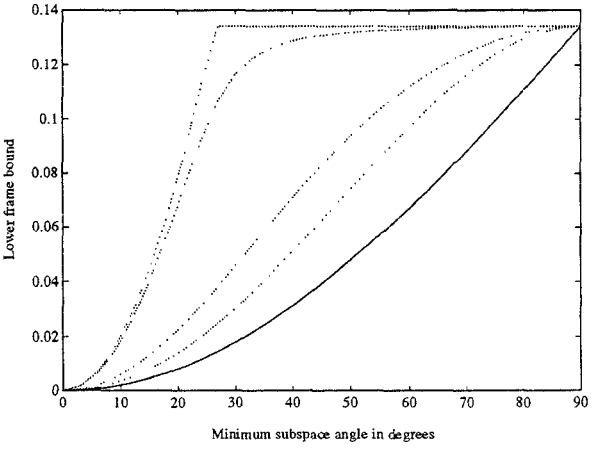

Figure C.5: Example III with $\gamma = \pi/6$. Solid Line: Lower frame bound estimate; Dashed lines: Actual lower frame bound for different values of ω

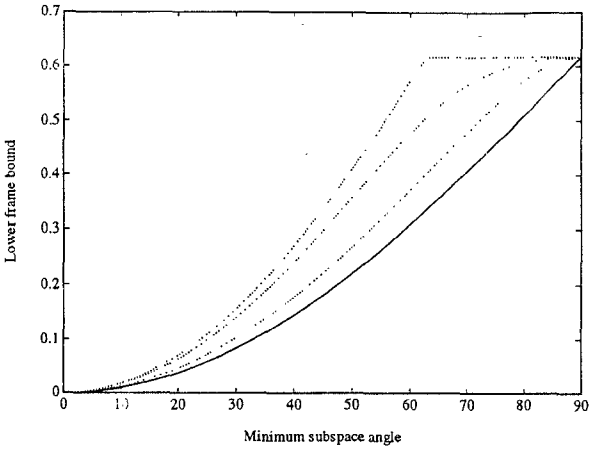

Figure C.6: Example III with $\gamma = 3\pi/8$. Solid Line: Lower frame bound estimate; Dashed lines: Actual lower frame bound for different values of ω

Example IV: Violation of Lower Frame Bound when $\theta_m = 0$

By this infinite-dimensional example (which can be found in [Gil91]) we show that the lower frame bound can indeed be zero in the case where $\theta_m = 0$.

Let $\{e_j\}$ be the standard orthonormal basis for ℓ^2 and let $\psi_j = e_{3j}$, $\phi_j = \sqrt{1-1/j}\ e_{3j} + \sqrt{1/j}\ e_{3j+1}$. Thus the sequences $\{\psi_j\}$, and $\{\phi_j\}$ are orthonormal

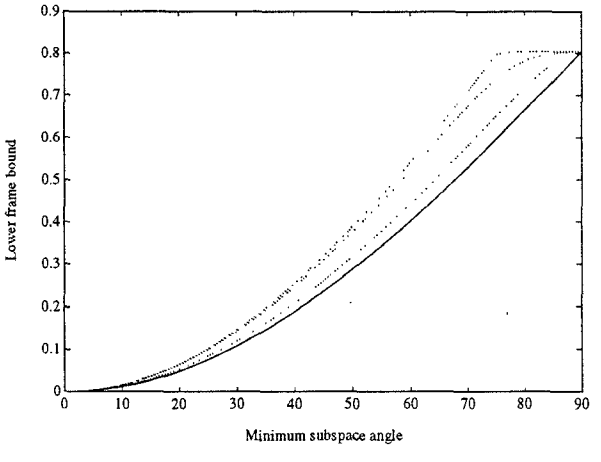

Figure C.7: Example III with $\gamma = 7\pi/16$. Solid Line: Lower frame bound estimate; Dashed lines: Actual lower frame bound for different values of ω

sequences and thereby frames for their respective closed spans. However if we consider the union of the two frames and take $e_{3k+1} \in \text{Span}\{\psi_j,\ \phi_j\}$ as a test vector, it is easily seen that

$$\sum_j |\langle e_{3k+1}, \psi_j \rangle|^2 + \sum_j |\langle e_{3k+1}, \phi_j \rangle|^2 = \frac{1}{k} = \frac{1}{k}\|e_{3k+1}\|^2.$$

Hence since $\frac{1}{k} \to 0$ as $k \to \infty$, the sequence $\{\psi_j,\ \phi_j\}$ is not a frame for its span.

C.3.3 Discussion

In this section we have provided a geometric characterization of conditions which guarantee that the union of two frames is a frame for the appropriate direct sum space. The main result of this section is contained in Theorem C.2 which says that given frames for subspaces M and N, the union of the frames is a frame for the direct sum space $M \oplus N$ provided that the minimum angle between the two subspaces is bounded away from zero. An estimate for the lower frame bound can be made in terms of the quantity $1 - \cos\theta_m$. As mentioned in Section C.3.2, the lower frame bound estimate in Theorem C.2 is in a sense the best estimate which can be made using the minimum subspace angle alone. Furthermore, we have shown that the lower frame bound is nonincreasing with respect to the lower frame bounds for the original subspaces.

Bibliography

[AK69] E. W. Aslaksen and J. R. Klauder. Continuous representation theory using the affine group. *Journal of Mathematical Physics*, 10(12):2267–2275, December 1969.

[Bar87] L. Baratchart. Recent and new results in L^2 rational approximation. In R. F. Curtain, editor, *Modelling, Robustness and Sensitivity Reduction in Control Systems*. Springer-Verlag, Berlin, 1987.

[Bat87] G. Battle. A block spin contruction of ondelettes. part i: Lemarie functions. *Comm. Math. Phys.*, 110:601–615, 1987.

[BG73] A. Bjorck and G. H. Golub. Numerical methods for computing angles betweeen linear subspaces. *Mathematics of Computation*, 27(123), July 1973.

[Chu92] C. K. Chui. *An Introduction to Wavelets*. Academic Press, San Diego, 1992.

[CMQW90] R. R. Coifman, Y. Meyer, S. Quake, and M. V. Wickerhauser. Signal processing and compression with wavelet packets. preprint,Yale University, April 1990.

[Cur88] R. F. Curtain. A synthesis of time and frequency domain methods for the control of infinite-dimensional systems: A system theoretic approach. Preprint, Univ. of Groningen, The Netherlands, September 1988.

[CW90] R. R. Coifman and M. V. Wickerhauser. Best-adapted wave packet basis. preprint,Yale University, 1990.

[CW92] W. R. Cluett and L. Wang. Frequency smoothing using Laguerre model. *IEE Proceedings-D*, 139(1):88–96, 1992.

[Cyb88] G. Cybenko. Continuous valued neural networks with two hidden layers are sufficient. Technical report, Department of Computer Science, Tufts University, Medford, MA, March 1988.

[Cyb89] G. Cybenko. Approximations by superpositions of a sigmoidal function. Technical Report CSRD 856, Center for Supercomputing Research and Development, University of Illinois, Urbana, February 1989.

[Dau83] J. Daugman. Six formal properties of two-dimensional anisotropic visual filters: Structural principles and frequency/orientation selectivity. *IEEE Transactions on Systems, Man, and Cybernetics*, SMC-13(5):882–887, September/October 1983.

[Dau88a] I. Daubechies. Orthonormal bases of compactly supported wavelets. *Communications on Pure and Applied Mathematics*, 41:909–996, 1988.

[Dau88b] I. Daubechies. Time-frequency localization operators: A geometric phase space approach. *IEEE Transactions on Information Theory*, 34(4):605–612, July 1988.

[Dau90] I. Daubechies. The wavelet transform, time-frequency localization and signal analysis. *IEEE Transactions on Information Theory*, 36(5):961–1005, September 1990.

[Dau92] I. Daubechies. *Ten Lectures on Wavelets*. CBMS-NSF regional conference series in applied mathematics. SIAM, Philadelphia, PA, 1992.

[DGM86] I. Daubechies, A. Grossmann, and Y. Meyer. Painless nonorthogonal expansions. *Journal of Mathematical Physics*, 27(5):1271–1283, May 1986.

[DM72] H. Dym and H. P. McKean. *Fourier Series and Integrals.* Academic Press, San Diego, 1972.

[DS52] R. J. Duffin and A. C. Schaeffer. A class of nonharmonic fourier series. *Trans. Amer. Math. Soc.*, 72:341–366, 1952.

[Dur70] P. L. Duren. *Theory of H^p Spaces*, volume 38. Academic Press, New York, 1970.

[DZP90] G. A. Dumont, C. C. Zervos, and G. L. Pageau. Laguerre-based adaptive control of *ph* in an industrial bleach plant extraction stage. *Automatica*, 26(4):781–787, 1990.

[Eyk74] P. Eykhoff. *System Identification.* Wiley, New York, 1974.

[FG] H. Feichtinger and K. Grochenig. Reconstruction of band-limited functions from irregular sampling values. Preprint.

[Gab46] D. Gabor. Theory of communication. *J. Inst. Elect. Eng.*, 93(III):429–457, 1946.

[Gar81] J. B. Garnett. *Bounded Analytic Functions*, volume 96. Academic Press, New York, 1981.

[Gil91] J. Gillis. Reconstruction of stochastic processes using frames. Technical Report SRC-TR-91-14, University of Maryland, Systems Research Center, College Park, MD, 1991.

[GLP90] K. Glover, J. Lam, and J. R. Partington. Rational approximation of a class of infinite-dimensional systems I: Singular values of Hankel operators. *Mathematics of Control, Signals, and Systems*, 3(4):325–344, 1990.

[GLP91a] K. Glover, J. Lam, and J. R. Partington. Rational approximation of a class of infinite-dimensional systems II: Optimal convergence rates of L_∞

approximants. *Mathematics of Control, Signals, and Systems*, 4(3):233–246, 1991.

[GLP91b] K. Glover, J. Lam, and J. R. Partington. Rational approximation of a class of infinite-dimensional systems: The L^2 case. In P. Nevai and A. Pinkus, editors, *Progress in Approximation Theory*. Academic Press, San Diego, 1991.

[GM84] A. Grossmann and J. Morlet. Decomposition of hardy functions into square integrable wavelets of constant shape. *SIAM Journal of Mathematical Analysis*, 15(4):723–736, July 1984.

[GMP85] A. Grossmann, J. Morlet, and T. Paul. Transforms associated to square integrable group representations i: General results. *Journal of Mathematical Physics*, 26(10):2473–2479, October 1985.

[GMP86] A. Grossmann, J. Morlet, and T. Paul. Transforms associated to square integrable group representations ii: Examples. *Ann. Inst. Henri Poincare*, 45(3):293–309, 1986.

[Gui63] E. A. Guillemin. *Theory of Linear Physical Systems*. John Wiley and Sons, Inc., New York, 1963.

[Hof88] K. Hoffman. *Banach Spaces of Analytic Functions*. Dover Publications, New York, 1988.

[HSW89] K. Hornik, M. Stinchcombe, and H. White. Multilayer feedforward networks are universal approximators. *Neural Networks*, 2:359–366, 1989.

[HSW90] K. Hornik, M. Stinchcombe, and H. White. Universal approximations of an unknown mapping and its derivatives using multilayer feedforward networks. Preprint, January 1990.

[HW89] C. E. Heil and D. F. Walnut. Continuous and discrete wavelet transforms. *SIAM Review*, 31(4):628–666, December 1989.

[Jaf89] S. Jaffard. These de l'ecole polytechnique, 1989.

[JL92] S. Jaffard and Ph. Laurencot. Orthonormal wavelets, analysis of operators, and applications to numerical analysis. In C. K. Chui, editor, *Wavelets: A Tutorial in Theory and Applications.* Academic Press, San Diego, 1992.

[KMMG87] R. Kronland-Martinet, J. Morlet, and A. Grossmann. Analysis of sound patterns through wavelet transforms. *Internat. J. Pattern Recog. Artif. Int.*, 1:273–302, 1987.

[Kup88] M. Kuperstein. Generalized neural model for adaptive sensory-motor control of single postures. In *Proceedings IEEE Inter. Conf. On Robotics and Automation*, pages 134–139, Philadelphia, Pa., April 1988.

[KW90] M. Kuperstein and Jyhpyng Wang. Neural controller for adaptive movements with unforseen payloads. *IEEE Trans. on Neural Networks*, 1(1):137–142, March 1990.

[Lju87] L. Ljung. *System Identification: Theory For The User.* Prentice Hall, Englewood Cliffs, New Jersey, 1987.

[LKTS92] J. Lin, W. Ki, K. Thompson, and S. Shamma. Cochlear filters design using a parallel dilating-biquads switched-capacitor filter bank. In *IEEE International Symposium on Circuits and Systems*, volume 4, pages 2053–2056, May 1992.

[LZ89] H. C. Lueng and V. W. Zue. Applications of error backpropagation to phonetic classification. In David S. Touretzky, editor, *Advances in Neural Information Processing Systems*, pages 206–231. Morgan Kaufman Publisher, 1989.

[MAFG82] J. Morlet, G. Arens, I Fourgeau, and D Girard. Wave propagation and sampling theory. *Geophysics*, 47(2):203–236, February 1982.

[Mak90a] P. M. Makila. Approximation of stable systems by Laguerre filters. *Automatica*, 26(2):333–345, 1990.

[Mak90b] P. M. Makila. Laguerre series approximation of infinite dimensional systems. *Automatica*, 26(6):985–995, 1990.

[Mak91] P. M. Makila. On identification of stable systems and optimal approximation. *Automatica*, 27(4):663–676, 1991.

[Mal89a] S. G. Mallat. Multiresolution approximations and wavelet orthonormal bases of $l^2(r)$. *Trans. of the AMS*, 315(1):69–87, September 1989.

[Mal89b] S. G. Mallat. Multifrequency channel decompositions of images and wavelet models. *IEEE Transactions On Acoustics Speech and Signal Processing*, 37(12):2091–2110, December 1989.

[Mal89c] S. G. Mallat. A theory for multiresolution signal decomposition: The wavelet representation. *IEEE Transactions On Pattern Analysis and Machine Intelligence*, 11(7):674–693, July 1989.

[Mea89] C. Mead. *Analog VLSI and Neural Systems.* Addison Wesley, 1989.

[Mey86] Y. Meyer. Principe d'incertitude, bases hilbertiennes et algebres d'operateurs, 1985–1986.

[MH] S. G. Mallat and W. L. Hwang. Singularity detection and processing with wavelets. Preprint.

[NP90] K. S. Narendra and K. Parthasarathy. Identification and control of dynamical systems using neural networks. *IEEE Trans. on Neural Networks*, 1(1):4–27, March 1990.

[Par91] J. Partington. Approximation of delay systems by fourier-Laguerre series. *Automatica*, 27(3):569–572, 1991.

[Pat91] Y. C. Pati. Frames generated by subspace addition. Technical Report SRC TR 91-55, University of Maryland, Systems Research Center, 1991.

[PK90] Y. C. Pati and P. S. Krishnaprasad. Discrete affine wavelet transforms for analysis and synthesis feedforward neural networks. In R. Lippman, J. Moody, and D. Touretzky, editors, *Advances in Neural Information Processing Systems III*, pages 743–749, San Mateo, CA, 1990. Morgan Kaufmann, Publishers.

[PK92] Y. C. Pati and P. S. Krishnaprasad. Analysis and synthesis of feedforward neural networks using discrete affine wavelet transforms. *IEEE Transactions on Neural Networks*, 1992. In Press. (Also Univ. of Md., Systems Research Center Technical Report SRC-TR-90-44).

[PZ88] M. Porat and Y. Y. Zeevi. The generalized Gabor scheme of image representation in biological and machine vision. *IEEE Transactions on Pattern Analysis and Machine Intellegence*, 10(4):452–468, July 1988.

[Sha85a] S. A. Shamma. Speech processing in the auditory system. i: Representation of speech sounds in the responses of the auditory-nerve. *J. Acoust. Soc. Am.*, 78:1612–1621, 1985.

[Sha85b] S. A. Shamma. Speech processing in the auditory system. ii: Lateral inhibition and the processing of speech evoked activity in the auditory-nerve. *J. Acoust. Soc. Am.*, 78:1622–1632, 1985.

[Ste73] G. W. Stewart. Error and perturbation bounds for subspaces associated with certain eigenvalue problems. *SIAM Review*, 15(4), October 1973.

[Str81] V. Strejc. Trends in identification. *Automatica*, 17(1):7–21, 1981.

[SW89] M. Stinchcombe and H. White. Universal approximations using feedforward networks with non-sigmoid hidden layer activation functions. In

Proceedings Inter. Joint Conf. on Neural Networks (IJCNN), pages 613–617, Washington D.C, 1989.

[Sze39] G. Szego. *Orthogonal Polynomials*, volume 23 of *AMS Colloquium*. American Mathmatical Society, Providence, Rhode Island, 1939.

[UR90] H. Unbehauen and G. P. Rao. Continuous-time approaches to system identification: A survey. *Automatica*, 26(1):23–35, 1990.

[Wah91] B. Wahlberg. System identification using Laguerre models. *IEEE Transactions on Automatic Control*, 36(5):551–562, 1991.

[Wel81] P. Wellstead. Non-parametric methods of system identification. *Automatica*, 17(1):55–69, 1981.

[Wic89] M. V. Wickerhauser. Acoustic signal compression with wave packets. preprint,Yale University, 1989.

[Wie56] N. Wiener. The theory of prediction. In E. F. Beckenback, editor, *Modern Mathematics for the Engineer*. McGraw-Hill, New York, 1956.

[You80] R. M. Young. *An Introduction to Nonharmonic Fourier Series*. Academic Press, New York, 1980.

[You81] P. Young. Parameter estimation for continuous time models. *Automatica*, 17(1):23–39, 1981.

[YWS92] X. Yang, K. Wang, and S. A. Shamma. Auditory representation of acoustic signals. *IEEE Transactions on Information Theory*, 38(2), 1992.